Characterizing the turnover of viral nonstructural proteins of the hepatitis C virus

Dissertation

zur Erlangung des Doktorgrades
der Naturwissenschaften (Dr. rer. nat.)

vorgelegt beim Fachbereich Biologie
der Johannes Gutenberg-Universität
in Mainz

von

Vanessa Haberger
geb. am 20.05.1990 in Mainz

Erstgutachter:
Zweitgutachter:

Langen, 2021
(D77)

Vom Fachbereich 10 der Johannes Gutenberg-Universität als Dissertation angenommen.

Dekan:

Gutachter:

Datum der Disputation:

„*Was wir wissen, ist ein Tropfen, was wir nicht wissen, ein Ozean.“*

Isaac Newton

Table of contents

1 Introduction

1.1 Hepatitis C virus

Hepatitis C virus (HCV) causes acute and chronic liver diseases. According to the WHO (World Health Organization) currently estimated 58 million people suffer from chronic HCV infection, with about 1.5 million new infections per year and approximately 290.000 people, who die each year due to HCV-associated liver cirrhosis and hepatocellular carcinoma (WHO HCV 2021). The WHO has launched the global HCV elimination program by 2030, but many barriers have to overcome. The treatment of a chronic infection with direct-acting antivirals agents (DAAs) allows a cure rate over 97%. However, these therapies are very cost-intensive and therefore not accessible for every patient. Another barrier to achieve HCV elimination is the absence of a prophylactic vaccine. For the development of effective cures and a vaccination, a better understanding of the viral life cycle is indispensable.

1.1.1 History

A new parenterally-transmitted hepatitis form was identified in the 1970s that was not caused by the hepatitis A or the hepatitis B virus (Feinstone et al. 1975). In 1988, after the development of a diagnostic test, scientists were able to identify the hepatitis C virus as a cause for the non-A, non-B hepatitis (NANBH) (Choo et al. 1989). Initial limitations impeded the establishment of *in vitro* systems based on subgenomic replicons to analyze the HCV replication. Virus replication and production of viral particles for analysis of the complete HCV life cycle however was not possible until a heterologous expression system was developed (Bartenschlager et al. 1994). In addition, the development of subgenomic replicon systems (Lohmann et al. 1999; Blight et al. 2000) and pseudoparticles (Bartosch et al. 2003) further enabled investigation on the life cycle.

For the host cell line, Huh7.5 were identified as convenient cells in being highly permissive for HCV and contributed to an improved cell culture system to study the HCV life cycle (Blight et al. 2002; Zhong et al. 2005). From the serum of a Japanese patient with fulminant hepatitis (JFH1) a clone was isolated, which replicates up to high levels without any adaptive mutations (Lindenbach et al. 2005; Wakita et al. 2005; Zhong et al. 2005). A higher infectivity was achieved with a generated chimera of a J6

and JFH1 isolate called Jc1 (Pietschmann et al. 2006), which represents a further improvement of the cell culture system.

1.1.2 Infection and pathogenesis

Since HCV is a blood-borne virus, infection occurs through parenteral exposure to contaminated blood, blood products or by the use of injectable drugs (Alter 2007; Frank et al. 2000). HCV is also transmitted by tattooing, hemodialysis, from an infected mother to the unborn child or by sexual activity (Sy and Jamal 2006; Clarke and Kulasegaram 2006; Roberts and Yeung 2002; Terrault 2002). Diagnostic HCV tests and inactivation of the virus minimizes the risk of infection by blood products. HCV virions can keep stability and infectivity after drying at room temperature for a long time (Ciesek et al. 2010). Due to this, a cross contamination of insufficient hospital hygiene is not excepted (Kamili et al. 2007).

The incubation period varies from a few weeks to several months. Because of flu-like symptoms or an absence of any symptoms the acute infection goes unnoticed. Infection with HCV is cleared in about 15% spontaneously, while the remaining 85% develop a chronic hepatitis (Alter 1997; Nawaz et al. 2015). A spontaneous elimination of HCV can occur due to virus-related factors like genotype, high rate of mutations or immune response suppression by viral antigens or through host-related factors, e.g., race, gender, age and rare immune responses (Janiak et al. 2018).

In acute HCV-related metabolic disturbances, the liver, skeletal muscle and adipose tissue are mainly targeted. In the liver ectopic fat, inflammation and oxidative stress is increased, which contribute to the development of steatosis (Chaudhari et al. 2021). Further inflammation and oxidative stress together with fibrogenesis and insulin resistance progress within 30 years to end-stage liver disease. This includes cirrhosis and a high risk for hepatocellular carcinoma (HCC), which is the third leading cause of cancer-related deaths worldwide (Pascual et al. 2016; Chaudhari et al. 2021). Beside the metabolic shift, the pathogenesis of a chronic infection originates from the affected immune response of the host (Irshad et al. 2013). Elevated levels of reactive oxygen species (ROS) causes persistent liver damage and exhausted liver regeneration leads to replaced non-functional connective tissue, which progresses into liver fibrosis (Rockey and Bissell 2006). In HCV positive cells, elevated ROS is produced due to ER stress, UPR (unfolded protein response), mitochondrial dysregulation, high cytosolic Ca^{2x} levels and NADPH oxidases (NOXs) (Medvedev et al. 2016). ROS contributes to

the HCV-associated pathogenesis and the induction of autophagy, which is required for viral replication and release (Ploen and Hildt 2015). Furthermore, ROS leads to the activation of Nrf2 (nuclear factor erythroid 2 (NF-E2) related factor 2). However, Nrf2 signaling is impaired upon HCV infection, which results in further increase of ROS and the activation of JNK (c-Jun N-terminal kinase). Activated JNK induces phosphorylation of IRS1/2 (insulin receptor substrate 1/2) on Ser/Thr residues and thereby impairs the insulin signaling (Medvedev et al. 2016). Moreover, increased expression of PGC-1α (peroxisome proliferator-activated receptor-gamma coactivator 1α), enhanced fatty acid uptake and upregulation of genes involved in cholesterol and lipid synthesis may contribute to oxidative stress-induces insulin resistance (Medvedev et al. 2016). Furthermore, Nrf2 activation due to defects in the autophagic flux, which results in p62 accumulation has been associated with drug resistance and cancer (Bender and Hildt 2019). In addition to metabolic shifts, oxidative stress, immune response and insulin, chronic HCV affects the iron metabolism. Iron is a central component for HCV replication and translation, however it is controversial whether iron promotes or suppresses viral replication (Chaudhari et al. 2021). A hepatic iron overload by high serum ferritin levels in chronic infected patients are considered as an independent risk factor for advanced liver fibrosis (Zou and Sun 2017; Chang et al. 2020). In several studies, statins, beta-blockers, Mediterranean diet and coffee were found to act as protective factors, which can reduce the risk of developing HCC (Pascual et al. 2016). Up to now, the development of tumor cells is still unclear, but the main factor might be the induction of oxidative stress. High ROS-levels result in DNA damage and its accumulation may lead to several genetic mutations and mutagenesis. (Kryston et al. 2011). Moreover, oncogenic properties were observed for some HCV proteins (Tang and Grisé 2009).

1.1.3 Diagnosis

In direct laboratory tests, HCV RNA and core antigen are characterized, while specific antibodies against HCV can be detected in an indirect test (Gupta et al. 2014).
The “gold standard” for the detection of active HCV replication is the screening of RNA by nucleic acid tests (NAT) in early infection even after 4-6 days (Gupta et al. 2014; Marwaha and Sachdev 2014). Viral RNA can be detected 1-3 weeks after infection by using target amplification with polymerase chain reaction (PCR) and signal amplification (hybrid capture or the branched DNA assay) (Chevaliez and Pawlotsky

2008). Quantitative real-time PCR assays progressively replace classical techniques and allow a direct quantification of the viral load and can detect very low RNA levels (10-15 IU/ml) (Chevaliez and Pawlotsky 2008).
Since the HCV core antigen levels follow HCV RNA dynamics, core can be detected by enzyme-linked immunosorbent assay (ELISA) and chemiluminescence immunoassays (CLIA) (Seme et al. 2005).
After approx. 6-8 weeks of infection, antibodies against HCV can be detected by ELISA (Gupta et al. 2014). Current generation of ELISA enables detection of HCV capsid antigen and antibodies against core and the nonstructural proteins NS3, NS4 and NS5A.

1.1.4 Therapy

Treatment against HCV started with the administration of interferon alpha (IFN-α), followed by a combination with ribavirin, which is a guanosine analogue with antiviral effects. To measure the success of a treatment, sustained virological response (SVR) was used as unit and is based on an undetectable level of HCV RNA 12 weeks (SVR12) or 24 weeks (SVR24) after the termination of the treatment (Lynch and Wu 2016). A quite low SVR of 7-11% by use of IFN-α and 28-31% in combination with ribavirin was obtained (Pawlotsky et al. 2015). For more than over two decades, HCV was then treated by pegylated IFN-α with ribavirin, which led to a moderate efficiency of 42-46%. However, the combinated therapy has severe side effects like depression, fatigue, flu-like symptoms and anemia (Pawlotsky et al. 2015).
Later in the year 2011, first-generation of direct-acting antivirals (DAAs) HCV NS3-NS4A protease inhibitors Telaprevir and Boceprevir were approved combined with pegylated IFN-α and ribavirin and increased the SVR rate to 67-75% (Ghany et al. 2011).
As a new generation of therapy, further inhibitors were developed to inhibit NS5A, nucleotide analogue inhibitors of the HCV RNA-dependent RNA polymerase (RdRp) NS5B and non-nucleoside inhibitors of the viral RdRp (Pawlotsky et al. 2015). All inhibitors had in common, that there are mainly active only against genotype 1 and exhibit a low barrier to resistance.
Therefore, second-generation of NS3-4A protease inhibitors were developed. This generation improved the barrier to resistance to a higher level and had pangenotypic

activity. Second-generation of NS5A inhibitors with pangenotypic activity but a low barrier to resistance followed (Pawlotsky et al. 2015).

Finally in 2014, two new IFN-α free DAA combinations have been approved. Harvoni® is a combination of Sofosbuvir (nucleotide analogue of HCV RNA polymerase NS5B) and Ledipasvir (NS5A inhibitor) in one pill and improved the SVR rate to 93-100% when administered daily for 8-24 weeks (Pawlotsky et al. 2015). Grazoprevir combined with Elbasvir in Zepatier® contains an NS3-4A and NS5A inhibitor, respectively and the combination of Sofosbuvir and Velpatasvir (NS5A inhibitor) is sold as Epclusa®. Further antiviral drugs are Vosevi™, a triple combination of Sofosbuvir, Velpatasvir and Voxilaprevir (NS3-4A inhibitor) as well as Mavyret™ for the administration of Glecaprevir (NS3-4A inhibitor) and Pibrentasvir (NS5A inhibitor) (WHO 2018; DGVS 2020).

To this day, new DAAs and combinations are being tested in clinical trials in the hope that HCV can be totally cured one day. However, the prohibitive pricing of the drugs as well as HCV resistance to DAAs are still limiting the therapy. Despite the high prevalence of HCV, only approx. 20% of infected individual have been diagnosed and only 7% have received treatment worldwide (Zhang et al. 2021). The major challenges remain in the implementation of diagnosis and new therapies, not only in low- to middle-income countries, but also in high-income countries (Pawlotsky et al. 2015). It is forecasted, that more people globally in 2040 die due to viral hepatitis than HIV, tuberculosis and malaria combined and demonstrate how crucial progresses on therapies and vaccines against HCV are (Foreman et al. 2018; Cox 2020).

1.1.5 Epidemiology

Studies on the global distribution of HCV in 138 countries and with 177 million HCV-infected people estimated the total HCV prevalence of about 2.5% (Petruzziello et al. 2016). The highest prevalence is estimated in central Asia and central Africa (> 3.5%). A moderate prevalence (1.5% - 3.5%) was observed in South-, East- and Southeast Asia, West-, East- and North Africa and Middle East, Latin America, Australasia and Eastern Europe. The lowest prevalence has occurred in Southern Africa, North America, Pacific Asia and Western and Central Europe (< 1.5 %) (Petruzziello et al. 2016).

The different HCV genotypes distinguish in their distribution worldwide. In the geographic distribution, shown in figure 1, genotype 1 is the most common and has

the highest prevalence in the high-income countries, genotype 2 is highly present in West Africa and genotype 3 in Asia. For genotype 4, the highest prevalence is in North Africa and the Middle East. In Central and Northern Africa and in Southeast Asia the genotypes 4 and 6 are mostly present (Petruzziello et al. 2016).

Discriminated in their proportion worldwide, genotype 1 has the highest (46.2%), followed by genotype 3 (30.1%), genotype 2 (9.1%), genotype 4 (8.3%), genotype 6 (5.4%) and genotype 5 (0.8%) (Warkad et al. 2018).

Compared with other infectious diseases such as tuberculosis, HIV and malaria that have a steady decline in prevalence and mortality over the last years, HCV infection remains on the rise and is a global health problem moving forward (Zhang et al. 2021).

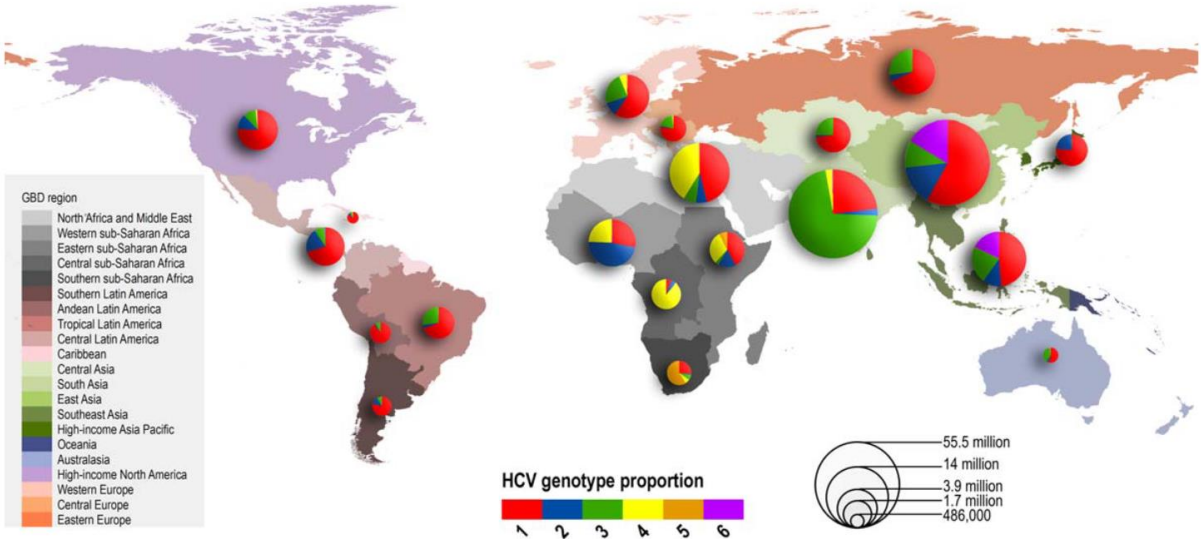

Figure 1 Relative prevalence and distribution of HCV genotypes worldwide. The most common genotype for each country and the number of seroprevalent cases is shown (Messina et al. 2015).

1.1.6 Classification of hepatitis C virus

HCV is an RNA virus that belongs to the genus of *Hepacivirius* within the family of *Flaviviridae* to which the yellow fever virus, dengue virus and Zika virus are also related to (Blázquez et al. 2014). It can be subdivided into 7 genotypes (1-7) and various subtypes (a, b, c, etc.) and distinguished in geographical distributions and medication (Kuiken and Simmonds 2009; Simmonds 2004). Within the genotypes the nucleotide sequence differs by about 30-35% and by another 20-25% within the subtypes (Irshad et al. 2010). Due to a lack of proof-reading function of the viral RNA-dependent RNA polymerase (RdRp), a high mutation rate of the viral genome occurs. Based on this, a high genetic diversity with different but closely related genomes (quasispecies) is

observed that makes treatment of chronic hepatitis C in patients challenging (Martell et al. 1992; Farci and Purcell 2000).

1.1.7 Genome organization

As a hallmark for flaviviruses, HCV has a single-stranded, positive-sense, uncapped RNA genome with a size of 9.6 kB. The single open reading frame (ORF) is flanked by highly structured 5' and 3' untranslated regions (UTR) harboring conserved structures required for viral replication (Lohmann et al. 1999). The internal ribosomal entry site (IRES) of the 5' UTR binds the 40S ribosomal subunit and initiates the translation of the viral genome in a cap-independent manner (Bartenschlager et al. 2013). The resulting polyprotein of about 3000 amino acids (aa) is cleaved by cellular and viral proteases into ten mature proteins: The structural proteins Core, E1 and E2 and the nonstructural proteins p7, NS2, NS3, NS4A, NS4B, NS5A and NS5B (Gu and Rice 2013; Neufeldt et al. 2018). The HCV genome organization is shown in figure 2. To assemble the viral particle, the structural proteins core, E1 and E2 envelope and form the nucleocapsid that harbors the viral RNA. The nonstructural proteins NS3-NS5B are not part of the viral particle and represent the replicon complex (RC), which is essential for viral replication and involved in the regulation of cellular processes (Bartenschlager et al. 2013). The ion channels p7 and NS2 are not part of the viral particle but required for viral assembly as p7/NS2 dictate the relocalization of core from LDs to ER (Bartenschlager et al. 2011; Madan and Bartenschlager 2015). The 3' UTR contains a short variable sequence (VAR), a poly (U/UC) region and a highly conserved 98 nucleotide sequence (X-tail) (Tanaka et al. 1996; Kolykhalov et al. 1996).

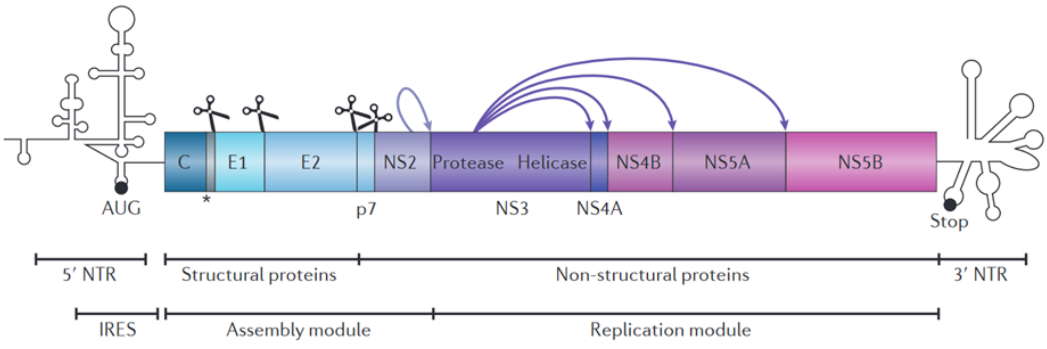

Figure 2 HCV genome organization.
The ORF of the HCV genome, flanked by 5' and 3' non-translated regions (NTR) with start and stop codons. The 5' NTR contains the internal ribosome entry site (IRES). The structural proteins core (C), E1 and E1 together with p7 and NS2 present the assembly module. The remaining nonstructural proteins NS3-NS5B are required for

RNA replication (replication module). Indicated scissors show the polyprotein cleavage by cellular proteases. The cleavage removing the carboxy-terminal regions of core is indicated by an asterisk. Cleavage by viral proteases is indicated with arrows (Bartenschlager et al. 2013).

1.1.8 Structural proteins

1.1.8.1 Core

The highly conserved RNA-binding protein core has a size of 21 kDa and forms the viral capsid (McLauchlan 2000). From three different domains, the RNA-binding domain 1 is hydrophilic and involved in oligomerization. The membrane-binding domain 2 is hydrophobic and binds the mature core at the endoplasmatic reticulum (ER) and on the surface of lipid droplets (LDs) where virion assembly takes place (Hope et al. 2002; Boulant et al. 2006). The hydrophobic domain 3 serves as signal peptide and mediates E1 translocation into the ER lumen. Subsequently, the signal peptide is cleaved by the cellular signal peptide peptidase, which leads to the maturation of core (McLauchlan 2000). The core protein mediates the recruitment of nonstructural proteins to the LDs (Miyanari et al. 2007). Furthermore, core has various regulatory functions and is involved in the HCV pathogenesis by affecting host cell functions (Khaliq et al. 2011). Core is involved in the deregulation of cell signaling pathways, which contribute to the development of HCC (Pascut et al. 2021). The up- or downregulation of miRNAs by core enables inhibition of the interferon response, promotes viral replication and alters hepatic lipid metabolism (Pascut et al. 2021). Recently, core was reported to inhibit the cleavage of MHC class I molecules and induce their degradation, thus suggesting that core functions as an immunoevasin (Hirano et al. 2021).

1.1.8.2 E1 and E2

The two envelope proteins E1 and E2 are type I transmembrane proteins, which form a heterodimer. After translocation to the ER the proteins get glycosylated, which is important for the proper folding and release (Khan et al. 2015). Depending on their glycosylation, the molecular size of E1 is ~33 kDa and of E2 ~70 kDa (Deleersnyder et al. 1997). The C-terminal putative fusion peptide of E1 play a role in E1E2 heterodimerization, assembly and release, while the α2-helix is involved in receptor interaction and infectivity (Moustafa et al. 2018). Moreover, E1 is required for the fusion between viral and endosomal membrane to release the nucleocapsid into the cytosol

(Ashfaq et al. 2011). Despite extensive research, the molecular mechanism of the fusion between the membranes is not clear (Tong et al. 2018). The E2 protein mediates host cell recognition and entry by interaction with the cellular receptors CD81 and scavenger receptor B1 (SRB1) (Scarselli et al. 2002; Dao Thi et al. 2012; Bankwitz et al. 2010) . Due to two hypervariable regions that are prone for mutations, the E2 protein allows the virus to evade neutralizing antibodies (Ashfaq et al. 2011). Recently, a study showed syntenin and HCV structural proteins expressing cells, which release exosomes containing E2, but lacking core and exhibit a higher resistance to neutralizing antibodies (Deng et al. 2019).

1.1.9 Nonstructural proteins

All nonstructural proteins are tethered to intracellular membranes by one or several transmembrane domains (TMD) or by amphipathic α-helices. The membrane topology and major functions of the HCV proteins are shown in figure 3.

1.1.9.1 p7

The small membrane protein p7 has a molecular weight of 7 kDa and is located in the ER where it oligomerizes to form a cation channel. The p7 protein has two transmembrane domains and is relevant for virus assembly and HCV infectivity (Griffin et al. 2003; Sakai et al. 2003; Steinmann et al. 2007). Ion channel-independent functions of p7 are subcellular localization of NS2, membrane-to-membrane adhesion at lipid rafts and membrane permeabilization (Tedbury et al. 2011; Lee et al. 2016a; Lee et al. 2020).

1.1.9.2 NS2

The hydrophobic protein NS2 has a size of 21-23 kDa and is essential for viral assembly, but dispensable for viral replication. The N-terminus is located at the ER membrane, while the C-terminus remains in the cytoplasm (Ashfaq et al. 2011). Together with the N-terminal part of the NS3 protein the C-terminus of NS2 forms a metalloproteases and mediates the release of NS3 by autocleavage (Moradpour et al. 2007; Ashfaq et al. 2011).

1.1.9.3 NS3

The N-terminal amino acids of the 70 kDa protein NS3 harbor a serine protease, which is involved in the cleavage of the vial polyprotein (Bartenschlager et al. 1993). NS3 can

modulate the innate immune response in infected cells by inhibiting the RIG-I and TLR3 signaling (Foy et al. 2005; Li et al. 2005). The C-terminus has an NTPase/helicase activity that converts double-stranded RNA or secondary structures into single-stranded RNA, which makes NS3 essential for the viral replication (Morikawa et al. 2011).

1.1.9.4 NS4A

NS4A serves as a cofactor for the NS3 protease and has a molecular size of 8 kDa. The anchoring of the NS3/NS4A complex on the ER membrane is mediated by the N-terminal transmembrane helix of NS4A (Brass et al. 2008). NS4A is involved in the activation of NS3 active site and contributes to the efficiency of their protease activity (Kim et al. 1996). In addition, NS4A is necessary for the hyperphosphorylation of NS5A (Lindenbach et al. 2007).

1.1.9.5 NS4B

The hydrophobic membrane protein NS4B has a size of 27 kDa and four transmembrane domains (TMD), which are tethered in the ER membrane (Lundin et al. 2006). NS4B induces the formation of the membranous web that is composed of ER-derived membranes, LDs and double-membrane vesicles (DMV) (Egger et al. 2002; Romero-Brey et al. 2012; Ferraris et al. 2010). The replicon complex is formed through a direct interaction of NS4B with NS4A and indirect interaction with NS3 and NS5A (Hügle et al. 2001).

1.1.9.6 NS5A

The RNA-binding phosphoprotein NS5A exists in two phosphorylation forms, a basally phosphorylated (hypophosphorylated) form with the size of 56 kDa and a hyperphosphorylated form with 58 kDa (Moradpour et al. 2007). NS5A is required for the viral replication, interaction with several cellular and viral proteins and is involved in the regulation of cell signaling pathways and immune responses (Ashfaq et al. 2011). NS5A is hydrophilic and composed of three domains with an amphipathic α-helix at the N-terminus, which mediates the attachment to the ER membrane (Brass et al. 2002). In addition, the domain I has a zinc binding motif, which is required for the RNA replication (Tellinghuisen et al. 2004). Domain II contributes to viral replication and domain III is involved in infectious particle assembly (Appel et al. 2008; Tellinghuisen et al. 2008; Ross-Thriepland et al. 2013). NS5A has an interferon-α-sensitivity-determining region (ISDR), which enables the repression of the antiviral interferon-

induced protein kinase R (PKR) (Gale et al. 1997). The phosphorylation forms of NS5A are supposed to act as a switch between viral replication and viral particle assembly/release in which the basal form may play a role in replication and the hyperphosphorylation is required for assembly and release (Masaki et al. 2014; Goonawardane et al. 2017). The hyperphosphorylation of NS5A depends on the NS3-mediated autocleavage between NS3 and NS4A and is followed by the release from the NS4A-5A polyprotein (Chiang et al. 2020). NS5A is able to modulate the MAPK (mitogen activated protein kinase) pathways, which can cause hepatocyte transformation and HCC formation, since MAPK signaling is involved in apoptosis, cell growth, ROS-dependent pathways and the PI3K (phosphatidylinositol 3-kinase) pathways (Macdonald et al. 2004). Furthermore, NS5A mediates the recruitment of the c-Raf kinase to the replicon complex where it gets activated and is required for the viral replication. The recruitment is resulting in the activation of the MEK/ERK (Mitogen-activated protein kinase kinase/extracellular signal-regulated kinase) signaling pathway (Bürckstümmer et al. 2006; Himmelsbach et al. 2009).

1.1.9.7 NS5B

NS5B is the RNA-dependent RNA polymerase (RdRp) with a molecular weight of 65 kDa and synthesizes the viral RNA. The α-helix form at the C-terminus region anchors the NS5B protein at the ER membrane (Moradpour et al. 2007). By using the plus-strand RNA as matrix, NS5B produces a complementary minus-strand RNA, from which a new plus-strand genome is directly synthesized (Ashfaq et al. 2011). Due to a lack of a proof-reading function, a lot of mutations can occur during viral replication, which results in various so-called quasispecies (Martell et al. 1992). As the NS5B protein is crucial for viral replication, it is a major target for antiviral agents (Ashfaq et al. 2011).

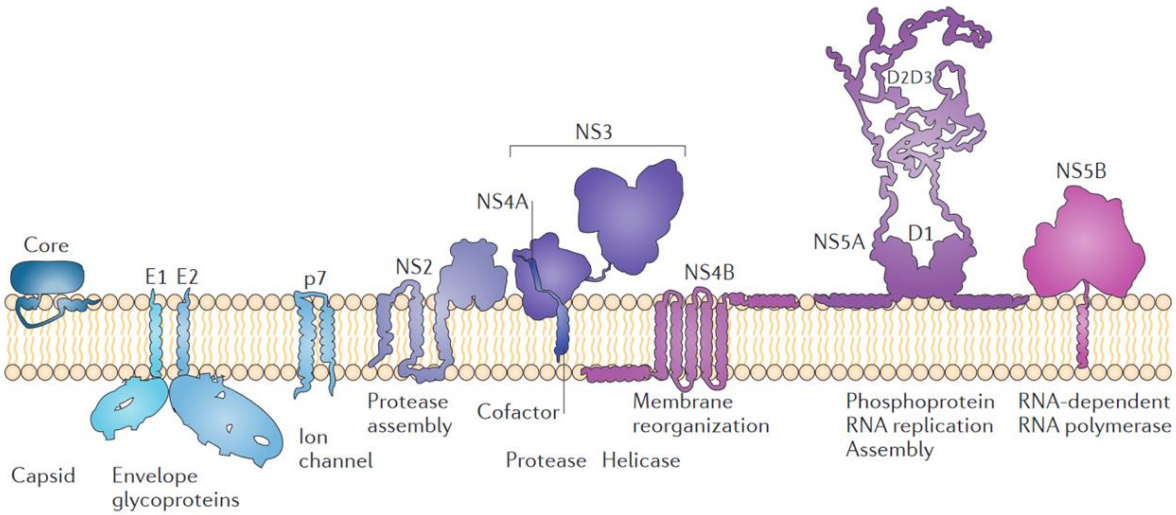

Figure 3 Membrane topology of viral proteins.
Membrane topology and major functions of the HCV proteins. The proteins are tethered to intracellular membranes by one or several transmembrane segments. Core and NS5A are tethered by amphipathic α-helices and NS3 via a small α-helix and via NS4A. NS4A is intercalated into the amino-terminal protease domain of NS3. Here, NS5A is shown as a dimer, but most HCV proteins form homo- or heterodimers or oligomeric complexes (Bartenschlager et al. 2013).

1.1.10 Life cycle of HCV

1.1.10.1 Entry and uncoating

HCV exclusively infects humans and chimpanzees with hepatocytes as the main target (Moradpour et al. 2007). After the primary infection, HCV particles circulate in the blood stream until they reach the surface of hepatocyctes. The virus enters the cell through an interaction with several cell receptors shown in figure 4 (Zeisel et al. 2013). The scavenger receptor B1 (SRB1) and the heparan sulfate proteoglycan (HSPG) syndecan-1 and syndecan-4 are required for the attachment of viral particles (Scarselli et al. 2002; Dao Thi et al. 2012; Shi et al. 2013; Lefèvre et al. 2014). Also required for the viral entry are the low density lipoprotein receptor (LDLR), tetraspanin CD81, claudin-1 (CLDN1) and occludin (OCLN), the cholesterol transporter Niemann-Pick C1-like (NPC1L1) and the transferrin receptor 1 (Agnello et al. 1999; Albecka et al. 2012; Scarselli et al. 2002; Pileri et al. 1998; Evans et al. 2007; Ploss et al. 2009; Sainz et al. 2012; Martin and Uprichard 2013). Due to this compilation of these surface proteins, hepatocytes are the target host cell for HCV (Reynolds et al. 2008).
The HCV entry occurs in a coordinated chronological and spatial order. The entry is initiated by binding of the viral particle to SRB1 and a modified lipid composition of the associated lipoproteins on the HCV particle where the CD81 binding site of the E2

glycoprotein is presented (Scarselli et al. 2002; Dao Thi et al. 2012; Bankwitz et al. 2010). The endopeptidase calpain-5 (CAPN5) and the ubiquitin ligase Casitas B-lineage lymphoma proto-oncogene B (CBLB) were found to form a complex with CD81 and support the HCV entry (Bruening et al. 2018). The transferrin receptor 1 is involved in the early step of the entry and is supposed to have a post-CD81 role (Martin and Uprichard 2013). Subsequently, attached viral particles move lateral to tight junctions and interact with CLDN1 (Harris et al. 2010; Harris et al. 2008). The formation of a CD81-CLDN1 co-receptor is involved in downstream processes of the viral entry, such as Rho GTPase signaling, protein kinase A (PKA) and the Ras/MEK/ERK pathway, which is promoted by the signaling of epidermal growth factor receptor (EGFR) or the ephrin type A receptor 2 (EphA2) (Brazzoli et al. 2008; Farquhar et al. 2012; Farquhar et al. 2008; Lupberger et al. 2011). The tight junction protein OCLN is essential for viral entry, but it is supposed to be involved at the late step of the entry (Benedicto et al. 2009). Together with the CD81-OCLD1 complex the lipoviral particles are endocytosed in a clathrin-dependent manner (Farquhar et al. 2012; Blanchard et al. 2006; Meertens et al. 2006). The internalized viral particles are transported retrograde on actin filaments to early endosomes (EE) (Coller et al. 2009). Due to the low pH in early endosomes, an E1-mediated fusion of the viral membrane and EE is induced, which results in the release of the viral genome into the cytoplasm (Blanchard et al. 2006). Subsequently, the uncoated viral RNA is translocated to the rough ER (rER) membrane.

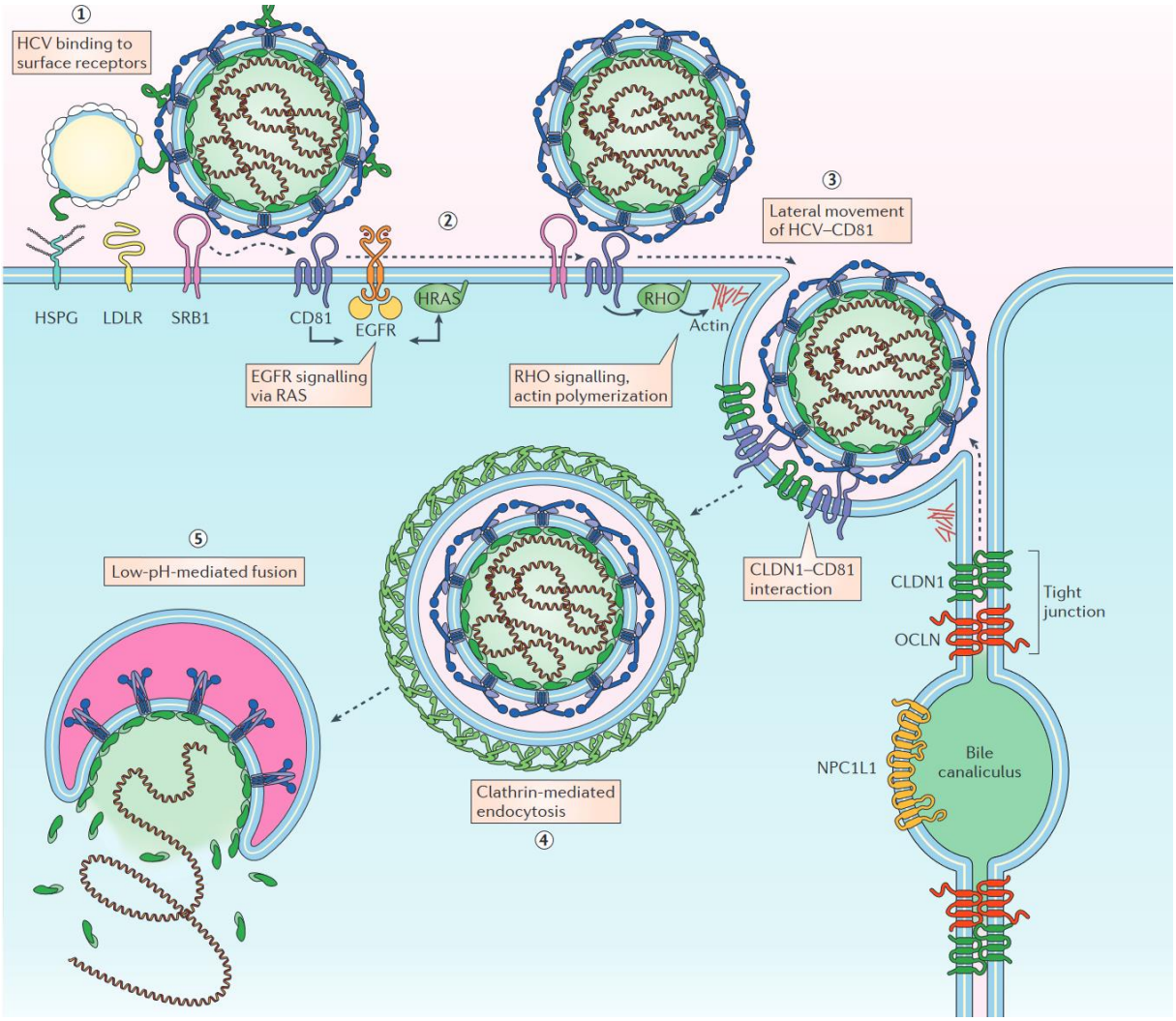

Figure 4 Entry and uncoating of HCV.
(1) The lipoviral particle (LVP) interacts with heparan sulphate proteoglycans (HSPGs), low-density-lipoprotein receptor (LDLR) and scavenger receptor class B member 1 (SRB1). The modified lipid composition of the associated lipoproteins on the LVP causes the exposure of the CD81 binding site of E2 glycoproteins. (2) Interaction of viral E2 and CD81 activates signal transduction through epidermal growth factor receptor (EGFR) via HRAS and through RHO GTPases. (3) These signaling events cause the lateral movement of the HCV-CD81 complex to sites of cell-cell contact and interaction of CD81 with claudin 1 (CLDN1). (4) HCV is internalized by endocytosis in a clathrin-dependent manner. (5) The low pH of the endosome induces fusion between the viral envelope and the bounding endosomal membrane. NPC1L1, Niemann–Pick C1-like 1; OCLN, occludin; HRAS, Harvey rat sarcoma viral oncogene homolog; RHO, Ras homologue (Lindenbach and Rice 2013).

1.1.10.2 HCV RNA translation and replication

The IRES-mediated translation of viral RNA is initiated at the rough ER where the polyprotein is synthesized. The viral polyprotein is co- and post-translationally cleaved by cellular and viral proteases into ten mature proteins, the structural proteins (core, E1 and E2) and the nonstructural proteins (p7, NS2, NS3, NS4A, NS4B, NS5A, NS5B)

(Penin et al. 2004; Bartenschlager et al. 2004; Lindenbach and Rice 2005). The cellular proteases cleave the structural proteins and p7, while viral proteases are required to cleave the nonstructural proteins (Moradpour et al. 2007).

Host cell factors and the viral proteins induce vesicular membrane alterations to form the so-called membranous web. It is composed of ER-derived membranes, LDs and double-membrane vesicles (DMV) (Egger et al. 2002; Romero-Brey et al. 2012; Ferraris et al. 2010). The oligomerized NS4B plays a major role in forming the scaffold for the membranous web (Gouttenoire et al. 2010b; Dubuisson and Cosset 2014). NS5A induces the DMV and the interaction with the phosphatidylinositol-4-kinase-III (PI4KIII), which induces the accumulation of phosphatidylinositol-4-phosphate (PI4P) within the membranous web and is crucial for its formation (Romero-Brey et al. 2012; Reiss et al. 2011). In addition, the PI4KIII induces the accumulation of cholesterol and other lipids into the membranes, which are essential for the viral replication (Diamond et al. 2010; Paul et al. 2013). The DMVs are highly enriched in sphingolipids and cholesterol. To ensure the establishment of cholesterol-enriched DMVs for viral replication, HCV hijacks the lipid transfer proteins (Stoeck et al. 2018).

Lipid droplets are intracellular storage organelles of excess fatty acids, cholesterol esters and triacylglycerides (TAG) surrounded by a phospholipid monolayer, which is coated with several proteins (Dubuisson and Cosset 2014). Synthesis of LDs can occur through the fusion of existing LDs or by an accumulation of neutral lipids in the ER membrane within the bilayer followed by forming lens-like structures (Wilfling et al. 2014; Choudhary et al. 2015). Proteins of the FIT (fat storage-inducing transmembrane protein)-family are required for budding of the mature lipid droplets from the ER and for the monolayer membrane of LDs, which consists of ER proteins (Choudhary et al. 2015). In the life cycle of HCV, LD-associated proteins play a crucial role in replication and morphogenesis. The interaction of nonstructural proteins with LDs, mediated by Rab18, promotes the viral replication (Salloum et al. 2013). Furthermore, the tail-interacting protein of 47 kDa interacts with NS5A and together with Rab9 involved in the shuttling of viral RNA from the RC to LDs where particle assembly takes place (Ploen et al. 2013a; Ploen et al. 2013b).

RNA replication is catalyzed by the RNA-dependent RNA polymerase activity of NS5B and supported by other viral nonstructural proteins and host cell factors like cyclophilin A and B as well as the liver-associated microRNA miR-122, which enhance the replication (Lohmann 2013; Tabata et al. 2020). The plus-stranded RNA serves as a

matrix for NS5B and is used for the synthesis of a negative-sense RNA that in turn is a matrix for the positive-sense RNA, which can be processed for RNA translation, replication or incorporated in viral particles (Bartenschlager et al. 2013; Shi and Suzuki 2018). The activity of NS5B was shown to depend on redox-sensitive posttranslational modifications like S-glutathionylation or cysteine modification (Kukhanova et al. 2019). Recently, the activation of mTOR (mammalian target of rapamycin) by HCV early during infection was demonstrated to be an antiviral response by the cells as viral RNA levels were low. HCV replication is restricted by mTORC1 through ULK1, which further modulates the levels of miR-122 and functions as a balance between viral replication, virion packaging and release (Johri et al. 2020). Moreover, a higher level of miR-22 is supported by the glycogen synthase kinase 3 (GSK3), which enhances viral replication (Saleh et al. 2018). HCV translation and replication is shown in figure 5.

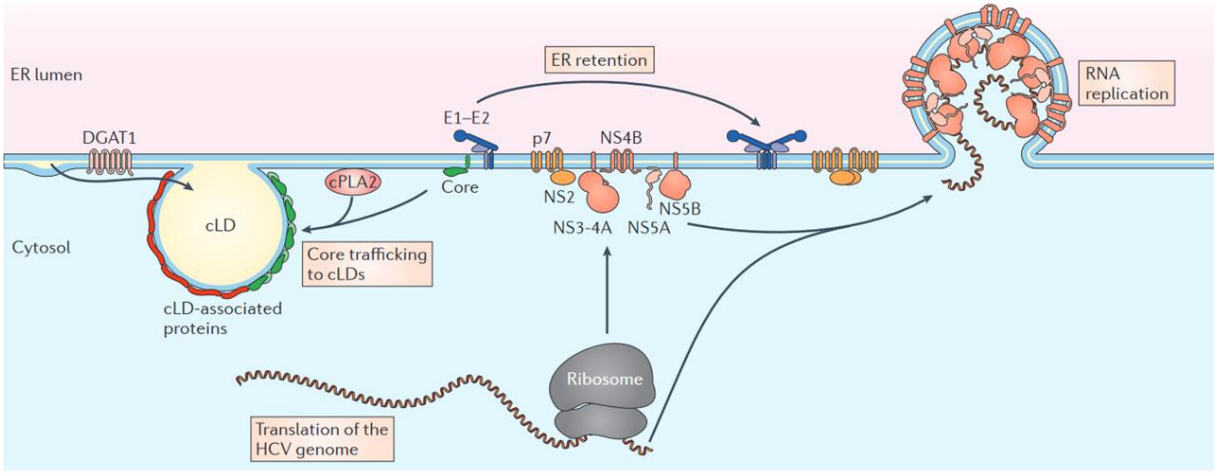

Figure 5 Translation and replication of HCV.
In the early step of the HCV life cycle, the viral gene is expressed into the polyprotein. The ten viral proteins, cleaved from the polyprotein, are recruited to the ER membrane. The RNA is replicated by the replicon complex, which consist of nonstructural proteins. The structural proteins E1 and E2 as well as p7 and NS2 remain in the ER membrane. Trafficking of core is mediated by the cytosolic phospholipase A2 (cPLA2) to cytosolic lipid droplets (cLD), which are formed by the diacylglycerol O-actetyltransferase 1 (DGAT1). Adapted from Lindenbach and Rice 2013.

1.1.10.3 Assembly and release

The complex process of assembly and release is the last step of the viral life cycle and tightly coupled to the host cell metabolism. Homodimerized core proteins are transported from the ER membrane to the cytosolic LDs, which is mediated by diacylglycerol acyltransferase-1 (DGAT1) and MAPK-regulated cytosolic phospholipase A2 (PLA2G4) (Barba et al. 1997; Boulant et al. 2006; Herker et al. 2010; Menzel et al. 2012). The accumulated core at the surface of LDs binds to viral RNA

and forms the nucleocapsid in close proximity to accumulated E1 and E2, which retain in the ER (Bartenschlager et al. 2011). Accumulation of the heterodimer E1E2 is mediated by NS2, p7 and SPCS1 (signalpeptidase complex unit 2) and crucial for the migration to the viral particle assembly site (Jirasko et al. 2010; Popescu et al. 2011; Ma et al. 2011; Stapleford and Lindenbach 2011; Gentzsch et al. 2013; Suzuki et al. 2013). By budding into the ER lumen, the capsid acquires the envelope, which consists of a bilayer membrane and E1-E2 complexes (Dubuisson and Cosset 2014). LVPs are formed through fusion or binding to lipoproteins and acquire their low buoyant density (Gastaminza et al. 2006; Gastaminza et al. 2008).

The release out of the host cell occurs on the classical secretory pathway through the Golgi (Counihan et al. 2011; Coller et al. 2012). Beside the classical way, LVPs release can also occur via the endosomal pathway independent of the very-low density lipoprotein (VLDL) pathway (Elgner et al. 2016b; Bayer et al. 2016). In studies with the multivesicular body (MVB) inhibitor U18666A and expression of dominant negative mutants of the ESCRT (endosomal sorting complexes required for transport) machinery, the release of LVPs was prevented and viral particles accumulated in the cytosol (Elgner et al. 2016b). Furthermore, fluorescent-tagged viral particles were colocalized with structural proteins on endosomal compartments (Bayer et al. 2016). HCV core was localized on endosomal structures and dominant negative mutants of Rab-GTPases, involved in the endosomal release, inhibited the release of viral particles (Lai et al. 2010; Coller et al. 2012; Mankouri et al. 2016). Moreover, HCV mediates the decrease of α-taxilin (Elgner et al. 2016a). α-taxilin interacts with free syntaxin4 (Stx4), a member of the t-SNARE complex, which interferes with the vesicular trafficking of MVBs (Nogami et al. 2003a; Nogami et al. 2003b). Through decrease of α-taxilin, HCV favors the SNARE complex formation and the release of viral particles. In line with this, in HCV-infected cells half-life of Stx4 is extended and an overexpression facilitates viral release, while silencing of Stx4 inhibits the release of HCV particles (Ren et al. 2017). In addition, knockdown of autophagy related genes like Beclin1 and Atg7 inhibit the release of HCV particles by the exosomal pathway (Shrivastava et al. 2016). Particle assembly and release are illustrated in figure 6.

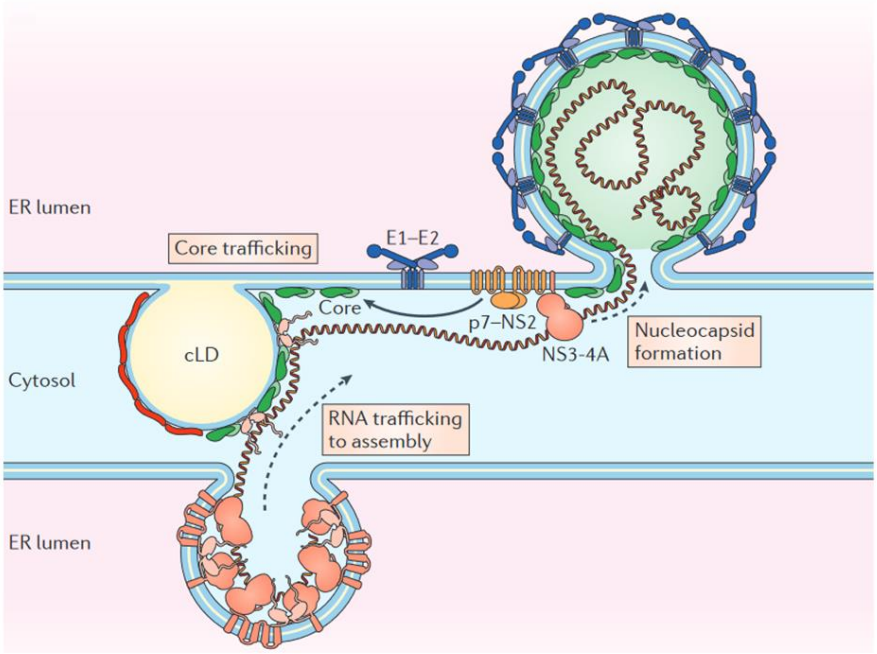

Figure 6 Particle assembly of HCV.
In the late step of the HCV life cycle, viral RNA is shuttled from the RC to cLDs where viral particles are assembled. Interaction of p7-NS2 and NS3-NS4A recruits core to the particle assembly site. The particles are assembled by recruitment of E1-E2 complexes and budding into the ER lumen. Adapted from Lindenbach and Rice 2013.

1.1.11 Viral particle

HCV particles represent lipoviral particles (LVP), therefore every step of the viral life cycle is related to the lipid metabolism (Popescu et al. 2014). The viral particle is surrounded by a host-derived lipid bilayer and the two envelope glycoproteins E1 and E2. The single-stranded RNA genome is encapsulated by the nucleocapsid, which consists of oligomerized core protein, shown in figure 7 (Lindenbach and Rice 2013).

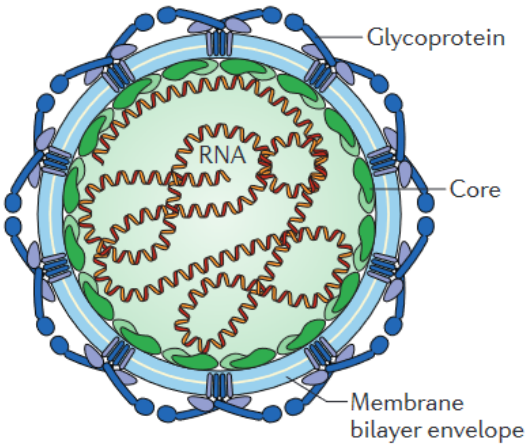

Figure 7 Model of the HCV particle.
The membrane bilayer contains the E1/E2 glycoprotein complex and surrounds the nucleocapsid containing core proteins and the viral RNA genome (Lindenbach and Rice 2013).

The formation of disulfide-linked complexes by E1E2 dimers during particle maturation contributes to the acid resistance of HCV particles (Vieyres et al. 2010; Tscherne et al. 2006). The putative fusion peptide of E1 is supposed to mediate the fusion between the viral and the endosomal membrane, which releases the viral capsid into the cytoplasm, while E2 interacts with several host cell receptors (Dubuisson and Cosset 2014).

Enveloped viral particles are 50-80 nm in diameter. Different populations of particles where observed, where enveloped particles are 60,7± 10,4 nm and non-enveloped particles smaller with 44,24 ± 4,74 nm (Gastaminza et al. 2010).

Up to now, HCV particles are not well characterized due to their low and heterogenous buoyant density when compared to other flaviviruses (André et al. 2002; Lindenbach et al. 2005). The mean density of *in vitro* viral particles is ~1,10 g/ml in which those with low density are more infectious (Gastaminza et al. 2010; Sabahi et al. 2010). Based on the production of lipoproteins in the host, viral particles from cultivated hepatoma cell lines differ from *in vivo* hepatocytes (Bartenschlager et al. 2011; Lindenbach and Rice 2013). LVPs from patient sera have a higher density (1,06-1,25 g/ml) and contain ApoA, ApoB, ApoC and ApoE, while density of cell-culture-derived particles (HCVcc) is lower and lack the ApoB protein (Merz et al. 2011). Regarding this, various cell lines were shown to produce infectious particles (HCVcc) depending on ApoE, but independent of ApoB (Lindenbach and Rice 2013). The lipid composition of viral particles resembles the very-low density lipoproteins (VLDL) and low density

lipoproteins, that's why HCV particles are called lipoviral particles (LVPs) (Merz et al. 2011; Lindenbach and Rice 2013).

Based on these findings and the pleomorphic structures in electron microscopy, two model systems were proposed, shown in figure 8. The first model is the two-particle model, where viral particles have a transient interaction with divisible serum lipoprotein particles (left panel in figure 8). And in the second model, the viral particle share the envelope with a lipoprotein as a hybrid-particle (right panel in figure 8) (Lindenbach and Rice 2013; Dubuisson and Cosset 2014). No matter which model reflects the real HCV particle, both describe a poor accessibility for specific antibodies against E1 and E2 glycoproteins as well as lipoproteins to be essential for HCV infection (Lindenbach and Rice 2013; Dubuisson and Cosset 2014).

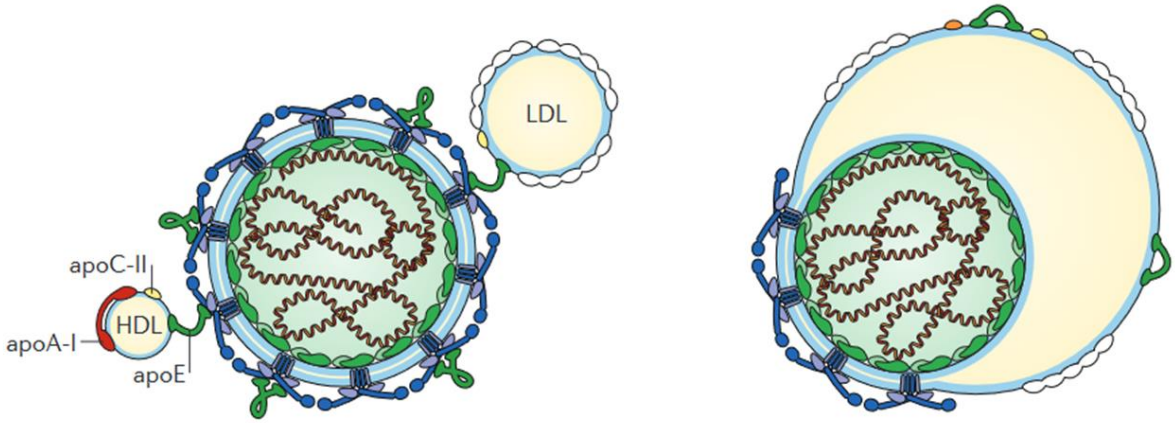

Figure 8 Two model systems for lipoviral particles.
(Left) The two-particle model, where the viral particle transiently interacts with lipoproteins. (Right) The hybrid-particle model, where the viral particle shares the envelope with a low or very-low density lipoprotein (Lindenbach and Rice 2013).

1.1.12 Model systems

The first attempts to develop a suitable model system failed, as HCV isolates from patients were not able to establish infections in cell culture. From the discovery in 1989 it took 8 years until HCV clones were able to infect chimpanzees, but failed to produce viral particles (Yanagi et al. 1997).

A breakthrough in *in vitro* studies was the establishment of a subgenomic replicon (genotype 1b), which allowed replication in the human hepatoma cell line Huh7 (Lohmann et al. 1999). The subgenomic replicon is a bicistronic RNA expresses an antibiotic resistance gene (e.g. neomycin) under control of the HCV IRES and containing the HCV nonstructural proteins NS3-NS5B under control of a second IRES. Antibiotic selection of RNA transfected Huh7 results in stable cell lines, which replicate

HCV at low levels. One clone of the stable cell line is named Huh9-13 (Lohmann et al. 1999). Due to a lack of the structural proteins core, E1 and E2, no infectious particles can be produced or released (Lohmann et al. 1999). Adaptive cell culture mutations in the HCV genome resulted in higher replication level *in vitro*, but production of viral particles was still prevented (Lohmann et al. 2001).

The replicon system enables studies on intracellular replication or antiviral effects, but not on viral entry. Hence, entry of HCV was studied with recombinant HCV-like particles or HCV E1E2 pseudoparticles (HCVpp) (Baumert et al. 1998; Bartosch et al. 2003).

Finally, in 2005, the isolation of a clone with genotype 2a from a Japanese patient with fulminant hepatitis (JFH1) was able to replicate in Huh7 cells and produce infectious viral particles (HCVcc) and enabled studies on the complete HCV life cycle in cell culture (Zhong et al. 2005; Lindenbach et al. 2005; Wakita et al. 2005).

Shortly afterwards, different chimeras were developed to study the life cycle. One chimera is a combination of the NS3-NS5B region of JFH1 and the core-NS2 region from another isolate of genotype 2a (J6) (Pietschmann et al. 2006). The chimera with a genotype breakpoint between NS2 and NS3 is called J6/JFH1 and a breakpoint within NS2 is named Jc1 (Lindenbach et al. 2006; Pietschmann et al. 2006; Catanese and Dorner 2015). The JFH1 region enables efficiently *in vitro* replication and infection, while the J6 region enhances production of viral particles.

Based on the Jc1 construct, a bicistronic luciferase reporter virus was developed in which enzyme activity is directly proportional to viral replication (Koutsoudakis et al. 2006). A NS5A-GFP variant of the Jc1 construct enables visualization of viral replicon complex, while an E1-mCherry variant can be used to monitor assembled viral particles (Moradpour et al. 2004; Bayer et al. 2016; Elgner et al. 2016b).

A replicon deficient virus was developed by a point mutation in the catalytic motif of the RNA-dependent RNA polymerase NS5B from GDD to GND, which can be used as a negative control (Wakita et al. 2005). The different HCV constructs are visualized in figure 9.

Up to now, human hepatoma cell line Huh7 and its derivates are the most permissive cells for HCV in cell culture. The Huh7.5 cell line is used the most for cell culture experiments. The cell line has a loss-of-function missense mutation in the retinoic acid-inducible gene I (RIG-I), therefore a higher production of infectious viral particles and spread *in vitro* (Blight et al. 2002; Sumpter et al. 2005). A limitation of Huh7.5 is the

lack of cell polarity, as it does not enable mimicking the compartmentalization of HCV receptors or the directionality of the secretory route like in polarized hepatocytes (Catanese and Dorner 2015). Furthermore, viral particles produced in Huh7 cells differ from the lipoviral particles in primary cell cultures or *in vivo* (Podevin et al. 2010). The natural host cell for HCV are primary human hepatocytes (PHH), which can be isolated from liver tissues after partial hepatectomy (Farquhar and McKeating 2008; Ploss et al. 2010; Zeisel et al. 2011). However, PHHs have several limitations like poor availability, high costs, loss of differentiation, short survival under cell culture conditions and poor permissiveness to HCV (Catanese and Dorner 2015).

Since the discovery of HCV, only human and chimpanzees have been found as natural hosts. Chimpanzees were the most important *in vivo* models for HCV study until HCV research on chimpanzees was banned in 2011 (Berggren et al. 2020). Additionally, difficulties in caring for chimpanzees, ethical aspects and the rare development of chronic liver disease after infection were leading to the development of an alternative and smaller animal model for HCV.

Transgenic mice were generated, which express full length HCV as well as specific HCV proteins and enable studies on HCV pathogenesis (Berggren et al. 2020). Specific lines of immunodeficient mice were developed to allow xenotransplantation of tissues or cell types, but the utility of this model is limited due to the lack of immune responses (Berggren et al. 2020). Genetically humanized mice expressing human HCV entry factors or knock-in of hepatocyte receptor genes were used for studies on the viral entry. However, replication and infectious particle production is low, highlighting the difficulty of developing an animal model, which does not natively sustain HCV infection (Berggren et al. 2020).

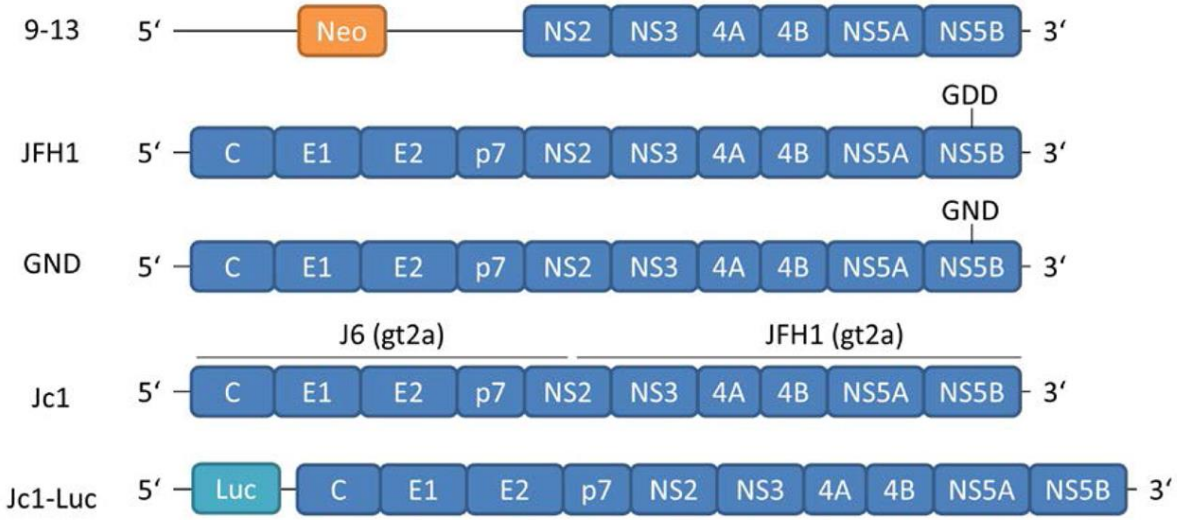

Figure 9 Schematic overview of different HCV constructs.
The bicistronic subgenomic replicon 9-13 consists of NS2-NS5B and a neomycin resistance gene. The JFH1 isolate (genotype 2a) and the replication deficient GND mutant (based on JFH1). The chimeric construct Jc1, which consists of structural proteins, p7 and parts from NS2 from the J6 isolate (genotype 2a) and the nonstructural proteins from the JFH1 isolate. The bicistonic reporter virus Jc1-Luc has an IRES-dependent luciferase prior to the Jc1 sequence. Adapted from Elgner 2016.

1.2 Protein degradation

In the changing environment of a living cell, proteins are involved in most of the processes and functions. The timely and proper activity of proteins is mainly regulated by their degradation (Cohen-Kaplan et al. 2016). The two major protein degradation systems in eukaryotic cells are the autophagy-lysosome and the ubiquitin-proteasome. Both are highly regulated and conserved and maintain the protein homeostasis and adaptation to environmental changes (Cohen-Kaplan et al. 2016). One degradation system is not independent from another as ubiquitination can target substrates for disposal via both pathways and activity is linked between the two systems (Korolchuk et al. 2010) . Hence, a crosstalk between autophagy and UPS is prevalent.

1.2.1 Autophagy

Macroautophagy (hereafter: autophagy; “self-eating”) is a highly regulated and conserved cellular quality control system, required to remove damaged proteins or organelles to maintain the cellular homeostasis (Mizushima et al. 2008). Autophagy

plays a role in programmed cell death, prevention of cancer, neurodegeneration, aging and innate and adaptive immunity (Eskelinen and Saftig 2009).
The catabolic process is induced as a response to nutrient starvation, elevated ROS levels or electrophiles, aggregation of damaged proteins and organelles or pathogen infection (Eskelinen and Saftig 2009).
Autophagy can be distinguished in macroautophagy for the disposal of organelles and proteins, microautophagy in which uptake of cargo occurs directly at the lysosome, and chaperone-mediated autophagy (CMA), where chaperones instead of membrane structures identify and sequester cargo (Parzych and Klionsky 2014). Pexophagy, mitophagy and ribophagy are subordinated to macroautophagy and describe the degradation of peroxisomes, mitochondira and ribosomes, respectively (Korolchuk et al. 2010). Furthermore, macro- and microautophagy can be divided in selective and nonselective degradation, while CMA is highly specific (Feng et al. 2014; Parzych and Klionsky 2014). The formation of autophagosomes is tightly regulated by more than 32 autophagy-related genes (Atg) (Kroemer et al. 2010). Moreover, the autophagosomal pathway is functionally connected to the endocytic pathway, which includes the release of exosomes. Both pathways have components of the ESCRT system, Rab GTPases and SNARE proteins in common (Medvedev et al. 2017a).

1.2.1.1 Initiation and nucleation

Under nutrient-rich conditions, the serine/threonine kinase mammalian target of rapamycin (mTOR kinase) represses autophagy through phosphorylation of the Unc-like kinase 1 and 2 (ULK1/2-complex) (Alers et al. 2012).
But during starvation or metabolic stress, the kinase activity of mTOR is inhibited by AMP-activated protein kinase (AMPK) and the ULK1/2 complex gets activated (Alers et al. 2012). The class III phosphatidylinositol-3-kinase (PI3K3) Vps34, Vps15, p150, Beclin-1 and Atg14 are generating phosphatidylinositol-3-phosphate (PI3P) (Carlsson and Simonsen 2015). PI3P recruits the effector DFCP1- (double FYVE-containing protein 1) and WIPI- (WD-repeat domain phosphoinositide interacting) proteins to promote formation of an ER-associated Ω.-structure, called omegasome. The omegasome is considered as intermediate structure for the formation of the isolation membrane (IM) (Axe et al. 2008; Itakura and Mizushima 2010).
Subsequently, the phagophore is formed, a crescent-shaped double membrane derived from the ER, Golgi-, mitochondrial or plasma membranes as well as

endosomes (Ploen and Hildt 2015; Yen et al. 2010; Reggiori et al. 2005; Ravikumar et al. 2010).

1.2.1.2 Elongation

By ubiquitin-like reactions, Atg12 is conjugated to Atg5, which require Atg7 (E1-like) and Atg10 (E2-like). The conjugate of Atg12-Atg5 associates with Atg16L to form the Atg12-Atg5-Atg16L complex (E3-like) (Ploen and Hildt 2015). The Atg4 cleaves the microtubule-associated protein 1 light chain (LC3) at its carboxy terminus. LC3 is being converted from its cytosolic form LC3-I to a phosphatidylethanolamine (PE)-conjugated form LC3-II by Atg7 and Atg3 (Fujita et al. 2008).
The two ubiquitin-like conjugation systems Atg5-Atg12-Atg16L and Atg4-Atg3-LC3 are required to elongate the phagophore and form the enclosed autophagosome (Mizushima et al. 2011).

1.2.1.3 Closure and maturation

The autophagy adaptor protein p62 (sequestosome 1/SQSTM1) is a cargo protein targeting other proteins that bind to p62 and interact with LC3. The interaction of p62 and LC3-II on the phagophore membrane leads to the engulfment of the substrates by closing autophagosome (Johansen and Lamark 2011).

1.2.1.4 Fusion

Enclosed and mature autophagosomes can fuse directly with lysosomes to form autolysosomes directed by the Rab7 GTPase protein (Mizushima et al. 2008). Another way is a Rab7-mediated fusion between late endosomes/multivesicular bodies (LE/MVBs) and autophagosomes to form amphisomes, followed by a fusion with lysosomes (Fader and Colombo 2009).
The autophagosomal SNARE (soluble N-ethylmaleimide sensitive factor attachment protein) syntaxin 17 (STX17) is also involved in the fusion of autophagosome-lysosome. Syntaxin17 is located on the membrane of enclosed autophagosomes and interacts with SNAP29 (synaptosomal-associated protein, 29 kDa) and SNARE VAMP8 (Vesicle-associated membrane protein 8) to promote the fusion with lysosomes (Itakura et al. 2012; Itakura and Mizushima 2013; Hegedűs et al. 2013).

1.2.1.5 Degradation

The integral membrane proteins, which include a vacuolar H^+ ATPase pump (v-ATPase) as well as ion channels, lipid transporters, receptors, solute carriers and

signaling complexes maintain the acidity in the lysosomal lumen (Mindell 2012). The low pH is an optimal condition for lysosomal hydrolases, which lyse the inner membrane and cleave the waste cargo (Mizushima et al. 2008). To protect the cell from lysosomal, degradative enzymes, the integrity of the limiting membrane has to be preserved during degradation by LIMP (lysosome integral membrane protein) and LAMP (lysosome-associated membrane proteins) (Schulze et al. 2009).

Degraded macromolecules are released back into the cytosol and serve as energy sources or are processed for recycling in order to de novo synthesis of molecules. A schematic model for autophagy is shown in figure 10.

The ubiquitin-binding protein p62 is degraded with the waste cargo during selective autophagy (Medvedev et al. 2017a). Therefore, LC3-II and p62 can be used to monitor autophagy, as decreased p62 levels and detection of LC3-II indicate enhanced autophagy, while accumulation of p62 and less LC3-II is a hint for insufficient autophagic flux (Kabeya et al. 2000).

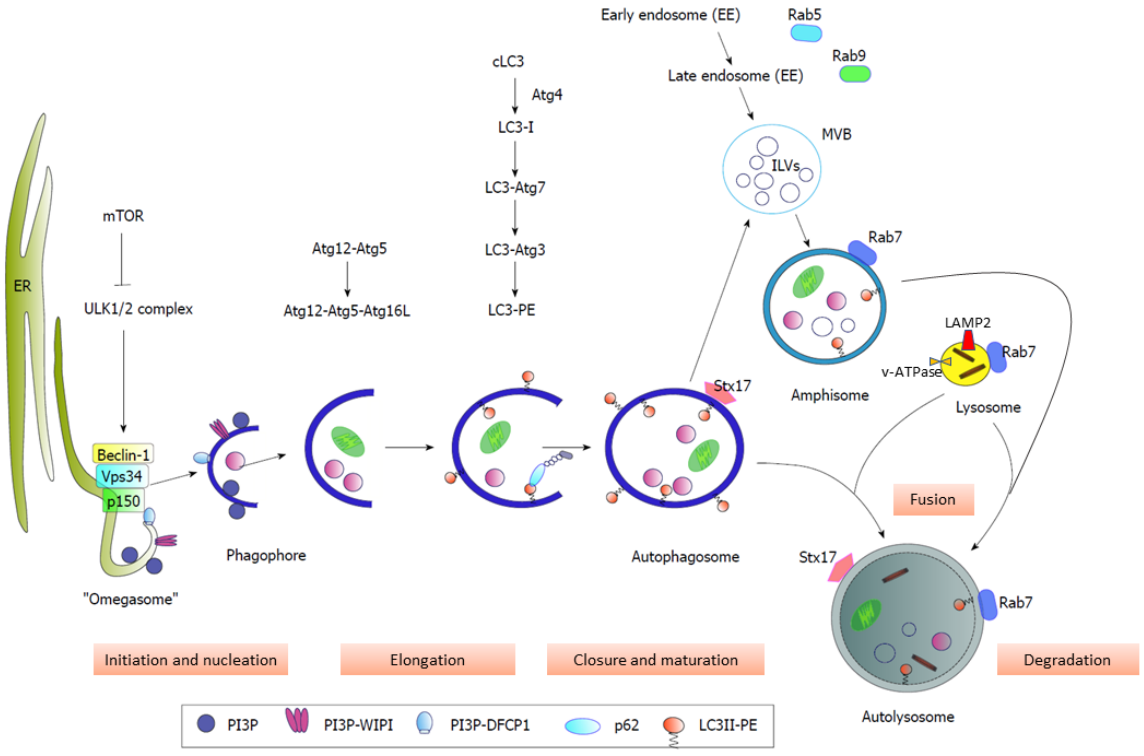

Figure 10 Schematic model for autophagy.
The mammalian target of rapamycin (mTOR) represses the ULK1/2 complex through phosphorylation. Inhibition of mTOR kinase results in the activation of autophagy. Beclin-1, Vps34 and p150 forms the PI3K complex, which induces with ULK1/2 complex a PI3P-enriched environment. Effector double FYVE-containing protein 1 (DFCP1) and WD-repeat domain phosphoinositide-interacting (WIPI) proteins are recruited by PI3P. The formation of an ER-associated Ω-structure (omegasome)

results in phagophore nucleation. For elongation, the Atg12-Atg5-Atg16L complex and PE-conjugated LC3II are required. Via p62 recycling material is recruited to the autophagosome and interaction with LC3II-PE leads to a closing of the phagophore. The mature autophagosomes can fuse directly with lysosomes to autolysosomes or fuse with late endosomes/multivesicular bodies to form amphisomes, followed by the fusion with lysosomes. Rab7 and the autophagosomal SNARE syntaxin 17 (STX17) are mediating the fusion between autophagosome and lysosome. Adapted and modified from Ploen and Hildt 2015.

1.2.1.6 Lysosome-associated membrane protein (LAMP)

The lysosome associated membrane proteins 1 and 2 (LAMP1 and LAMP2) are major protein components of the lysosomal membrane and involved in the autophagosomal process. LAMP1 and LAMP2 are type I transmembrane proteins with a luminal domain, a transmembrane domain and a C-terminal cytoplasmic tail (Eskelinen 2006). LAMP1 and LAMP2 have a 37% amino acid homology and a polypeptide backbone with the molecular mass of 40-45 kDa. However, after glycosylation the mass is approx. 120 kDa (Eskelinen 2006).

The glycoprotein LAMP2 is located in the membrane of lysosomes and late endosomes and required for maturation and structural integrity of the membrane (Eskelinen 2006). Furthermore, LAMP2 is involved in the transport of unfolded proteins and RNA to the lysosomes (Arias and Cuervo 2011; Fujiwara et al. 2013).

Due to alternative splicing, LAMP2 has three isoforms, LAMP2A, LAMP2B and LAMP2C. Deficiency of LAMP2 in human, mice and hepatocytes is characterized by autophagic vacuoles (Nishino et al. 2000; Nishino 2003; Tanaka et al. 2000; Eskelinen et al. 2002). A downregulation of LAMP2 showed a decreased expression of Stx17 and translocation to the autophagosomes. Thereby, LAMP2 is involved in the fusion of the autophagosomes with lysosomes (Hubert et al. 2016).

1.2.1.7 HCV and autophagy

Many RNA viruses are known to exploit autophagy for their life cycle. HCV depends on the autophagic machinery for its entry, replication, assembly and release. In several studies it was reported, that autophagy is crucial for the viral replication and for the release of viral particles (Tanida et al. 2009; Shrivastava et al. 2016; Ploen et al. 2013b; Ren et al. 2016). Additionally, activated autophagy represses the innate immune system and contributes to the survival of infected hepatocytes and HCV-associated pathogenesis of the liver (Ploen and Hildt 2015; Ríos-Ocampo et al. 2019).

There are two possible mechanisms discussed, how HCV mediates indirect induction of autophagy. The first is the elevated ROS level through HCV, which induces oxidative stress (Bartosch et al. 2009; Medvedev et al. 2017b). The second mechanism is the induced ER stress triggered by the concentration of E1E2 dimers in the ER membrane as well as the membranous web where HCV replication takes place (Choukhi et al. 1998; Asselah et al. 2010; Tardif et al. 2002; Sir et al. 2008; Ke and Chen 2011a, 2011b).

The high ROS levels, which are induced by HCV, cause the phosphorylation of serine-349 of the p62 protein and activate autophagy indirectly (Medvedev et al. 2017b). Phosphorylated p62 has a higher affinity to Keap1 and disrupt the interaction between Keap1 and Nrf2 (nuclear factor erythroid 2 (NF-E2) related factor 2), followed by the activation of Nrf2 and the targeting of Keap1 towards autophagosomal degradation (Medvedev et al. 2017b). Through activation of Nrf2 in a non-canonical way, Nrf2 is withdrawn from proteasomal degradation and translocate to the nucleus to bind to sMAF (small musculoaponeurotic fibrosarcoma) proteins on ARE (antioxidant response element) sequences for the expression of cytoprotective genes (Bender and Hildt 2019). However, HCV core triggers the delocalization of sMAF proteins from the nucleus to the replicon complex for interaction with NS3, which prevent binding of sMAF with Nfr2 on ARE sequences, resulting in further increased ROS levels and activation of autophagy (Carvajal-Yepes et al. 2011). Additionally, NS5A interferes with Nrf2-activation via a crosstalk with the MAPK signaling cascade. The phosphorylation of Nrf2 is triggered by the MAPK/ERK pathway, which results in the dissociation of Nrf2 to Keap1 and the activation of Nrf2 (Bender and Hildt 2019). Interaction of NS5A and PI4KA (phosphatidylinositol-4-kinase III α) is required for tethering the membranes between ER and mitochondria, resulting in mitochondrial fragmentation (Siu et al. 2016). Hence, the HCV structural protein core as well as the nonstructural protein NS5A are considered to be the main activators of ROS production (Bender and Hildt 2019).

At the ER the replicon complex of HCV is assembled, which induces ER stress and UPR. This leads to the activation of ATF6 (activating transcription factor 6), IRE1 (inositol-requiring enzyme 1), and the double-stranded RNA-activated PERK (protein kinase-like ER kinase) (Chu and Ou 2021). The core protein was also indicated to be sufficient for induction of ER stress, although it activated only ATF6 and PERK, but not IRE1 (Wang et al. 2014).

The interaction of NS4B with Rab5, Vps34 and Beclin-1 inhibits the mTOR kinase and can be considered as direct effect on autophagy activation (Li et al. 2010; Su et al. 2011). NS3/4A further triggers autophagy directly by interaction with human immunity-associated GTPase family M (IRGM) protein, Atg5, Atg10 and LC3 (Grégoire et al. 2011). NS5A induces the formation of LC3II-containing double membrane vesicles (DMVs) as well as multi membrane vesicles (MMVs), which mediate the fusion of autophagosomes and lysosomes (Ferraris et al. 2010; Romero-Brey et al. 2012; Romero-Brey and Bartenschlager 2014; Shrivastava et al. 2012). DMVs have a morphological similarity to autophagosomes, but can be distinguished in their size as DMVs have an average diameter of ~200 nm and autophagosomes 500-1000 nm (Tabata et al. 2020). Another difference is the duration of autophagosomal biogenesis. In nutrient-starved cells, the progression of phagophores to autophagosomes took ~10 min whereas that induced by HCV took ~30 min (Wang and Ou 2018). Autophagosomal factors like markers of early endosomes (EE), late endosomes (LE), lipid droplets (LDs), mitochondria and Rab proteins are localized in the membranous web (Romero-Brey et al. 2012).

A previous study on activation of autophagy in Huh7.5.1 KO cells showed that HCV induces Atg5- and Atg14-dependent selective autophagy in the early stage of infection to promote replication, while in the late stage of infection an Atg5-dependent impairment of the autophagic flux prevent autophagosomal degradation and favors viral propagation (Mori et al. 2018). To mediate the RNA replication, it was shown that HCV induces the localization of lipid rafts to autophagosomes (Kim et al. 2017). However, HCV-induced phagophores were shown to play a role for viral replication rather than autophagosomes (Fahmy and Labonté 2017; Wang et al. 2017). Conversely to favor viral replication, in several studies IFN-induced autophagy was shown to suppress HCV replication (Chan and Ou 2017).

Furthermore, it was reported that HCV downregulates the autophagosomal SNARE protein syntaxin 17 to prevent formation of autolysosomes and to favor the release of viral particles (Ren et al. 2016). Thereby, HCV affects an equilibrium between release and intracellular degradation of viral particles.

Moreover, beside the VLDL pathway LVPs are released through the endosomal route via exosomes (Elgner et al. 2016b). This reflects a further association of HCV with autophagy, as the biogenesis of autophagosomal membranes is closely connected to endosomes and components involved in endosomal trafficking. Despite many studies

on autophagy-associated viral replication, morphogenesis and release the crosstalk between the HCV life cycle and autophagy is not fully understood. Whether further HCV life-cycle processes can be associated with autophagy still needs to be elucidated. Hereof, to examine the autophagy-associated fate of excess nonstructural proteins will not only clarify a non-existing protein accumulation in the host cell, but could also reflect another host related-factor to restrict viral replication via the autophagic flux.

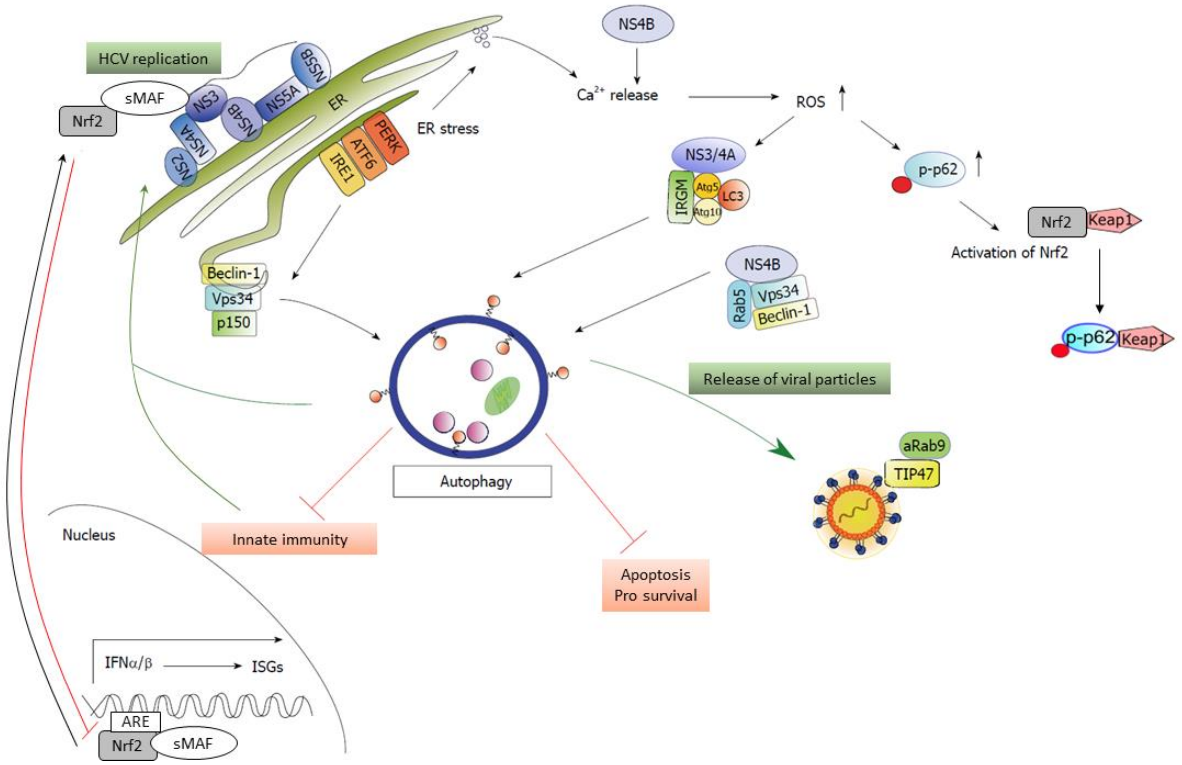

Figure 11 Schematic model of the crosstalk between autophagy and HCV.
The HCV replication complex assembles at the ER, which induces ER stress and unfolded protein response (UPR). UPR activates the signaling pathways ATF6, IRE1 and PERK followed by autophagy. NS4B interferes with Ca^{2+} homeostasis, that results in elevated reactive oxygen species (ROS) and activation of the IRE1 and ATF6 pathway, which triggers UPR. Due to elevated ROS levels p62 is phosphorylated and activates Nrf2. sMAF translocate from the nucleus to NS3 and interacts with Nrf2 resulting in the prevented binding to ARE sequence for cytoprotective genes. Autophagy is stimulated by the complex of Rab5, Vps34 and Beclin-1 with NS4B. The human immunity-associated GTPase family M (IRGM) protein interacts with NS3/4A and Atg5, Atg10 and LC3, which further triggers autophagy. Activated autophagy favors HCV replication and viral particle release. Interaction between TIP47 and Rab9 (aRab9) on the particles is crucial. Based on HCV-induced autophagy, the inhibition of apoptosis favors cell survival and the innate immunity is impaired. Adapted and modified from Ploen and Hildt 2015.

1.2.2 Proteasome system

1.2.2.1 Ubiquitin-dependent degradation

The ubiquitin-proteasome system (UPS) acts in a highly regulated manner to degrade ubiquitinated substrates. The degradation of ubiquitinated molecules can occur through the autophagic pathway or the UPS. Three types of enzymes are involved in the ubiquitination. E1 is the ubiquitin-activating enzyme and two are known in mammals. E2 is a ubiquitin-carrier protein, also called ubiquitin-conjugating enzyme, around 40 are thought to be encoded in the mammalian genome. And E3 is a ubiquitin ligase, from which the cell possesses several hundred (Korolchuk et al. 2010; Cohen-Kaplan et al. 2016).

The enzyme E1 induces the ATP-dependent activation of ubiquitin (Ub) at its C-terminal glycine residue. Ubiquitin is transferred to the ubiquitin-carrier protein E2. Subsequently, E2 forms a complex with an E3 ligase, which specifically binds to a substrate and performs its ubiquitination. Ubiquitin is either transferred directly from E2 to the lysine (K) residue of the substrate or is conjugated to an internal cysteine residue of the E3 ligase. The lysine residue of ubiquitin enables an attachment of additional molecules to create a ubiquitin chain to mark the substrate for proteasomal degradation (Ciechanover 1994; Finley 2009). Ub can be attached to a substrate as monoubiquitination, multiple monoubiquitination or polyubiquitination (Cohen-Kaplan et al. 2016). Moreover, Ub chains can be elongated by E4, an additional type of ligase, which is termed as Ub-chain elongation factor (Koegl et al. 1999).

The length of the Ub chain and the lysine residue, through which the chain is linked to, determine the fate of the substrate (Pickart 2000). First it was reported, that short-lived proteins are marked selectively by K48-linked Ub chains. However, all chain types are probably involved in the degradation via proteasome (Cohen-Kaplan et al. 2016). As another degradation signal for UPS, K63 Ub chains and monoubiquitination can also target substrates to selective autophagy for degradation (Olzmann et al. 2007; Tan et al. 2008; Wooten et al. 2008; Kim et al. 2008).

The barrel-shaped 26S proteasome is composed of a 20S core particle (CP), which is coated by one or two 19S regulatory particles (RP) that recognize polyubiquitinated substrates The deubiquitinating enzymes (DUB) mediate the removal of the Ub chain on the substrate followed by an unfolding and transfer into the proteolytic chamber of the 20S complex (Gallastegui and Groll 2010; Livneh et al. 2016).

Substrates are degraded into oligopeptides by a combination of trypsin-like, chymotrypsin-like and peptidyl-glutamyl peptide-hydrolyzing activities and are released into the cytoplasm or nucleoplasm (Heinemeyer et al. 1997; Orlowski 1990; Rivett 1989). The UPS commonly mediates the degradation of short-lived proteins like regulatory proteins, while long-loved proteins are preferentially degraded through the autophagic pathway. However, several studies reported that, *vice versa*, a degradation of long-lived proteins can occur by the proteasome and short-lived by autophagy (Cohen-Kaplan et al. 2016).

1.2.2.2 Ubiquitin-independent degradation

Beside polyubiquitinated proteins a ubiquitin-independent proteolysis of the proteasome was described (Orlowski and Wilk 2003). Several Ub-independent substrates contain a sequence, which mediates their proteasomal targeting (‘degron’), like IκBα, p35 and Nkx3.1 (Fortmann et al. 2015; Takasugi et al. 2016; Rao et al. 2012). Moreover, a high structural flexibility and oxidation of proteins contribute to Ub-independent degradation (Cohen-Kaplan et al. 2016).

1.2.2.3 HCV and UPS

HCV-induced elevated intracellular reactive oxygen species (ROS) trigger ER stress followed by induction of unfolded protein response (UPR) and phosphorylation of p62. In uninfected cells, phosphorylated p62 binds to Kelch-like ECH-associated protein 1 (Keap1) and activate Nrf2 through its dissociation from Keap1. Nrf2 translocate from the cytosol to the nucleus, where it binds to ARE sequences together with sMAF proteins to activate cytoprotective genes (Kensler et al. 2007; Kensler and Wakabayashi 2010; Ichimura et al. 2013). During HCV infection, Nrf2 and sMAF translocate to the replicon complex and bind to NS3, while expression of cytoprotective genes is prevented. In addition, the activity of the constitutive proteasome is decreased, as the expression of the catalytic active subunit of the proteasome (PSMB5) depends on Nrf2-ARE signaling (Kwak and Kensler 2006; Carvajal-Yepes et al. 2011).

Furthermore, the proteasome activator PA28γ interacts with core and is involved in viral particle production (Moriishi et al. 2010; Kwak et al. 2017).Knockdown of PA28γ results in enhanced ubiquitination of core and impaired particle production with no effect on RNA replication (Moriishi et al. 2010). Conversely, the knockdown of E3 ubiquitin ligase E6AP reduced ubiquitination of core and enhanced virus production

(Moriishi et al. 2010). Through interaction with NS5B, the retinoblastoma tumor-suppressor protein (pRb) and the tumor suppressor NORE1A are targeted to proteasomal degradation, which promotes cell proliferation (Munakata et al. 2005; Munakata et al. 2007; Arora et al. 2017). Another interaction with NS5B was shown for the E3 ligase TRIM26, which mediates a K27-linked ubiquitination of NS5B at residue K51, and thus promotes the interaction between NS5B and NS5A, that is crucial for the assembly of the RC (Liang et al. 2021). To favor its replication, HCV mediates the ubiquitination and proteasomal degradation of suppressor of cytokine signaling 3 (SOCS3) (Shao et al. 2010).

In *in vivo* studies HCV was reported to affect the antigen process, as NS3 mutations impair the induction of HCV-specific $CD8^+$ cells by the immunoproteasome. Moreover, the low-molecular-mass protein 7 (LMP7) is involved in peptidase activities in the immunoproteasome and downregulated through binding to NS3, which interferes with the viral antigen processing for presentation by MHC class I molecules (Shoji 2012). The IFN-γ-induced immunoproteasomes influence the outcome of $CD8^+$ cytotoxic T lymphocyte responses. It was reported, that in HCV-infected cells the induction of the immunoproteasome is suppressed in a protein kinase R(PKR)-dependent manner to evade the immune responses (Oh et al. 2016). Thus, HCV exploit the proteasome to target host cell proteins for degradation as well as the immunoproteasome to regulate innate and adaptive immunity for the facilitation of the viral life cycle.

2 Aim of this study

As the hepatitis C virus possesses a single ORF, one polyprotein is synthesized and processed into structural and nonstructural proteins. Hence, there are equal amounts of viral structural and nonstructural proteins in the cell. Structural proteins are part of the viral particle, in which some are released from the host cell and others are lysosomal degraded, while the fate of the nonstructural proteins is unclear. Since accumulation of viral nonstructural proteins was assumed but not observed yet, excess nonstructural proteins must be degraded. Despite the preliminary data, the cellular degradation pathways for the turnover of the remaining nonstructural proteins of HCV are still not fully clarified. Furthermore, HCV is known to exploit autophagy in a great extent to favor its replication and release.

This project aimed to investigate the fate of the HCV nonstructural proteins with a major focus on autophagosomal-lysosomal pathway. For this purpose, *de novo* protein translation was inhibited and autophagy modulated to determine the autolysosomal turnover of NS3, NS4B, NS5A as well as NS5B in comparison to proteasomal degradation.

The impact of the autophagosome marker LC3 as well as the lysosomal marker LAMP2 on the turnover of NS3 and NS5A was determined. A closer look on the subcellular localization of NS3, NS4B, NS5A and NS5B in cell fractions further elucidated the contribution of autophagy on the turnover of nonstructural proteins.

3 Materials

3.1 Cells

3.1.1 Prokaryotic cells

Strain	Genotype	Source
E. coli DH5α	F- endA1 glnV44 thi-1 recA1 relA1 gyrA96 deoR nupG purB20 φ80dlacZΔM15Δ(lacZYA-argF)U169, hsdR17($r_K^-m_K^+$), λ^-	Invitrogen, Karlsruhe, DE
E. coli TOP10	F- mcrA Δ(mrr-hsdRMS-mcrBC) φ80lacZΔM15 ΔlacX74 nupG recA1 araD139 Δ(ara-leu)7697 galE15 galK16 rpsL(Str^R) endA1 λ^-	Invitrogen, Karlsruhe, DE

3.1.2 Eukaryotic cells

Strain	**Description**	**Source**
Huh7.5	Human hepatoma cell line derived from Huh7 cells	Blight et al. 2002
Huh7.5-LC3 (clone 6 and clone 18)	Huh7.5 cells stably overexpressing LC3 under selection with 750 µg/ml G418	This work
Huh7.5-LAMP2 KO (clone 3 and clone 13)	Stable LAMP2 knockout Huh7.5 cells, generated via CRISPR/Cas9 with sgRNA1-LAMP2	This work
Huh7.5-off target (clone 4 and clone 10)	Huh7.5 cells transfected with unspecific sgRNA served as control for CRISPR/Cas9 cells	This work
Huh9-13 (Huh7 I377/NS3-3‘/wt/9-13)	Huh7 cells stably producing the HCV subgenomic replicon I377/NS3-3’ under selection with 1 mg/ml Neomycin (Geneticin, G418)	Lohmann et al. 1999

3.2 Plasmids

Plasmid	Description	Source
pcDNA3.1+/C-(K)DYK MAP1LC3B cDNA ORF clone	LC3 expression construct with a C-terminal DYKDDDDK tag	Genscript (CloneID OHu18146)
pFK-Jc1	Chimera of the HCV genotype 2a isolates JFH1 and J6 producing higher titers of infectious particles	Pietschmann et al. 2006
pSpCas9(BB)-2A-Puro (PX459) V2.0	CRISPR/Cas9 cloning plasmid	Addgene # 62988 (Ran et al. 2013)
pUC18	Empty expression vector, served as control	Invirtogen, Karlsruhe, DE
PX459_LAMP2(1)	CRISPR/Cas9 plasmid, which codes for sgRNA1-LAMP2	Matthias Dusemund (2019)
PX459_off target	CRISPR/Cas9 plasmid, which codes for unspecific sgRNA	Dr. Fabian Elgner

3.3 Oligonucleotides

3.3.1 RT-qPCR-Primer

Description	Sequence (5' → 3')
JFH1-fwd (R6-260-R19)	ATG ACC ACA AGG CCT TTC G
JFH1-rev (R6-130-146)	CGG GAG AGC CAT AGT GG

3.3.2 Cloning primers

Description	Sequence (5' → 3')
crRNA_off-target_fwd	CAC CGC ACT ACC AGA GCT AAC TCA

crRNA_off-target_rev	AAA CTG AGT TAG CTC TGG TAG TGC
LAMP2_sgRNA1_fwd	CAC CGC CCA ATA CAA CTC ACT CCA C
LAMP2_sgRNA1_rev	AAA CGT GGA GTG AGT TGT ATT GGG C

3.3.3 Sequencing primers

Description	Sequence (5' → 3')
LAMP2_sgRNA1_fwd	GCG TAC AGG AGT GGC ACA GC
LAMP2_sgRNA1_rev	CCA TTG CAC AGA CTC TGA GGG ATG

3.3.4 siRNA

siRNA	Target	Manufacturer
LAMP2 siRNA, sc-29390 (10 µM stock solution in RNase-free H_2O)	LAMP2	Santa Cruz Biotechnology, Inc., USA
Scrambled RNA, sc-37007 (10 µM stock solution in RNase-free H_2O)	Unspecific control	Santa Cruz Biotechnology, Inc., USA

3.4 Antibodies

3.4.1 Primary antibodies

Antibody	Species, clonality	Dilution (WB/IF)	Manufacturer
Anti-EEA1	Rabbit, monoclonal	1:1000 / -	Thermo Fisher Scientific, Schwerte, DE
Anti-GAPDH	Mouse, monoclonal	1:10.000 / -	Santa Cruz Biotechnology, Inc., USA
Anti-HCV-NS3	Mouse, monoclonal	1:1000 / 1:200	Abcam, Cambridge, UK

Anti-HCV-NS3	Mouse, monoclonal	1:500 / 1:50	ViroStat, Inc., USA
Anti-HCV-NS4B	Mouse, monoclonal	1:500 / 1:100	ViroStat, Inc., USA
Anti-HCV-NS5A	Rabbit, polyclonal	1:1000 / 1:200	Bürckstümmer et al. 2006
Anti-HCV-NS5B	Rabbit, polyclonal	1:500 / 1:100	Abcam, Cambridge, UK
Anti-LAMP2	Goat, polyclonal	- / 1:200	R&D Systems, Inc., USA
Anti-LAMP2	Rabbit, monoclonal	1:200 / -	Abcam, Cambridge, UK
Anti-LC3	Mouse, monoclonal	- / 1:100	Genetex, Inc., USA
Anti-LC3	Rabbit, polyclonal	1:1000 / 1:100	MBL, Inc., USA
Anti-p62	Guinea pig, polyclonal	1:1000 / 1:200	Progen Biotechnik, Heidelberg, DE
Anti-PSMB4	Goat, polyclonal	- / 1:100	Abcam, Cambridge, UK
Anti-PSMB5	Rabbit, polyclonal	1:500 / -	Abcam, Cambridge, UK
Anti-Rab7a	Goat, polyclonal	1:1000 / -	MyBioScource, Inc., USA
Anti-β-Actin	Mouse, monoclonal	1:10.000 / -	Sigma-Aldrich, USA

3.4.2 Secondary antibodies

Antibody	**Species, clonality**	**Dilution WB/IF**	**Manufacturer**
Anti-goat IgG Cy3	Donkey, polyclonal	- / 1:400	Jackson ImmunoResearch Europe Ltd., Suffolk, UK

Anti-goat IRDye680RD	Donkey, polyclonal	1:10.000 / -	LI-COR Biosciences GmbH, Bad Homburg, DE
Anti-guinea pig IRDye800CW	Donkey, polyclonal	1:10.000 / -	LI-COR Biosciences GmbH, Bad Homburg, DE
Anti-mouse IgG-Alexa488	Donkey, polyclonal	- / 1:1000	Thermo Fisher Scientific, Schwerte, DE
Anti-mouse IgG-Cy3	Donkey, polyclonal	- / 1:400	Jackson ImmunoResearch Europe Ltd., Suffolk, UK
Anti-mouse IRDye680RD	Donkey, polyclonal	1:10.000 / -	LI-COR Biosciences GmbH, Bad Homburg, DE
Anti-mouse IRDye800CW	Donkey, polyclonal	1:10.000 / -	LI-COR Biosciences GmbH, Bad Homburg, DE
Anti-rabbit IgG Cy3	Donkey, polyclonal	- / 1:400	Jackson ImmunoResearch Europe Ltd., Suffolk, UK
Anti-rabbit IgG-Alexa488	Donkey, polyclonal	- / 1:1000	Thermo Fisher Scientific, Schwerte, DE
Anti-rabbit IRDye680RD	Donkey, polyclonal	1:10.000 / -	LI-COR Biosciences GmbH, Bad Homburg, DE
Anti-rabbit IRDye800CW	Donkey, polyclonal	1:10.000 / -	LI-COR Biosciences GmbH, Bad Homburg, DE

3.5 Fluorescent dye

Dye	Dilution IF	Manufacturer
DAPI (0.1 mg/ml stock in PBS)	1:300	Carl-Roth, Karlsruhe, DE

3.6 Molecular weight markers

3.6.1 DNA markers

Description	Manufacturer
Gene Ruler^{TM} 1 kB Plus DNA ladder	Thermo Fisher Scientific, Schwerte, DE

3.6.2 Protein markers

Description	Manufacturer
PageRuler^{TM} Prestained Protein Ladder	Thermo Fisher Scientific, Schwerte, DE
PageRuler^{TM} Plus Prestained Protein Ladder	Thermo Fisher Scientific, Schwerte, DE

3.7 Enzymes

Enzyme	Manufacturer
AseI	NEB, Frankfurt am Main, DE
RevertAid H Minus Reverse Transcriptase	Thermo Fisher Scientific, Schwerte, DE
RQ1 RNase-Free DNase	Promega, Fitchburg, USA
T7 RNA-Polymerase	Biozym, Hessisch Oldendorf, DE

3.8 Inhibitors

Inhibitor	Target	Manufacturer
Protease inhibitors		
Aprotinin	Serine protease	Sigma.Aldrich, Seelze, DE
Leupeptin	Serine and cysteine protease	Sigma.Aldrich, Seelze, DE
Pepstatin	Acid-, aspartatic proteases	Sigma.Aldrich, Seelze. DE
PMSF	Serine protease	Carl-Roth, Karlsruhe, DE
Phosphatase inhibitor		
Phosphatase inhibitor cocktail	Phosphatases	Sigma.Aldrich, Seelze. DE
RNase inhibitors		
RiboLock RNase Inhibitor	RNase	Thermo Fisher Scientific, Schwerte, DE
ScriptGuard RNase Inhibitor	RNase	Biozym, Hessisch Oldendorf, DE
Protein synthesis inhibitor		
Cycloheximide (CHX)	The translocation step in protein synthesis	Sigma.Aldrich, Seelze. DE
Modulators of Autophagy		
Bafilomycin-A1 (BFLA)	Vacuolar H^+-ATPase	Sigma.Aldrich, Seelze. DE
LY-294002	Phosphatidylinositol 3-kinase (PI3K)	Selleckchem, USA
Rapamycin	mTOR	Selleckchem, USA
Wortmannin	Phosphatidylinositol 3-kinase (PI3K)	Selleckchem, USA
Modulators of UPS		

Bortezomib	20S proteasome	Selleckchem, USA
PD169316	p38 mitogen-activated protein kinases (MAPK)	Sigma.Aldrich, Seelze. DE

3.9 Reagents for cell culture

Reagent	Manufacturer
DMEM (Dulbecco's Modified Eagles Medium) 4.5 g/l glucose	Lonza, Basel, CH
PBS without Ca^{2+} and Mg^{2+}	Paul-Ehrlich-Institut, Langen, DE
FCS (fetal calf serum)	Biochrom GmbH, Berlin, DE
L-glutamine	Biochrom GmbH, Berlin, DE
G418 (Geneticin)	Calbiochem, Darmstadt, DE
Penicillin/Streptomycin	Paul-Ehrlich-Institut, Langen, DE
Puromycin	Sigma.Aldrich, Seelze. DE
Trypsin/EDTA	Paul-Ehrlich-Institut, Langen, DE

3.10 Chemicals

Chemicals	Manufacturer
10 mM dNTPs	Thermo Fisher Scientific, Schwerte, DE
5x Reaction buffer for RT	Thermo Fisher Scientific, Schwerte, DE
10x T7-Scribe transcription buffer	Biozym, Hessisch Oldendorf, DE
6-Aminohexanoic acid	Carl-Roth, Karlsruhe, DE
Acetone	Carl-Roth, Karlsruhe, DE
Agarose	Genaxxon, Biberach, DE
Ampicillin	Carl-Roth-Karlsruhe, DE
APS (Ammoniumperoxodisulfate)	Carl-Roth, Karlsruhe, DE
BSA (Bovine serum albumin)	PAA, Linz, AT
Bradford reagent	Sigma-Aldrich, Seelze, DE
Bromphenol blue	Merck, Darmstadt, DE

Chloroform	Carl-Roth, Karlsruhe, DE
Chloroform/Isoamylalcohol, Roti-C/I	Carl-Roth, Karlsruhe, DE
DMSO (Dimetyl sulfoxide)	Genaxxon, Ulm, DE
EDTA (Ethylendiaminotetraacetic acid)	Paul-Ehrlich-Institut, Langen, DE
Ethanol	Carl-Roth, Karlsruhe, DE
Ethidiumbromide	AppliChem, Darmstadt, DE
Formaldehyde 37.5%	Carl-Roth, Karlsruhe, DE
Isopropanol	Carl-Roth, Karlsruhe, DE
Maxima Probe SYBR Green qPCR Master Mix	Thermo Fisher Scientific, Schwerte, DE
Methanol	Carl-Roth, Karlsruhe, DE
Mowiol	Sigma-Aldrich, Seelze, DE
NEBuffer 3.1	NEB, Frankfurt am Main, DE
N-TER peptide	Sigma-Aldrich, Seelze, DE
NTP-Mix	Thermo Fisher Scientific, Schwerte, DE
Optiprep (Iodixanol)	Progen Biotechnik, Heidelberg, DE
Phenol	Applichem, Darmstadt, DE
Polyethylenimine (PEI)	Polysciences, Eppelheim, DE
Random Hexamer Primer	Thermo Fisher Scientific, Schwerte, DE
Roti®-Block	Carl-Roth, Karlsruhe, DE
Roti-Phenol/Chloroform/Isoamylalcohol	Carl-Roth, Karlsruhe, DE
Rotiphorese Gel 40 (Acrylamide/bisacrylamide)	Carl-Roth, Karlsruhe, DE
RQ1 RNase-Free DNase 10x Reaction Buffer	Promega, Fitchburg, USA
RQ1 DNase stop solution	Promega, Fitchburg, USA
Sodium acetate	Paul-Ehrlich-Institut, Langen, DE
Sodium desoxycholat	Carl-Roth, Karlsruhe, DE
SDS 10%	Paul-Ehrlich-Institut, Langen, DE
siRNA Dilution Buffer	Sigma-Aldrich, Seelze, DE
Sucrose	Carl-Roth, Karlsruhe, DE

TEMED	Carl-Roth, Karlsruhe, DE
Trichlormethan/Chloroform	Carl-Roth, Karlsruhe, DE
Tris	Paul-Ehrlich-Institut, Langen, DE
Tris-HCl	Paul-Ehrlich-Institut, Langen, DE
Triton-X-100	Fluka, Deisenhofen, DE
Tween20	Genaxxon, Ulm, DE
β-Mercaptoethanol	Sigma-Aldrich, Seelze, DE

3.11 Kits

Kit	Manufacturer
Cellscript T7-Scribe™ Standard RNA IVT Kit	Biozym, Hessisch Oldendorf, DE
DNeasy Blood & Tissue Kit	Qiagen, Hilden, DE
Lysosome Isolation Kit	Sigma-Aldrich, Seelze, DE
Maxima™ SYBR Green qPCR Kit	Thermo Fisher Scientific, Schwerte, DE
N-TER™ Nanoparticle siRNA Transfection System	Sigma-Aldrich, Seelze, DE
QIAamp Viral RNA Mini Kit	Qiagen, Hilden, DE
Qiagen Plasmid Maxi Kit	Qiagen, Hilden, DE

3.12 Buffers and solutions

Buffer	Composition
Anode buffer I	20% Ethanol (v/v) 300 mM Tris
Anode buffer II	20% Ethanol (v/v) 25 mM Tris
Cathode buffer	20% Ethanol (v/v) 40 mM 6-Aminohexanoic acid
DNA loading dye (6x)	10 mM Tris HCl pH 7.6 0.03% Bromphenol blue 0.03% Xylene Cyanol

	60% Glycerol 60 mM EDTA
Lysogeny broth medium (LB)	1% Trypton (w/v) 0.5% Yeast extract (w/v) 1% Sodium chloride (w/v)
Mounting medium (Mowiol)	10% Mowiol (w/v) 25% Glycerol (w/v) 2.5% DABCO 100 mM Tris/HCl pH 8.5
Phosphate buffered saline (PBS) 10x	80.0 g NaCl 2.0 g KCl 14.4 g Na_2HPO_4 2.4 g KH_2PO_4 ad 1 L ddH_2O
Radioimmunoprecipitation assay buffer (RIPA)	50 mM Tris-HCl pH 7.2 150 mM NaCl 0.1% SDS (w/v) 1% Sodium desoxycholat (w/v) 1% Triton X-100
SDS loading buffer (4x)	4% SDS (w/v) 125 mM Tris-HCl pH 6.8 10% Glycerol (v/v) 10% ß-Mercaptoethanol (v/v) 0.02% Bromphenol blue (w/v)
SDS running buffer (10x)	0.25 M Tris 2 M Glycin 1% SDS (w/v) pH 8.3
Separation gel buffer	1.5 M Tris-HCl 0.4% SDS (w/v) pH 8.8
Stacking gel buffer	0.5 M Tris 0.4% SDS (w/v) pH 6.7

TAE-Puffer (50x)	2 M Tris 1 M NaAc 50 mM EDTA pH 8.0
TBS-T (10x)	200 mM Tris-HCl pH 7.8 1.5 M NaCl 0.5% Tween

3.13 Devices

3.13.1 Electrophoresis

System	Manufacturer
Horizontal electrophoresis system HE33	GE Healthcare Europe GmbH, Freiburg, DE
Mighty small multiple gel caster SE200	GE Healthcare Europe GmbH, Freiburg, DE
Mighty small II vertical electrophoresis system SE 250	GE Healthcare Europe GmbH, Freiburg; DE
Standard power pack P25	Biometra GmbH, Göttingen, DE
TE77 ECL semi dry transfer unit	GE Healthcare Europe GmbH, Freiburg, DE

3.13.2 Microscopy

Mircoscope	Manufacturer
Axiovert 40C	Carl Zeiss AG, Jena, DE
Confocal Laser Scanning Microscope 510 meta	Carl Zeiss AG, Jena, DE
Confocal Laser Scanning Microscope TCS SP8	Leica Microsystems, Wetzlar, DE

3.13.3 Imaging

Imaging system	Manufacturer
INTAS-Imaging System	Intas, Göttingen, DE
Odyssey CLx Imaging System	LI-COR, Bad Homburg, DE

3.13.4 PCR-Cycler

PCR Cycler	Manufacturer
LightCycler® 480 Instrument II	Roche, Mannheim, DE

3.13.5 Centrifuges

Centrifuge	Manufacturer
Heraeus Cyrofuge 5500i	Thermo Fisher Scientific, Schwerte, DE
Heraeus Fresco 17 centrifuge	Thermo Fisher Scientific, Schwerte, DE
Heraeus Fresco 21 centrifuge	Thermo Fisher Scientific, Schwerte, DE
Heraeus Megafuge 16R	Thermo Fisher Scientific, Schwerte, DE
Heraeus Multifuge 1S-R	Thermo Fisher Scientific, Schwerte, DE
Heraeus Multifuge X3 FR	Thermo Fisher Scientific, Schwerte, DE
Heraeus Sepatech Cryofuge 8500	Thermo Fisher Scientific, Schwerte, DE
Microcentrifuge	Carl-Roth, Karlsruhe, DE
Optima L-70 Ultracentrifuge	Beckman Coulter, Krefeld, DE
Optima XPN-80 Ultracentrifuge	Beckman Coulter, Krefeld, DE

3.13.6 Other devices

Device	Manufacturer
Accujet® pro	Brand GmbH & Co. KG, Wertheim, DE
Electroporator Gene Pulser MXcell™	BioRad, USA
Incubator BBD 6220	Heraeus, Osterode, DE
Incubator Innova 44	New Brunswick Scientific, Enfield, USA
Infinite M1000	Tecan, Männedorf, CH
NanoDrop™ One C	Thermo Fisher Scientific, Schwerte, DE
Neubauer chamber	Marienfeld, Lauda-Königshofen, DE
pH-Meter 766 Calimatic	Knick, Berlin, DE
RCT Classic magnetic stirrer	IKA, Staufen, DE
Refractometer	Bausch & Lomb, USA
Rocking Plattform	Biometra, Göttingen, DE
Sartorius analytical balance	Sartorius, Goettingen, DE

Sartorius balance LP 6000 200S	Sartorius, Goettingen, DE
Sonopuls HD 2200	Bandelin Sonopuls, Berlin, DE
SterilGardRIII Advance	The Baker Company, ME, USA
Stuart roller mixer SRT9	Bibby Scientific, UK
Thermomixer 5436	Eppendorf, Enfield, USA
Thermomixer compact	Eppendorf, Hamburg, DE
VacuSafe vacuum pump	Integra Bioscience, Zizers, CH
Vortex®Genie 2	Scientific Industries, USA
Waterbath 1228-2F	VWR, Darmstadt, DE

3.14 Relevant materials

Material	Manufactuer
Cell culture flasks (T25, T75, T175)	Greiner Bio-One, Frickenhausen, DE
Cell culture plates (6, 12, 24, 96 wells)	Greiner Bio-One, Frickenhausen, DE
Cell scrapers	A. Hartenstein, Würzburg, DE
Coverslips, 18mm	Carl Roth, Karlsruhe, DE
Electroporation cuvettes, 4 mm	VWR, Darmstadt, DE
Falcon tubes (15 ml, 50 ml)	Greiner Bio-One, Frickenhausen, DE
Filter tips (20 µl, 100 µl, 300 µl, 1 ml)	Sarstedt, Nümbrecht, DE
Graduated pipettes (5, 10, 25 ml)	Greiner Bio-One, Frickenhausen, DE
Microscope slides SuperFrost	Carl Roth, Karlsruhe, DE
Parafilm	Bemis, Bonn, DE
Phase Lock Gel Heavy, 2 ml	5 PRIME GmbH, Hilden, DE
Pipette tips (2,5 µl, 20 µl, 100 µl, 1 ml)	Sarstedt, Nümbrecht, DE
Roti®-Fluoro PVDF membrane	Carl Roth, Karlsruhe, DE
RotiLabo® syringe filter 0,22 µm	Carl Roth, Karlsruhe, DE
Safe-lock micro test tubes (1.5 ml, 2 ml)	Sarstedt, Nümbrecht, DE
Sterican® single-use hypodermic needles	B. Braun, Melsungen, DE
Syringes (10 ml, 20 ml)	B. Braun, Melsungen, DE

Whatman filter paper, 3 mm	VWR, Darmstadt, DE

3.15 Software

Software	Manufacturer
Citavi 5	Swiss Academic Software GmbH, CH
GraphPad Prism 8.4.3	GraphPad, USA
i-control 1.8	Tecan, Männedorf, CH
Image Studio	LI-COR, Bad Homburg, DE
Image Studio Lite 5.2	LI-COR, Bad Homburg, DE
ImageJ Fiji	Wayne Rassband, USA
INTAS GDS	Intas, Göttingen, DE
LAS X	Leica, Wetzlar, DE
LightCycler 480 SW 1.5	Roche Diagnostics, Mannheim, DE
MS Office	Microsoft, Redmond, USA
Zen 2012	Zeiss, Jena, DE

4 Methods

4.1 Cell biology

4.1.1 Prokaryotic cell culture

E.coli strain TOP10 or DH5α from glycerol stocks were cultivated for 16 h in LB medium at 37°C and 200 rpm in Erlenmeyer flasks. For selection of transformed bacteria, 100 µg/ml ampicillin was added to the LB medium. For new glycerol stocks, 5 ml of the overnight culture was pelleted and mixed with 50% glycerol (v/v) for storage at -80°C.

4.1.2 Eukaryotic cell culture

In this study, the HCV permissive Huh7-derived cell line Huh7.5 and HCV subgenomic replicon cells Huh9-13 were used (Blight et al. 2002; Lohmann et al. 1999). Furthermore, Huh7.5 CRISPR-Cas9 LAMP2 knockout (Huh7.5-LAMP2 KO) and Huh7.5 with an LC3 overexpression (Huh7.5-LC3) were generated and cultivated. All cell lines were grown in Dulbecco's modified Eagle's medium (4.5 g/l glucose) supplemented with 10% fetal calf serum, 2 mM L-glutamine, 100 units/mL penicillin and 100 µg/mL streptomycin (DMEM complete) at 37°C, 5% CO_2 and ≥90% humidity. For Huh9-13 cells, 1 mg/ml G418 (Geneticin) was added to DMEM complete. Huh7.5-LC3, harboring the pcDNA3.1+/C-(K)DYK MAP1LC3B cDNA ORF clone, were cultivated in DMEM complete with 750 µg/mL G418 for selection of clones.
Cells were passaged at ~90% confluency through washing with 10 ml PBS and 3 ml trypsin/EDTA for 5 min at 37°C to detach the cells from the flask. Enzymatic activity of trypsin was stopped with 7 ml DMEM complete. Cells were resuspended and seeded at 1:2 to 1:10 dilutions in fresh medium.

4.1.3 Electroporation of Huh7.5 cells

Huh7.5 cells with a confluence of ~90% were harvested as described in 4.1.2 and washed twice with ice cold PBS. Cells were resuspended in 50 ml PBS, counted and adjusted to $5x10^6$ cells/ml in PBS. 800 µl of the cell suspension and 10 µg *in vitro* transcribed RNA (chapter 4.2.7) were mixed and transferred to a 4 mm electroporation cuvette. Cells were electroporated in a Gene Pulser MXcell™ with 300 V and 950 µF to allow the entry of HCV RNA by the cell membrane. After 10 min incubation at room temperature, cells were diluted in 12 ml DMEM complete and seeded in a T75 cell culture flask. 3-4 h after electroporation medium was changed to remove cell debris and dead cells. Transfected cells were cultured as normal Huh7.5 cells.

4.1.4 Transfection of Huh7.5 cells

Seeded Huh7.5 or Huh7.5-Jc1 cells were transfected with 1 µg plasmid DNA and 10 µl PEI/µg plasmid DNA in 200 µl PBS. After 15 sec vortexing and 15 min incubation at room temperature, the transfection mix was added dropwise to 2 ml DMEM complete in a 6 well plate. To minimize cytotoxic effects of PEI, medium was changed after 16 h post transfection.

4.1.5 Silencing of gene expression

For transfection of siRNA, the N-TER^{TM} Nanoparticle siRNA Transfection System was used according to the manufacturer's protocol. 50 nM of siRNA LAMP2 or scrRNA was mixed with N-TER^{TM} reagent in DMEM complete and added dropwise to Huh7.5-Jc1 cells, respectively. 16 h post transfection medium was changed. Cells were harvested 96 h after transfection with RIPA lysis buffer and analyzed by Western blot.

4.1.6 CRISPR-Cas9 knockout cells

The sgRNA coding DNA oligopairs for LAMP2 sgRNA1 or off-target sgRNA (chapter 3.3.2) were annealed, phosphorylated and ligated into the vector pSpCas9(BB)-2A-Puro (PX459) V2 according to the instructions from the Zhang lab (Le Cong et al. 2013; Ran et al. 2013). Huh7.5 cells were transfected with the plasmids by PEI (chapter 4.1.4). 48 h after transfection, cells were selected with DMEM complete supplemented with 5 µg/ml Puromycin up to four weeks. Medium was changed twice a week to remove dead cells. Monoclonal colonies were washed once and covered with PBS. A microscope was used to pick the colonies with a 100µl pipette tip under sterile conditions. Picked colonies were transferred into DMEM complete without Puromycin in a 96 well plate. Confluent cells were passaged into a 24 well, followed by a 12 well and 6 well plate. Knockout was confirmed by immunofluorescence staining, Western blot and gene sequencing.

4.1.7 Modulation of protein degradation pathways

To examine the turnover of nonstructural proteins, degradation was inhibited or enhanced with several modulators. Huh7.5-Jc1 and Huh9-13 cells were treated each with 50 nM Bafilomycin A1 (hereafter: BFLA), 100 nM Rapamycin, 20 µM LY294002, 5 µM Wortmannin, 10 nM Bortezomib or 5 µM PD169316 for 16 h to modulate degradation by autophagy or proteasome. Wortmannin and LY294002 block autophagosome formation and were used to investigate the degradation at an early

stage, while BFLA inhibits autophagosomal-lysosomal fusion in the late step of autophagy. Rapamycin inhibits the mTOR signaling which allows induction of autophagy. For the UPS, the 20S proteasomal inhibitor Bortezomib was used and PD169316 to enhance proteasomal degradation. Every substance was diluted in fresh DMEM and cells were treated 16 h before cell lysis or fixation.

4.1.8 Cell harvest and lysis

For Western blot lysates, cells were washed once with PBS and lysed 5 min on ice with 200 µl RIPA buffer supplemented with protease- and phosphatase-inhibitors. Lysed cells were scraped from the cell culture plate and transferred into a 1.5 ml reaction tube. Lysates were sonicated 10 sec at 30% power and centrifuged for 10 min at full speed and 4°C to get rid of cell debris.

4.2 Molecular biology

4.2.1 Agarose gel electrophoresis

Plasmid DNA and RNA were analyzed by agarose gel electrophoresis. For DNA 0.7% (w/v) and for RNA 1% (w/v), agarose was dissolved in 1x TEA buffer by heating. The cooled, liquid agarose was poured into a horizontal gel chamber and 0.1 µg/ml ethidiumbromide was added. The solid gel was placed in an electrophoresis chamber containing 1x TAE buffer. Samples were supplemented with 6x loading buffer and loaded into the gel pockets. Nucleic acids were separated at 90 V and visualized with UV-light (254/365 nm) at the INTAS imaging system.

4.2.2 Determination of nucleic acid concentration

A nanophotometer was used to determine nucleic acid concentration. The absorbance (A) of the aromatic nucleobases was measured at 260 nm wavelength (λ). For determination of purity, absorbance was measured at λ=230 nm for solvents and λ=280 nm for proteins. Pure DNA samples should obtain the ratio $A_{260/280}$=1.8 and RNA samples $A_{260/280}$=2.0 as well as the ratio $A_{260/230}$=2.0-2.2.

4.2.3 Isolation of plasmid DNA

Plasmid DNA was isolated from *E.coli* DH5α or *E.coli* TOP10 using the QIAGEN Plasmid Maxi Kit according to the manufacturer's protocol. DNA was extracted from 500 ml bacterial overnight culture. Bacteria are lysed under alkaline conditions with SDS. DNA is bound to the column, washed and precipitated by isopropanol. The pellet was resuspended in ddH_2O and stored at -20°C.

4.2.4 Restriction endonuclease digestion

To linearize circular plasmid DNA containing HCV genomes, 40 µg pFK-Jc1 was digested using 40 U of restriction enzyme *AseI* and NEBuffer3.1. Digestion of DNA was performed according to the manufacturer's protocol.

4.2.5 Transformation of competent bacteria

For transformation of chemically competent *E.coli* DH5α or *E.coli* TOP10, 100 ng plasmid DNA were added to 100 µl competent cells and incubated on ice for 30 min. After a heat shock for 90 sec at 42°C, cells were incubated 2 min on ice. 400 µl LB medium was added and incubated at 37°C for 1 h with shaking (700 rpm). The suspension was added to 250 µl LB medium with ampicillin in an Erlenmeyer flask and incubated at 37°C and 200 rpm overnight.

4.2.6 Phenol/chloroform extraction of nucleic acids

The nucleic acids were extracted from aqueous solution with phenol/chloroform extraction. The solution was mixed with 0.1 volume 3 M sodium acetate (pH 5.2) and one volume phenol/chloroform/isoamylalcohol (25:24:1) and transferred into a Phase lock tube. After centrifugation for 5 min at 17.000 g and 4°C, one volume of chloroform/isoamylalcohol (24:1) was added and centrifuged again. The upper aqueous solution was transferred into a new reaction tube. To precipitate nucleic acids, solution was mixed with 2.5 volume ice cold ethanol for DNA or 0.7 volume of isopropanol for RNA. After centrifugation for 60 min at 17.000 g and 4°C, the supernatant was discarded and the pellet washed with 70% ethanol. The pellet was air dried and resuspended in ddH_2O for DNA and DEPC-H_2O for RNA.

4.2.7 *In vitro* T7 transcription

Isolated, linearized and purified plasmid DNA with a T7 promoter was used to generate HCV genome by T7 transcription. The T7 Scribe™ Standard RNA IVT Kit was used and reaction mixed according to the manufacturer's protocol (table 1).

Table 1 T7 transcription.

Reagent	Volume	Final concentration
Linearized DNA		4 µg
10x T7-Scribe transcription buffer	2 µl	1x

100 mM ATP	1.5 µl	7.5 mM
100 mM CTP	1.5 µl	7.5 mM
100 mM UTP	1.5 µl	7.5 mM
100 mM GTP	1.5 µl	7.5 mM
100 mM DTT	2.0 µl	10 mM
ScriptGuard RNase inhibitor	0.5 µl	
T7-Scribe enzyme solution	2 µl	
RNase free water	ad 20 µl	

Reaction mixture was incubated 2 h at 37°C. Plasmid DNA was digested by 1 µl RNase free DNase I for 15 min at 37°C. Transcribed RNA was purified by phenol/chloroform extraction (chapter 4.2.6) and resuspended in DEPC-H_2O. For electroporation, 10 µg RNA aliquots were prepared and stored at -20°C.

4.2.8 RNA isolation

For viral RNA isolation, 140 µl of each fraction from membrane flotation assay was used. RNA was isolated with the QIAamp Viral RNA Mini Kit (spin protocol) according to the manufacturer's instructions. For elution of viral RNA, 60 µl elution buffer was used.

4.2.9 cDNA synthesis

The remaining DNA in purified RNA samples was digested and the cDNA synthesized (table 2).

Table 2 DNA digestion and cDNA synthesis.

Reagent	Volume	Incubation
Purified RNA	8 µl	1 h at 37°C
RQ1 RNase-free DNase I	1 µl	
RQ1 RNase-free DNase10x reaction buffer	1 µl	
RQ1 DNase Stop solution	1 µl	10 min at 65°C
Random Hexamer Primer	1 µl	15 min at 65°C

Master mix for first strand cDNA synthesis		
5x RT buffer	4 µl	10 min at room temperature, followed by 1 h at 42°C and 10 min at 72°C
dNTP mix (10 mM)	2 µl	
RevertAid^{TM} H Minus RT (200 U/µl)	1 µl	
Nuclease-free water	1 µl	

Nascent cDNA was cooled on ice, diluted 1:10 in nuclease-free water for RT-qPCR and stored at -20°C.

4.2.10 Real-Time qPCR

Detection and quantification of HCV transcripts was performed with the synthesized cDNA by real-time qPCR at the LightCycler 480 system. 3 µl of diluted cDNA was mixed on ice with specific HCV primers (chapter 3.3.1) and 2x Maxima SYBR Green qPCR Maser mix as shown in table 3. Each sample was pipetted in duplicates.

Table 3 RT-qPCR sample composition.

Component	Volume (per sample)
Diluted cDNA	3 µl
Forward primer (10 µM)	0.25 µl
Reverse primer (10 µM)	0.25 µl
2x Maxima SYBR Green Master Mix	5 µl
Nuclease-free water	1.5 µl

The fluorescent dye SYBR Green intercalates in the complementary DNA. The fluorescence intensity of SYBR Green is proportional to the amount of amplified DNA and measured after each cycle. For quantification of HCV RNA, a provided HCV standard was used. The RT-qPCR program is shown in table 4.

Table 4 RT-qPCR program.

Program	Temperature (°C)	Hold time (sec)	Slope (°C/sec)	Cycles
Denaturating	95	600	20	1
Cycling	95	15	20	45
	56	30	20	
	72	30	5	
Melting	95	60	20	1
	60	30	20	
	95	0	0.1	
Cooling	40	30	20	1

4.3 Protein biochemistry

4.3.1 Half-life determination

To determine half-life of nonstructural proteins, cells were treated with Cycloheximide (CHX) and several modulators for autophagy and proteasome (see chapter 4.1.7). For this, seeded Huh9-13 cells as well as Huh7.5-Jc1 48 hpe were used. After 16 h of treatment, the 0 min timepoint was harvested. For timepoint 15 min to 120 min, every treatment was refreshed and mixed with Cycloheximide at a concentration of 142 µM to prevent *de novo* protein translation. The cells were harvested with RIPA buffer and analyzed by Western blot. The half-life was calculated from nonlinear regression equation of the mean values.

4.3.2 Autolysosome isolation

Lysosomes and autolysosomes were isolated from three to four weeks post electroporation cultivated Huh7.5-Jc1 by the Lysosome Isolation Kit according to the manufacturer's protocol. Crude lysosomal fractions (CLF) were resuspended in 1x extraction buffer and further purified by OptiPrep density gradient with ultracentrifugation. Subsequently, remaining rough ER and mitochondria in fractions were precipitated by 8 mM calcium chloride. Immediately, fractions were mixed with SDS loading buffer (4x) and stored at -20°C.

4.3.3 Isolation of HCV RC by membrane flotation assay

HCV replicon complex (RC) was isolated through subcellular fractionation by an OptiPrep density gradient with ultracentrifugation. For this, a membrane flotation assay was performed as described by Vogt and Ott 2015.

Four T175 flasks of three to four weeks cultivated Huh7.5-Jc1 cells were washed with PBS and harvested in ice cold PBS by scraping. Cells were washed with PBS and centrifuged at 400 g for 5 min. 6 ml cold sucrose (250 mM) in PBS supplemented with 1% protease inhibitor and 1% phosphatase inhibitor cocktail (PBS-Sucrose-P/P) was mixed with the cell pellet. For cell lysis a Potter-Elvehjem and a stirrer was used with a duration of 5 min for breakage. To remove nuclei, unlysed cells and cellular debris, lysed cells were centrifuged for 10 min at 2500 g and 4°C. The post-nuclear supernatant (PNS) was mixed on ice 1:1 with 60% (w/v) OptiPrep medium (Iodixanol) to obtain a gradient input of 30% Iodixanol-PNS. The gradient was performed on ice with 4 ml PNS containing Iodixanol (30%) suspension at the bottom of an ultracentrifuge tube, followed by 4 ml of 20% and 4 ml of 10% Iodixanol mixed in PBS-Sucrose-P/P. OptiPrep gradient was ultracentrifuged for 16 h at 209.000 g and 4°C using a SW41Ti rotor with slowest acceleration and no brake. After 16 h, 23 fractions with each 500 µl were collected from the top of the gradient. To determine refractive indices at the refractometer, 20 µl of each fraction was used. 150 µl of each fraction and the PNS (control) was mixed with 50 µl SDS loading buffer (4x) for gel electrophoresis and Western blot analysis. For RNA quantification, 140 µl of each fraction was used for RNA isolation and subsequent cDNA synthesis for RT-qPCR. All fractions were stored at -20°C.

4.3.4 Protein quantification by Bradford assay

The protein amount in cell lysates was determined using Bradford assay. The reagent contains the Coomassie-Brilliant-Blue G-250 dye, which binds to proteins. The binding shifts the light absorption maximum from 465 nm to 595 nm. 2 µl cell lysate were mixed with 100 µl Bradford reagent in a 96 well plate and incubated 5 min at room temperature in exclusion of light. Each sample was pipetted in duplicates. The absorption at λ=595 nm was measured using the Tecan reader (Infinite M1000) and protein concentration was calculated based on a BSA standard curve.

4.3.5 SDS-PAGE

To separate proteins depending on their molecular weight, the sodium dodecyl sulfate polyacrylamide gel electrophoresis (SDS-PAGE) was used. The gel is composed of a stacking gel and a separation gel. The polymer density of the stacking gel is 4% and allows proteins to concentrate. In the separation gel, the SDS-denatured proteins are separated and the polymer density varies from 8-14% depending on the size of the target protein. The composition of the gels is shown in table 5. The equal amount of protein (20-60 µg) was denatured in SDS loading buffer (4x) by heating at 95°C for 10 min and separated in a vertical chamber at 90-120 V. In case of the samples from autolysosome isolation and membrane flotation assay, determination of protein concentration was skipped and the maximal volume per gel pocket in equal amounts was used.

Table 5 Composition of the stacking and separation gel.

Reagent	**Stacking gel**	**Separation gel**			
	4%	**8%**	**10%**	**12%**	**14%**
Stacking gel buffer (4x)	15 ml	-	-	-	-
Separation gel buffer (4x)	-	20 ml	20 ml	20 ml	20 ml
Rotiphorese Gel 40 (29:1)	6 ml	16 ml	20 ml	24 ml	28 ml
ddH_2O	45 ml	44 ml	40 ml	36 ml	32 ml
APS	600 µl	800 µl	800 µl	800 µl	800 µl
TEMED	60 µl	80 µl	80 µl	80 µl	80 µl

4.3.6 Western blot

After separation by SDS-PAGE, proteins were transferred on a methanol-activated PVDF membrane. A semi-dry blotting chamber and discontinuous buffer system were used with an electric field of 1.3 mA/cm^2 for 1 h. After blotting, unspecific binding of antibodies was blocked for 1 h by 1x Roti®-Block blocking solution at room temperature. The primary antibody was diluted in blocking solution and membrane incubated for 1h at room temperature or at 4°C overnight. Unbound antibody was removed by 3x 10 min washing steps with TBS-T. The membrane was incubated with

fluorophore-conjugated secondary antibody diluted in blocking solution for 1h at room temperature in exclusion of light, followed by repeat of TBS-T washing steps to remove unbound antibody. Proteins were detected by using the Li-Cor Odyssey CLx imaging system. Protein signals were analyzed by densitometric quantification using the Li-Cor Image Studio software.

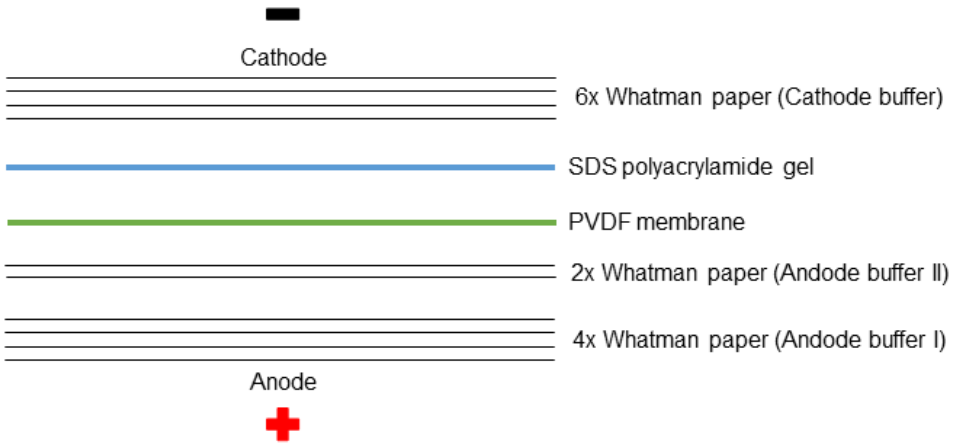

Figure 12 Principle for a semi-dry Western blot stack.
PVDF membrane and Whatman paper were adjusted to the size of the gel. The Whatman paper were soaked in the respective buffer and air bubble-free stacked together with the gel as shown in the figure.

4.3.7 Indirect immunofluorescence microscopy

Immunostaining was performed with fluorophore-labeled antibodies to analyze the intracellular localization and distribution of proteins. Cells were grown on 18 mm cover slips in a 12-well plate and washed once with PBS. Fixation was performed either with 3.7% formaldehyde in PBS for 20 min at room temperature or with Ethanol/Acetone 1:1 for 30 min at -20°C. Cells were washed 3x 5 min in PBS and permeabilized with 0.5% Triton X-100 in PBS for 10 min at room temperature. After permeabilization, cells were washed again 3x 5 min in PBS and unspecific antibody binding blocked by 1% BSA in PBS for 15 min at room temperature. Afterwards, cells were incubated in 50 µl primary antibody diluted in PBS for 1h at room temperature or overnight at 4°C in a humid chamber. Unbound primary antibody was removed by washing 3x 5 min in PBS. Then cells were incubated with 50 µl fluorophore-labeled secondary antibody and DAPI to stain the nuclei for 1 h at room temperature under exclusion of light. Unspecifically bound antibody was removed again by washing 3x 5 min in PBS and coverslips were mounted with Mowiol on microscope slides. Stained cells were stored at 4°C in the dark until analysis at the confocal laser scanning microscope.

4.4 Microscopy

4.4.1 Confocal laser scanning microscopy

The localization and distribution of the stained cells was analyzed by a confocal laser scanning microscope (CLSM) at the LSM 510 Meta (Zeiss) or at the CLSM TCS SP8 (Leica). In conventional fluorescence microscopy, all fluorophores in the sample are excited by a fluorescent lamp. Thus, the emitted fluorescence from the entire sample is detected. With CLSM, a confocal arranged pinhole aperture filters the light from higher or lower levels. Therefore, only the emitted fluorescence of a certain layer is detected. Furthermore, fluorophores are excited with monochromatic light from a laser and the emitted fluorescence is sequentially detected by a dot matrix. Then, detected and amplified light quanta can be digitally combined by the computer to form a finished image. A z-stack can capture multiple layers of a sample and create a three-dimensional image of the cell. The used objectives were 100x and 40x (NA, 1.46).
To analyze the colocalization, the tMOC (threshold Mander's overlap coefficient) was calculated using ImageJ Fiji software. The tMOC is independent from the intensity of the fluorescence signal and ranges from 0 to 1. A coefficient of 1 is defined as absolute colocalization.
Total fluorescence per cell was calculated using ImageJ Fiji and the formula: Corrected total cell fluorescence (CTCF) = integrated density - (area of selected cell x mean fluorescence of background readings).

4.5 Statistical analysis

All results are described as means ± standard errors of the means (SEMs) from at least three biological replicates. The bars in the figures represent SEMs. The significance of the results was analyzed by two-tailed unpaired Student's *t* test, using GraphPad Prism 8.4.3 software. In histograms showing relative changes compared with the control cells, the control group was arbitrarily set as 1. Here, a SEM for the control group cannot be reported, as standardization of the measured values (relative to the control group) was performed for each of the independent assays. Therefore, measurements for the treatment groups in each assay were dependent (matched). Statistical significance is represented in the figures as follows: *P<0.05, **P<0.01, ***P<0.001. ****P<0.0001.

5 Results

5.1 Prolonged half-life of NS proteins by autophagy inhibitors

5.1.1 Half-life of NS3 is extended after inhibition of the autophagic flux and the proteasome

To study the relevance of autophagosomal and proteasomal degradation of HCV nonstructural proteins, half-life was investigated in the presence of inhibitors or activators of autophagy or proteasome. For this purpose, the half-life was determined in Jc1 electroporated Huh7.5 cells.

For activation of autophagy, the mTOR inhibitor Rapamycin was used. To inhibit autophagic flux in an early stage, cells were treated with LY294002 and Wortmannin. Late stage of autophagy was inhibited through BFLA, which targets the vacuolar H^+-ATPase and therefore prevent acidification of lysosomes. To investigate the fate via the ubiquitin-proteasome-system (UPS), Bortezomib was used to inhibit and PD169316 to induce proteasomal degradation. After incubation, the reagent cycloheximide (CHX) was added to the cells to prevent *de novo* protein translation in combination with refreshed treatment with modulators against autophagy and the proteasome for a small screening. Changes in protein half-life then can be considered as an influence of respective degradation pathway on the turnover of nonstructural proteins.

In figure 13A, a simplified graph of the half-life is depicted. Half-life of NS3 was decreased after autophagy-induced treatment with Rapamycin, while inhibition of early and late autophagy with Wortmannin, LY294002 and BFLA showed a higher half-life compared to the DMSO control.
Half-life was aligned with proteasomal degradation. For this, Huh7.5-Jc1 cells were exposed to Bortezomib, which showed a higher half-life for NS3 and lower in PD169316 cells when compared to DMSO (Figure 13A).
In Figure 13B, each measured protein amount of NS3 after use of modulators and cycloheximide is displayed, in which a strong decline of the regression line indicates short half-lives and a minor decline a long half-life of the protein. Based on these non-linear regression line, half-life for each treatment was calculated.
NS3 half-life in untreated Huh7.5-Jc1 cells was 271 min similar to 301 min of the DMSO control. Rapamycin with 209 min and PD169316 with 244 min had shorter half-lives for

NS3. For BFLA, a half-life of 306 min was calculated, Wortmannin had 446 min, LY294002 508 min and proteasome inhibitor Bortezomib 440 min and thereby longer than the DMSO control (Figure 13B).

The impact of almost all modulators on the half-life indicates that both pathways, the autophagic as well as proteasomal, are involved in the turnover of HCV NS3 protein.

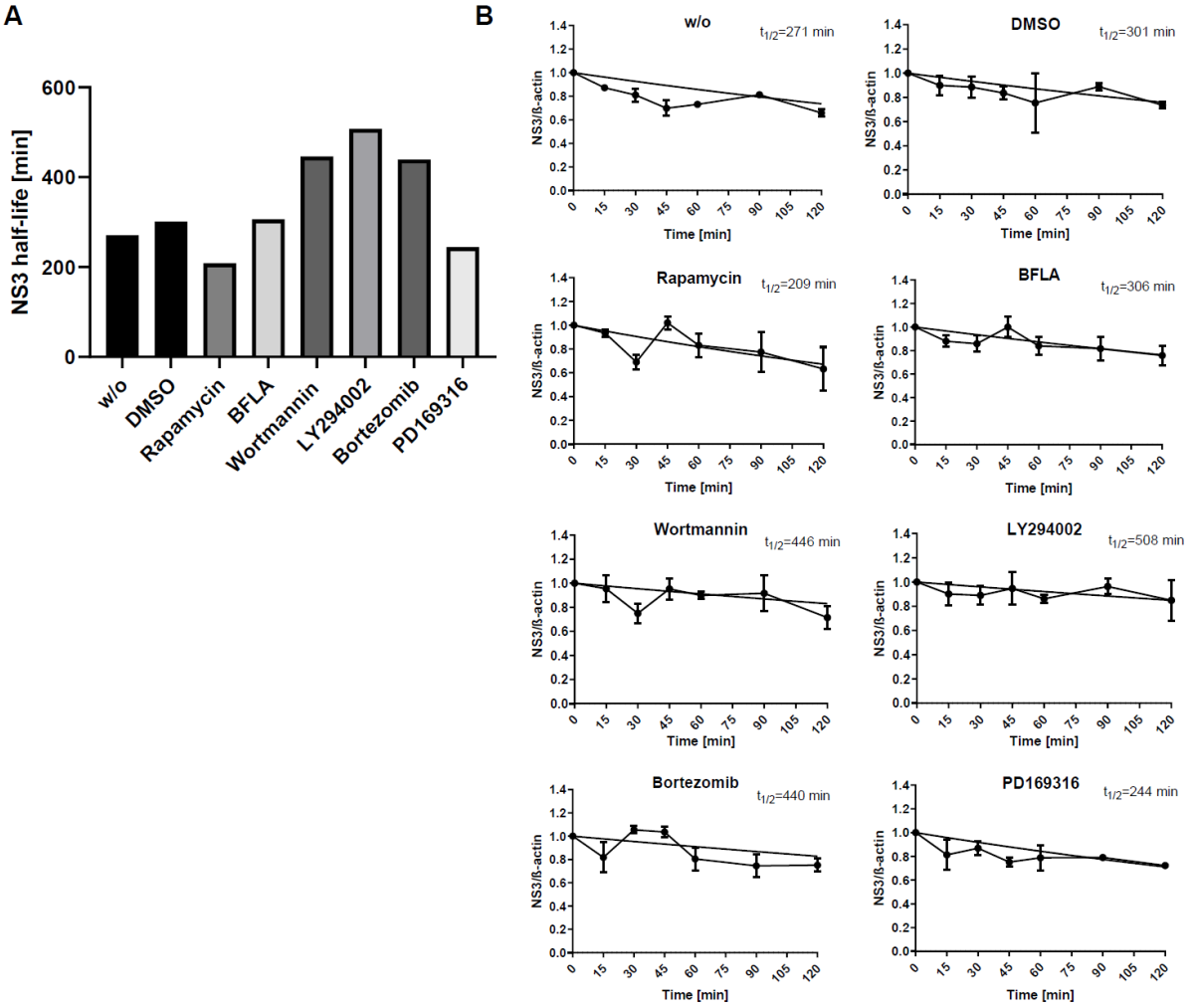

Figure 13 Altered half-life of NS3 after modulation of the autophagosomal and proteasomal pathway.
(**A**) Huh7.5-Jc1 were treated 16 h each with Rapamycin (100 nM), BFLA (50 nM), Wortmannin (5 µM) and LY294002 (20 µM) to modulate autophagy and Bortezomib (10 nM) and PD169316 (5 µM) to modulate proteasome. Subsequently, Cycloheximide (142 µM) was added to prevent *de novo* protein translation of NS3. Half-life of NS3 is indicated as mean of at least three independent experiments for each treatment; (**B**) NS3 bands of Western blot analysis were normalized to ß-actin (at least n=3, mean ± SEM). NS3 half-life was calculated for each treatment with one phase decay as exponential equation and constrains set to Y0=1 and plateau=1 as non-linear regression by GraphPad Prism 8.4.3.

5.1.2 Inhibited autophagy results in longer half-life of NS5A, while proteasomal inhibition was unaltered

Like for NS3, the relevance of the degradation route by calculation of half-life was examined in Huh7.5-Jc1 treated with the modulators mentioned before and CHX.

Compared to the DMSO control, cells treated with Rapamycin showed a decreased half-life of NS5A, while for LY294002, Wortmannin and BFLA a higher half-life was detected.
In Bortezomib-treated cells, half-life was slightly increased for NS5A and lower in PD169316 cells as in the DMSO control (Figure 14A).
Particularly, for untreated and DMSO-treated cells, the half-life of NS5A was 189 min and 197 min, respectively (Figure 14B). Shorter time was observed when using Rapamycin with 162 min or PD169316 with 177 min. Prolonged half-life for NS5A was calculated when Huh7.5-Jc1 were exposed to BFLA with 349 min, Wortmannin with 307 min and LY294002 with 499 min and slightly for Bortezomib with 205 min (Figure 14B).

As inhibited autophagy increased and induction decreased half-life, while proteasome treatment seemed to be unaffected, these results can indicate an importance of the autophagosomal degradation pathway for NS5A.

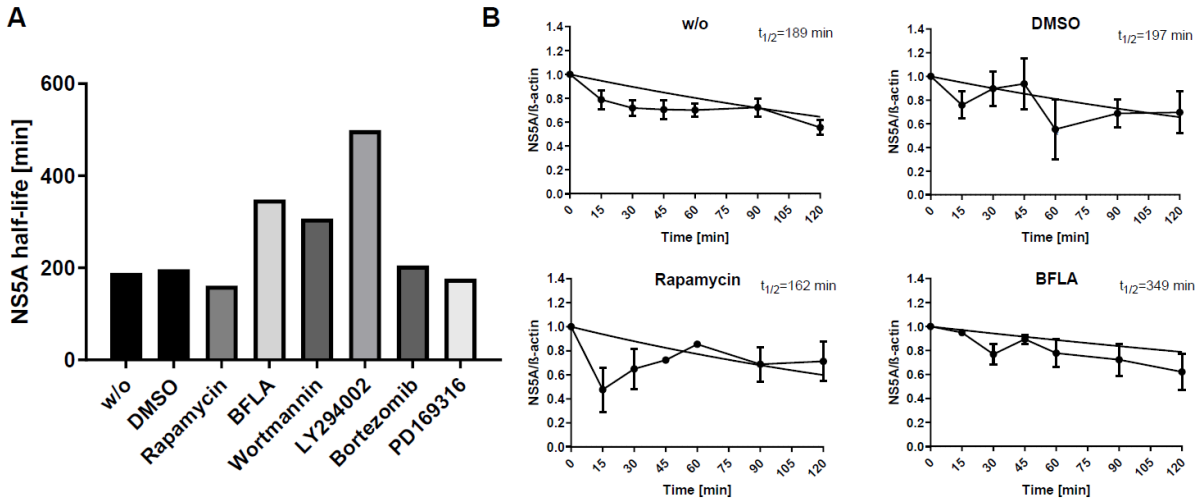

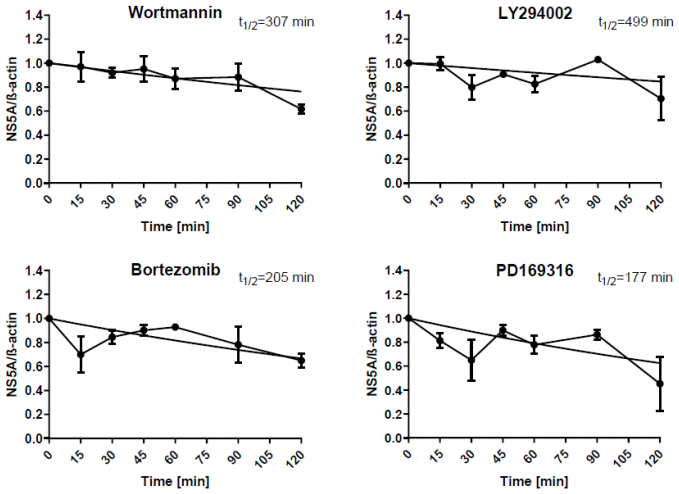

Figure 14 Autophagosomal route plays a role in determining the half-life of NS5A.
(**A**) Huh7.5-Jc1 were treated 16 h each with Rapamycin (100 nM), BFLA (50 nM), Wortmannin (5 µM) and LY294002 (20 µM) to modulate autophagy and Bortezomib (10 nM) and PD169316 (5 µM) to modulate proteasome. Subsequently, Cycloheximide (142 µM) was added to prevent *de novo* protein translation of NS5A. Half-life of NS5A is indicated as mean of at least three independent experiments for each treatment; (**B**) NS5A bands of Western blot analysis were normalized to ß-actin (at least n=3, mean ± SEM). NS5A half-life was calculated for each treatment with one phase decay as exponential equation and constrains set to Y0=1 and plateau=1 as non-linear regression by GraphPad Prism 8.4.3.

5.1.3 Half-life between the phosphorylation states of NS5A differs

Huh7.5-Jc1 cells were treated with modulators against autophagy or the UPS and with CHX to examine the relevance of these two degradation routes, which clarifies the fate of NS5A. The phosphoprotein NS5A possesses two different phosphorylation states. Basally/hypophosphorylated NS5A is involved in viral replication, whereas hyperphosphorylated NS5A is crucial for viral assembly (Moradpour et al. 2007; Masaki et al. 2014; Goonawardane et al. 2017). In Western blot analysis, basally phosphorylated NS5A can be detected at 56 kDa, while hyperphosphorylated NS5A has a molecular weight of 58 kDa and therefore enables separate calculation of each half-life. To distinguish between the two phospho-states and their half-life can indicate to which part of NS5A, or viral life-cycle step autophagy interferes regarding the protein turnover.

Similar to whole NS5A (both phosphorylation states together) the basally phosphorylated NS5A showed a shorter half-life in cells treated with Rapamycin and

PD169316 and prolonged half-life in cells treated with BFLA, Wortmannin, LY294002 and Bortezomib (Figure 15A).

Particularly, untreated cells had a half-life of 224 min and DMSO-treated 237 min for basally phosphorylated NS5A. The time was shorter with Rapamycin 196 min and longer with autophagy inhibitors BFLA with 344 min, Wortmannin with 343 min and LY294002 with 373 min. In parallel, Bortezomib led to a longer half-life of 320 min and PD169316 with 184 min to a shorter when compared to the DMSO control (Figure 15B).

Quite contrary to basal phosphorylation of NS5A, the half-life of hyperphosphorylated NS5A was higher in Rapamycin and PD169316 treated cells as well as after treatment with LY294002 (Figure 15C). Shorter half-life than in DMSO control cells could be observed after treatment with BFLA, Wortmannin and Bortezomib.

Both, untreated and DMSO-treated cells, had a half-life for NS5A of 183 min, higher for Rapamycin with 417 min, LY294002 with 236 min and PD169316 with 250 min (Figure 15D). A strong decline compared to the control cells was observed after use of BFLA with 150 min calculated, Wortmannin with 154 min and Bortezomib with 116 min.

To sum it up, the calculated half-lives of basally phosphorylated NS5A can be compared to those of the whole NS5A, as it shows a stronger effect of modulators against autophagy when compared to the UPS modulators, suggesting that basally phosphorylated NS5A is targeted to autophagic degradation.

Compared to basally phosphorylated NS5A, half-life of the hyperphosphorylated form indeed differed. Since Rapamycin as an activator of autophagy strongly changed half-life, autophagy is assumed as well, but may occur in another time-dependent degradation as basally phosphorylated NS5A.

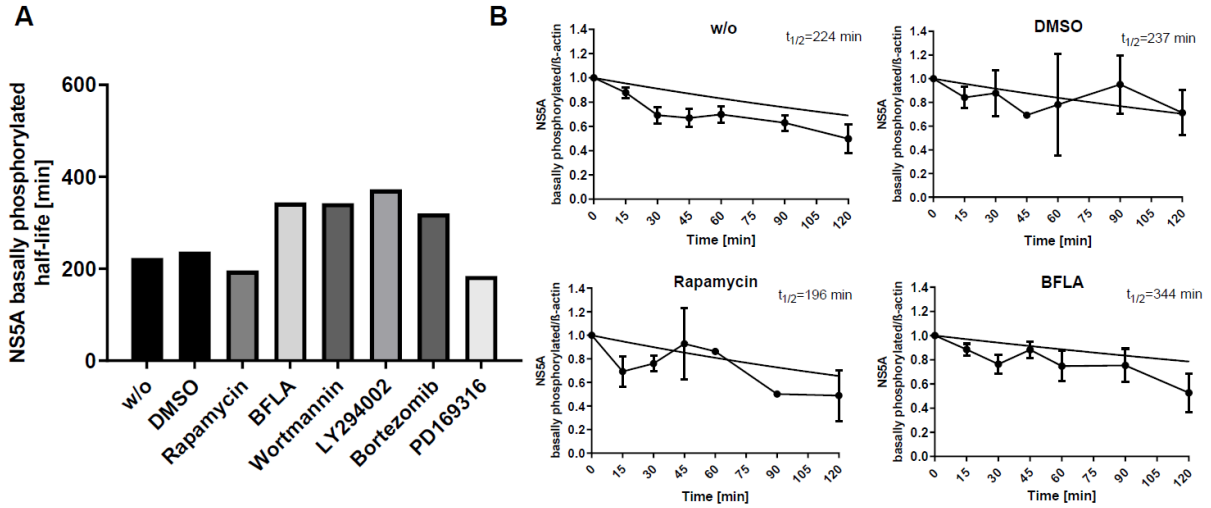

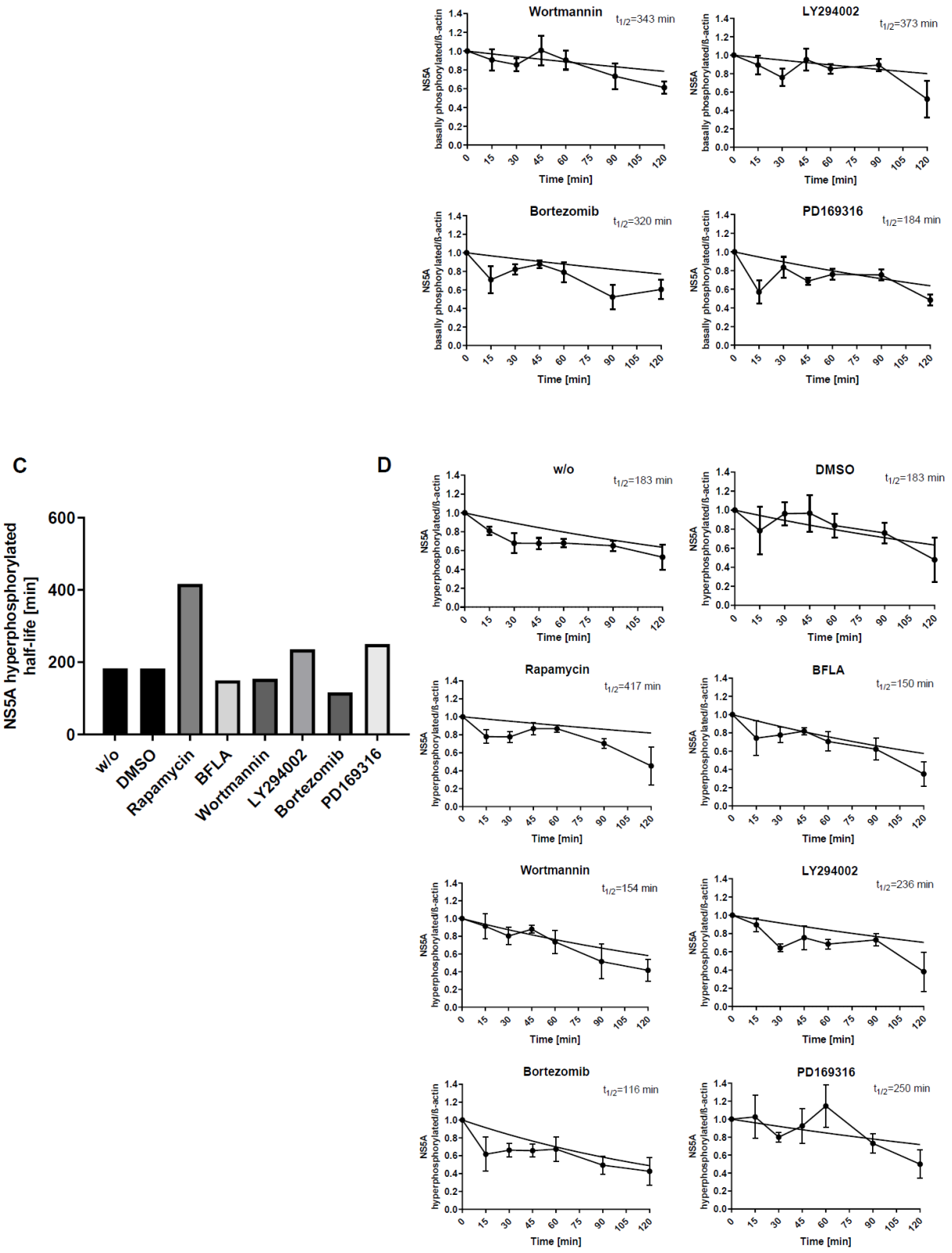

Figure 15 Altered half-life between basally and hyperphosphorylated NS5A after modulated autophagosomal and proteasomal degradation.
(**A**) Huh7.5-Jc1 were treated 16 h each with Rapamycin (100 nM), BFLA (50 nM), Wortmannin (5 µM) and LY294002 (20 µM) to modulate autophagy and Bortezomib (10 nM) and PD169316 (5 µM) to modulate proteasome. Subsequently, Cycloheximide (142 µM) was added to prevent *de novo* protein translation of basally phosphorylated NS5A. Half-life of basally phosphorylated NS5A is indicated as mean of at least three

independent experiments for each treatment; (**B**) Basally phosphorylated NS5A bands of Western blot analysis were normalized to ß-actin (at least n=3, mean ± SEM). NS5A half-life in basal phosphorylation was calculated for each treatment with one phase decay as exponential equation and constrains set to Y0=1 and plateau=1 as non-linear regression by GraphPad Prism 8.4.3; (**C**) Huh7.5-Jc1 were treated 16 h each with Rapamycin (100 nM), BFLA (50 nM), Wortmannin (5 µM) and LY294002 (20 µM) to modulate autophagy and Bortezomib (10 nM) and PD169316 (5 µM) to modulate proteasome. Subsequently, Cycloheximide (142 µM) was added to prevent *de novo* protein translation of hyperphosphorylated NS5A. Half-life of hyperphosphorylated NS5A is indicated as mean of at least three independent experiments for each treatment; (**D**) Hyperphosphorylated NS5A bands of Western blot analysis were normalized to ß-actin (at least n=3, mean ± SEM). NS5A half-life in hyperphosphorylation was calculated for each treatment with one phase decay as exponential equation and constrains set to Y0=1 and plateau=1 as non-linear regression by GraphPad Prism 8.4.3.

5.1.4 Modulation of both, autophagic and proteasomal degradation, has an impact on NS5B half-life

To examine the role of autophagy in the fate of the viral RNA-dependent RNA polymerase (RdRp) NS5B, half-life was determined by the use of CHX and treatment with different modulators for autophagy. The proteasomal pathway was modulated as well, to compare results with those for autophagosomal turnover. Rapamycin, BFLA, Wortmannin and LY294002 act as modulators for autophagy, while Bortezomib and PD169316 were used to modulate the UPS. As before for NS3 and NS5A, treated Huh7.5-Jc1 cells were lysed at each timepoint and analyzed via Western blot analysis. Signal intensities were again used for the calculation of the half-life of NS5B for each treatment, respectively.

As seen in figure 16A, the calculated mean of the half-life for NS5B from untreated cells was equal to the DMSO control. Enhancement of autophagosomal degradation by Rapamycin showed a decrease in half-life, while it was prolonged after inhibition of autophagy by BFLA, Wortmannin or LY294002 when compared to the control cells. Half-life was shorter with enhanced proteasomal degradation under treatment with PD169316 and slightly increased in comparison to the control cells with proteasome inhibitor Bortezomib (Figure 16A).

Untreated Huh7.5-Jc1 cells had a NS5B half-life of 501 min, while for DMSO control cells, 546 min were calculated. NS5B in Rapamycin-treated cells had a half-life of 288 min, for BFLA 618 min, 704 min for LY294002 and strong prolonged with 1636 min for

Wortmannin. The calculated NS5B half-life after Bortezomib treatment was 571 min and after PD169316 128 min (Figure 16B).

Taken all together, the strong effect of activators for autophagy and UPS as well as for inhibition of the autophagic flux on the half-life of NS5B assume an importance of both degradation pathways.

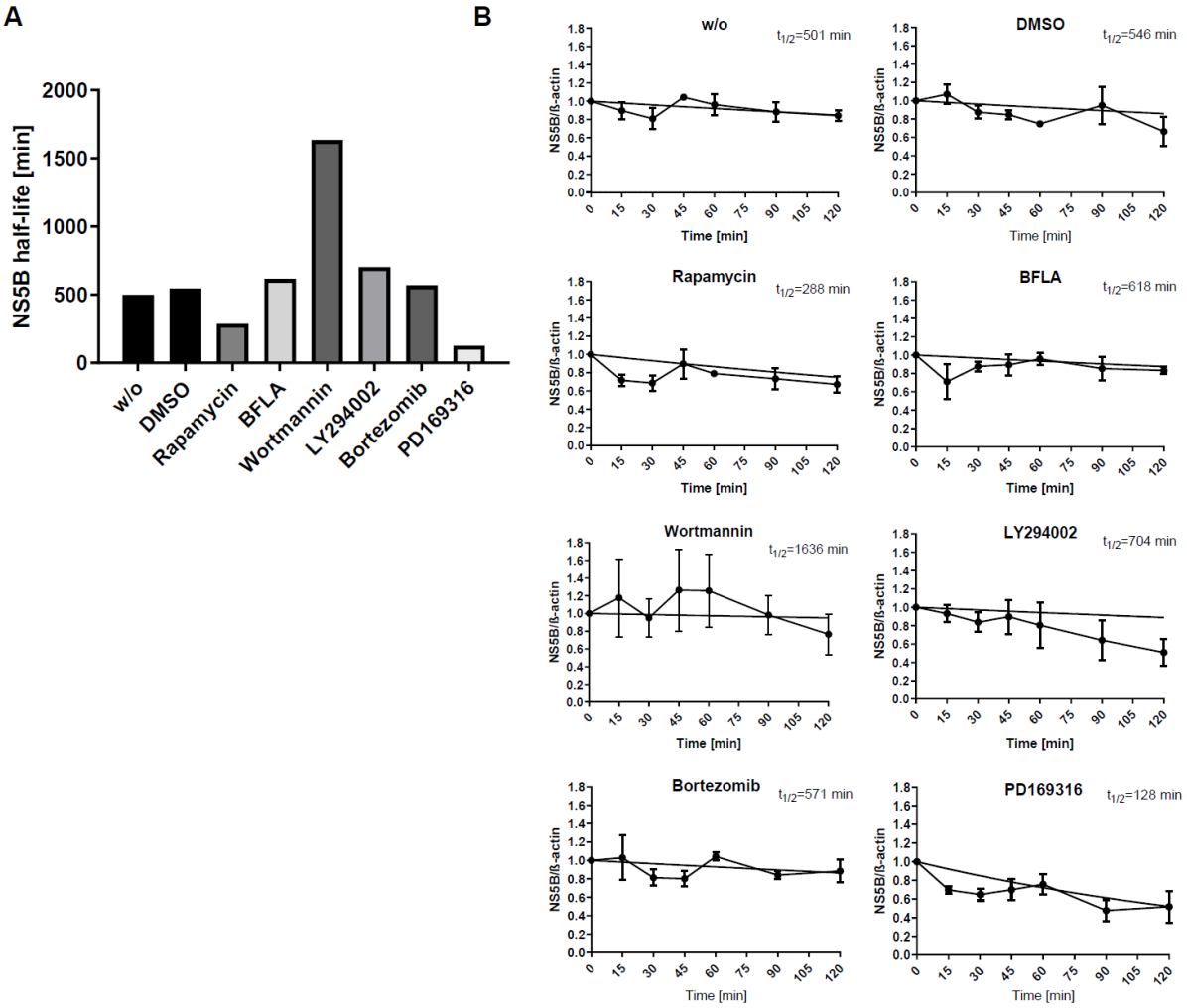

Figure 16 Decreased half-life of NS5B after autophagy and UPS induction.
(**A**) Huh7.5-Jc1 were treated 16 h each with Rapamycin (100 nM), BFLA (50 nM), Wortmannin (5 µM) and LY294002 (20 µM) to modulate autophagy and Bortezomib (10 nM) and PD169316 (5 µM) to modulate proteasome. Subsequently, Cycloheximide (142 µM) was added to prevent *de novo* protein translation of NS5B. Half-life of NS5B is indicated as mean of at least three independent experiments for each treatment; (**B**) NS5B bands of Western blot analysis were normalized to ß-actin (at least n=3, mean ± SEM). NS5B half-life was calculated for each treatment with one phase decay as exponential equation and constrains set to Y0=1 and plateau=1 as non-linear regression by GraphPad Prism 8.4.3.

5.1.5 Altered half-life for NS4B due to modulated autophagy

Beside NS3, NS5A and NS5B, the turnover for the nonstructural protein NS4B regarding autophagy was investigated as well. Here, Huh9-13 cells were treated with the same modulators for both pathways as mentioned before and with CHX, to prevent *de novo* protein translation. Based on Western blot analysis, the half-life for NS4B was calculated for each treatment. Furthermore, as the anti-NS4B antibody is more suitable against HCV genotype 1, but Huh7.5-Jc1 harbor the genotype 2, the subgenomic replicon cells Huh9-13 were used to investigate the half-life of NS4B. Since the HCV genome in Huh9-13 lack the structural proteins and thereby cannot produce viral particles, it has to be considered that it does not represent the full HCV life-cycle.

As seen in the simplified graph for half-life, the calculated mean half-life after Western blot analysis for DMSO was slightly increased compared to untreated cells.
A shorter half-life was observed for Rapamycin and PD169316, while it was strongly increased with BFLA. NS4B half-life for Wortmannin, LY294002 and Bortezomib was similar to DMSO control cells, but slightly increased in untreated Huh9-13 (Figure 17A).

The half-life more detailed showed for untreated and DMSO-treated cells a duration of 211 min and 314 min, respectively. Huh9-13 cells had a shorter half-life of 147 min for Rapamycin and 163 min for PD169316 after the respective induction of autophagy and UPS. By using the inhibitors, BFLA-treated cells had a half-life of 577 min, with Wortmannin 282 min, after LY294002 355 min and with proteasome inhibitor Bortezomib 278 min (Figure 17B).

Summarized, especially due to the effect of BFLA, there is a strong tendency of NS4B to be targeted to autophagy for its turnover. A potential accumulation of NS4B after the inhibition of the UPS, which is indicated by an extended half-life, is not assumed due to an equal half-life to the control cells.

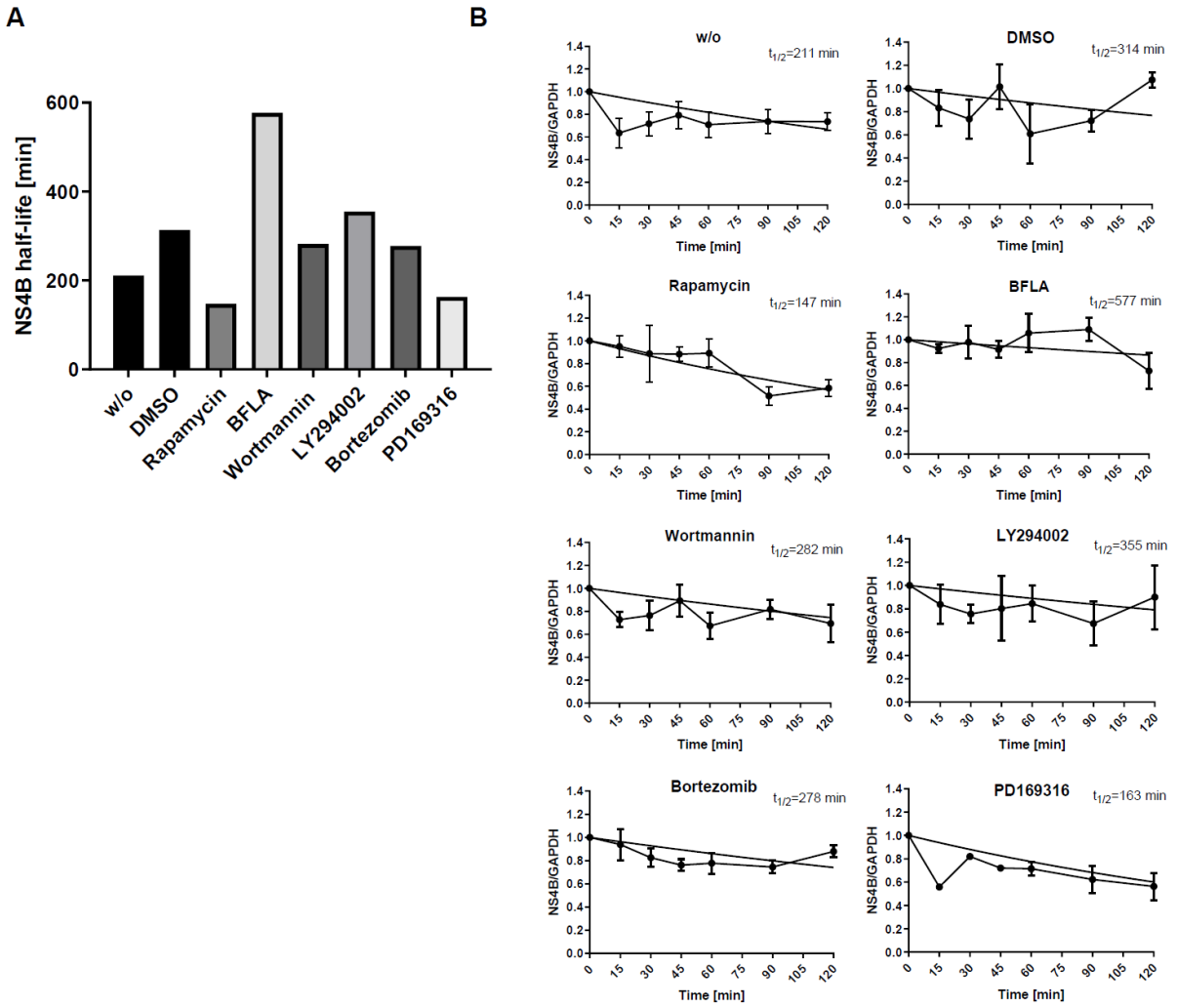

Figure 17 Modulated autophagy has a strong effect on the half-life of NS4B. (**A**) Huh9-13 cells were treated 16 h each with Rapamycin (100 nM), BFLA (50 nM), Wortmannin (5 µM) and LY294002 (20 µM) to modulate autophagy and Bortezomib (10 nM) and PD169316 (5 µM) to modulate proteasome. Subsequently, Cycloheximide (142 µM) was added to prevent *de novo* protein translation of NS4B. Half-life of NS4B is indicated as mean of at least three independent experiments for each treatment; (**B**) NS4B bands of Western blot analysis were normalized to GAPDH (at least n=3, mean ± SEM). NS4B half-life was calculated for each treatment with one phase decay as exponential equation and constrains set to Y0=1 and plateau=1 as non-linear regression by GraphPad Prism 8.4.3.

5.2 Affected NS5A phosphorylation upon modulation of autophagy and UPS

In addition to determine the half-life of NS5A under treatment with modulators for autophagy or the proteasome and CHX by Western blot, the two phosphorylation states of NS5A were considered separately. Basal phosphorylated NS5A is involved in viral replication, while hyperphosphorylated NS5A plays a role in viral assembly (Moradpour et al. 2007; Masaki et al. 2014; Goonawardane et al. 2017).

As shown in figure 18A, the quotient between both phosphorylation states was calculated to obtain a ratio. Thereby, changes in the ratio within the timepoints of a treatment or as well between the different treatments can be examined to figure out the influence of the degradation pathways on NS5A.

For untreated and DMSO treated Huh7.5-Jc1 as the control, the amount of NS5A at basal phosphorylation and hyperphosphorylation is steady from timepoint 0 min to 120 min.

The ratio of basal phosphorylated NS5A increased after treatment with autophagy inhibitors BFLA, Wortmannin and LY294002 as well as with autophagy induction by Rapamycin. Simultaneously, the hyperphosphorylated NS5A decreased. For Rapamycin and Wortmannin, the ratio for the 120 min timepoint is comparable to 0 min.

After treatment with proteasome inhibitor Bortezomib, a slight increase of basal phosphorylated NS5A was observed. The ratio of hyper- to basal phosphorylation was unaffected. A strong increase of basal phosphorylated NS5A was shown for PD169316 at timepoint 30-60 min, while no changes occurred for hyperphosphorylation (Figure 18A).

Based on these results, phosphorylation seems to be affected within the timespan and between different modulated degradation pathways in which hyperphosphorylated NS5A is may targeted to autophagosomal compartments for disposal.

A

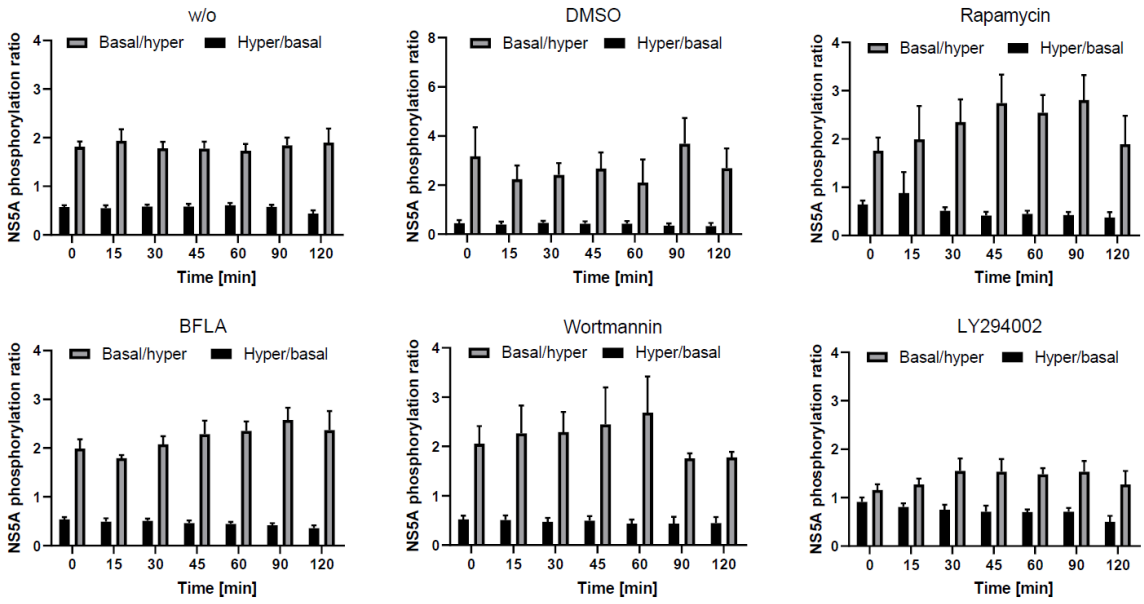

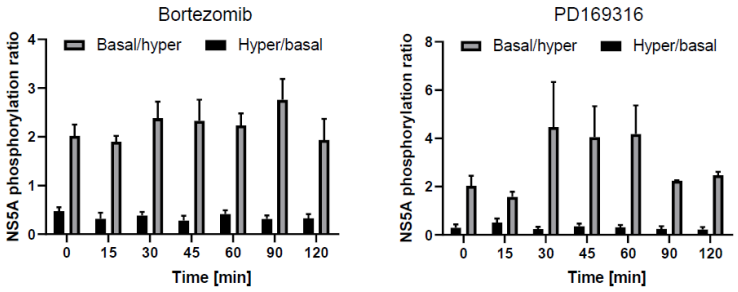

Figure 18 Modulation of autophagy or UPS changed NS5A phosphorylation.
(**A**) Huh7.5-Jc1 were treated 16 h each with Rapamycin (100 nM), BFLA (50 nM), Wortmannin (5 µM) and LY294002 (20 µM) to modulate autophagy and Bortezomib (10 nM) and PD169316 (5 µM) to modulate proteasome. Subsequently, Cycloheximide (142 µM) was added to prevent *de novo* protein translation of NS5A. Western blot bands of basal phosphorylated and hyperphosphorylated NS5A were quantified separate and normalized to ß-actin (at least n=3, mean ± SEM), The quotient between the two phosphorylation states was calculated for the phosphorylation ratio.

5.3 Modulators for autophagy affect colocalization of NS proteins with LAMP2-positive structures

5.3.1 NS3 and NS5A can be detected in LAMP2-positive structures

To investigate the turnover of NS3 and NS5A in treated cells in more detail, the subcellular localization of NS3 and NS5A was analyzed by immunofluorescence staining and confocal laser scanning microscopy. Huh7.5 cells were transfected by electroporation with HCV RNA (Jc1) and treated with modulators for autophagy and proteasome. Rapamycin serves as activator of autophagy, while BFLA, Wortmannin and LY294002 inhibit autophagy. To induce proteasomal degradation, PD169316 was used and *vice versa* for inhibition Bortezomib was chosen. Here, the lysosomal marker protein LAMP2 was used to investigate whether the lysosomal structures harbor NS proteins for the degradation process.

By using proteasomal modulators and the staining against LAMP2, it can be examined whether the NS proteins are shifted e.g., after inhibition, towards the autophagic route or not. Thereby, it allows insight on the switch or equilibrium between autophagy and UPS.

To quantify a colocalization between NS proteins and LAMP2, the tMOC (threshold Mander's overlap coefficient) was calculated. This coefficient is independent from the intensity of the fluorescence signal and 1 reflects an absolute colocalization.

Colocalization of NS3 to lysosomal marker protein LAMP2 was observed in cells treated with DMSO, BFLA and Wortmannin. Moreover, a more pronounced accumulation of NS3 can be observed after BFLA treatment.
Huh7.5-Jc1 cells showed less proximity of NS3 to LAMP2 after treatment with Rapamycin, LY294002, Bortezomib and PD169316 (Figure 19A).
Z-stacking and virtual cutting the organelles by clipping could visualize the autolysosomes containing NS3 (Figure 19B).
Calculation of the tMOC showed a slightly higher colocalization of about 62% for BFLA and 46% for Wortmannin when compared to untreated (44%) and DMSO (58%). In Huh7.5-Jc1 with Rapamycin, LY294002, Bortezomib and PD169316, less colocalization was observed (Figure 19C).

For NS5A, close proximity was in PD169316-treated cells, while treatment with BFLA, and Bortezomib were unchanged and Rapamycin-, Wortmannin- and LY294002-treated cells showed no proximity to LAMP2-positives structures (Figure 19D).
A closer look to the proximity of NS5A to LAMP2-stained autolysosomes can be observed in figure 19E.
Analysis of the tMOC for NS5A showed a colocalization after PD169316 treatment of about 80%, while BFLA and Bortezomib treatment led to similar tMOC like untreated or DMSO treated cells of approx. 50-60%. With Rapamycin, Wortmannin and LY294002, colocalization of NS5A to LAMP2-positive structures was reduced compared to the control (Figure 19F).
These observations imply, that autophagy may is involved in the disposal of NS3 and NS5A as the viral proteins show an accumulation, increased colocalization or close proximity to LAMP2-positive structures during inhibition of the autophagic flux. And *vice versa*, after induction less colocalization was observed, which is may due to accelerated degradation of the waste cargo in autolysosomes.

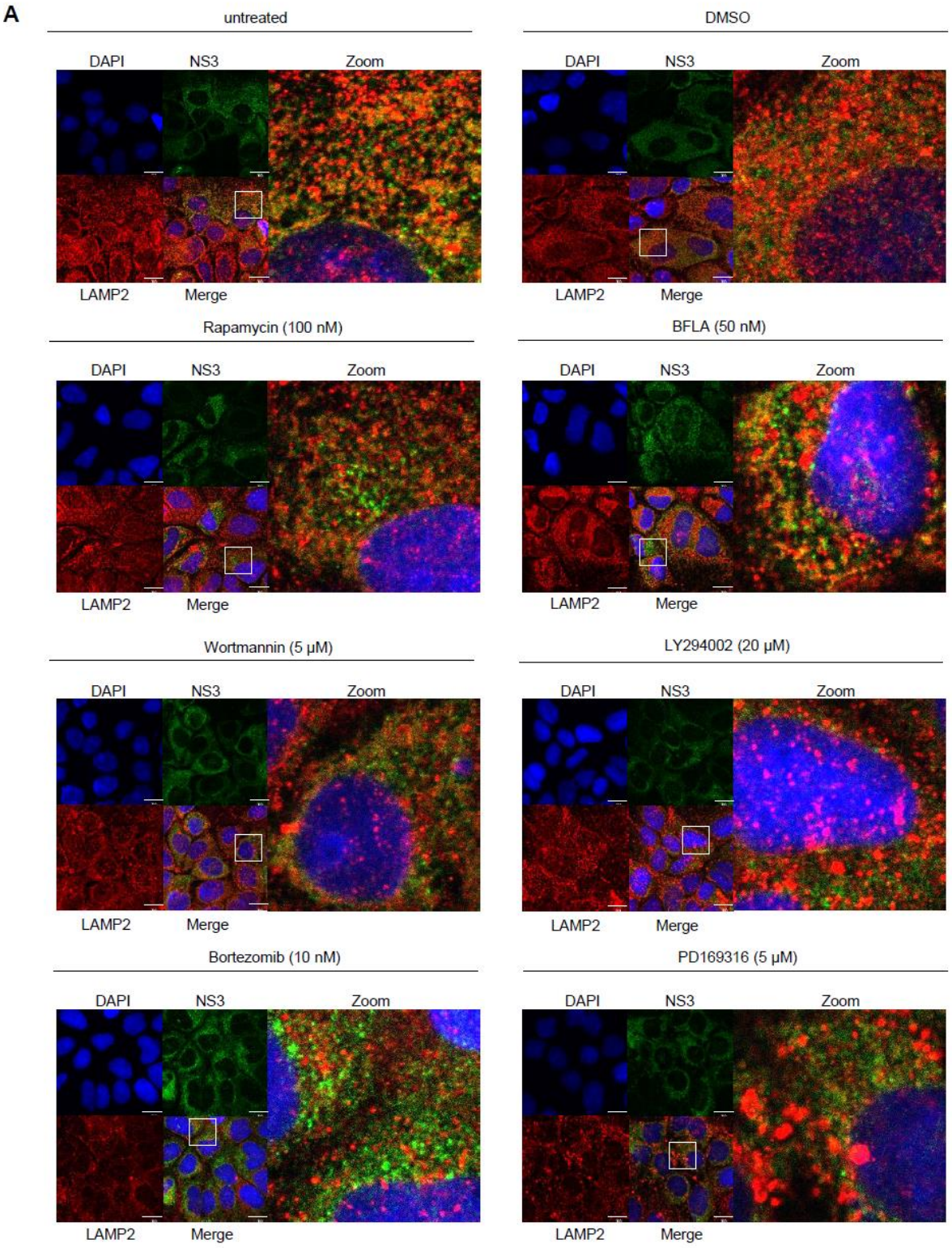
A
untreated
DMSO
Rapamycin (100 nM)
BFLA (50 nM)
Wortmannin (5 µM)
LY294002 (20 µM)
Bortezomib (10 nM)
PD169316 (5 µM)
DAPI
NS3
Zoom
LAMP2
Merge

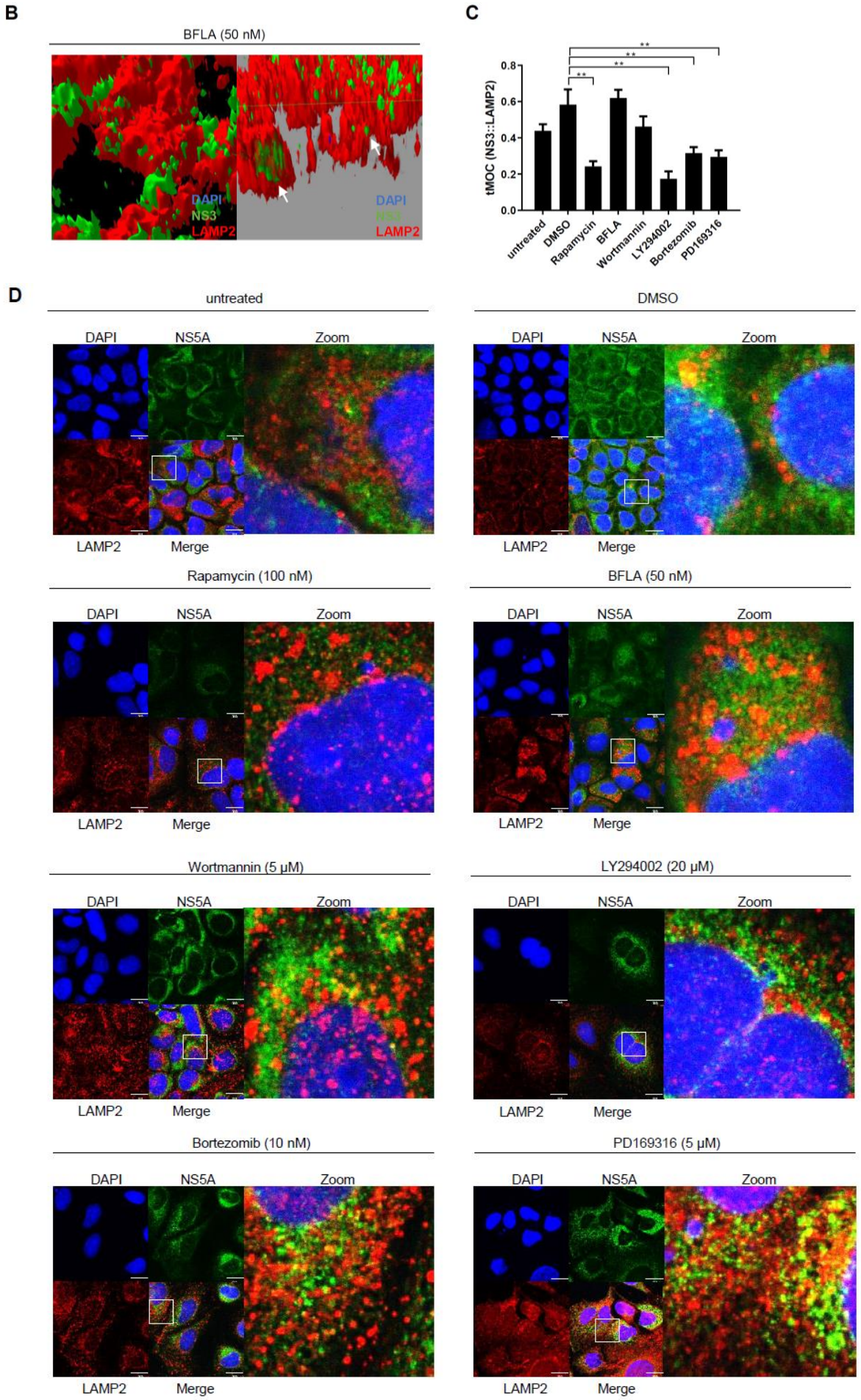
B
BFLA (50 nM)
DAPI
NS3
LAMP2
DAPI
NS3
LAMP2
C
tMOC (NS3::LAMP2)
0.8
0.6
0.4
0.2
0.0
**
**
**
**
untreated
DMSO
Rapamycin
BFLA
Wortmannin
LY294002
Bortezomib
PD169316
D
untreated
DMSO
Rapamycin (100 nM)
BFLA (50 nM)
Wortmannin (5 μM)
LY294002 (20 μM)
Bortezomib (10 nM)
PD169316 (5 μM)
DAPI
NS5A
Zoom
LAMP2
Merge

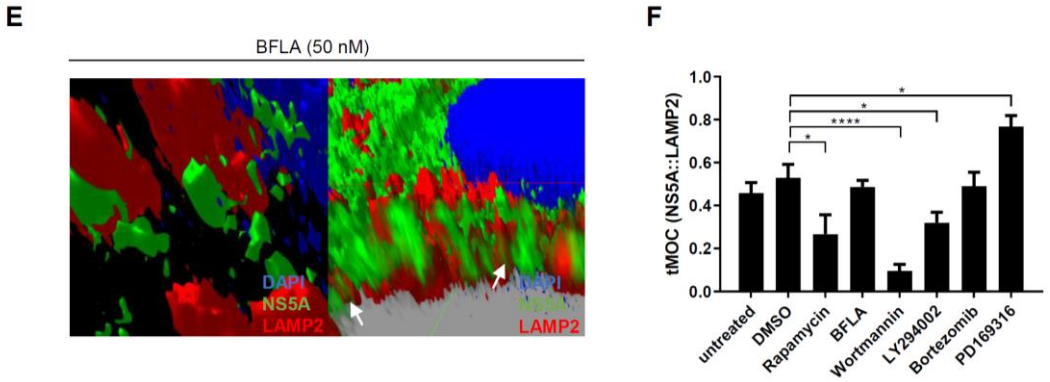

Figure 19 Colocalization and close proximity to LAMP2-positive structures is altered after treatment.
(**A**) CLSM analysis of HCV-positive Huh7.5 cells treated with modulators against autophagy and proteasome. The cells were stained using NS3-(green) and LAMP2-specific (red) antibodies. Nuclei were stained with DAPI (blue). Laser intensity was kept constant. Magnifications, x100 with Zoom-in 2.0. Higher magnification of indicated areas is marked with white squares. Scale bar represents 10 µM; (**B**) Z-stacking (Left) and clipping (Right) of stained, BFLA-treated Huh7.5-Jc1. White square and arrows indicate LAMP2-positve structures together with NS3; (**C**) Colocalization of NS3 and LAMP2-positive structures by tMOC from a minimum of 7 cells (mean ± SEM). Two-tailed unpaired *t*-test, **p<0.01; (**D**) CLSM analysis of HCV-positive Huh7.5 cells treated with modulators against autophagy and proteasome. The cells were stained using NS5A-(green) and LAMP2-specific (red) antibodies. Nuclei were stained with DAPI (blue). Laser intensity was kept constant. Magnifications, x100 with Zoom-in 2.0. Higher magnification of indicated areas is marked with white squares. Scale bar represents 10 µM; (**E**) Z-stacking (Left) and clipping (Right) of stained, BFLA-treated Huh7.5-Jc1. White square and arrows indicate LAMP2-positve structures together with NS5A; (**F**) Colocalization of NS5A and LAMP2-positive structures by tMOC from a minimum of 7 cells (mean ± SEM). Two-tailed unpaired *t*-test, *p<0.05, ****p<0.0001.

5.3.2 Colocalization of NS5B with LAMP2 or PSMB4 decreased after treatment

The distribution of the RNA-dependent RNA polymerase NS5B and the colocalization of NS5B with LAMP2 or PSMB4 was examined by immunofluorescence staining. Huh7.5-Jc1 cells were treated with modulators for autophagy and lysosomes were visualized by a LAMP2 staining. To investigate the fate of NS5B via the UPS, cells were treated with Bortezomib and stained against NS5B and the proteasome subunit beta type 4 (PSMB4). Colocalization of NS proteins with LAMP2-positive structures reflects lysosomes or autolysosomes, which contain NS protein for their disposal. Likewise, a proximity to the proteasomal marker PSMB4 is an evidence of interaction between the proteasome and NS proteins.

While colocalization of NS5B to LAMP2 was absent in untreated and Rapamycin-treated cells, NS5B was in close proximity to LAMP2-positive structures after treatment

with LY294002 and BFLA. In Huh7.5-Jc1 cells incubated with Bortezomib, localization and distribution did not change (Figure 20A).
Calculation of the threshold Mander's overlap coefficient (tMOC) showed less colocalization of about 17% for Rapamycin, 6% for BFLA and 11% for LY294002 when compared to the control, which had a calculated colocalization between NS5B and LAMP2 of about 24% (Figure 20B).
When stained with PSMB4, NS5B had a colocalization of about 36% in untreated and 20% on Bortezomib-treated cells (Figure 20C).

To conclude from this, the colocalization of NS5B to LAMP2 was not solely decreased after Rapamycin, but after each treatment. However, since colocalization of NS5B to PSMB4 in Bortezomib-treated cells was low as well and no accumulation was observed, the proteasome cannot be determined as single degradation route. Therefore, both pathways can be involved for NS5B disposal so far.

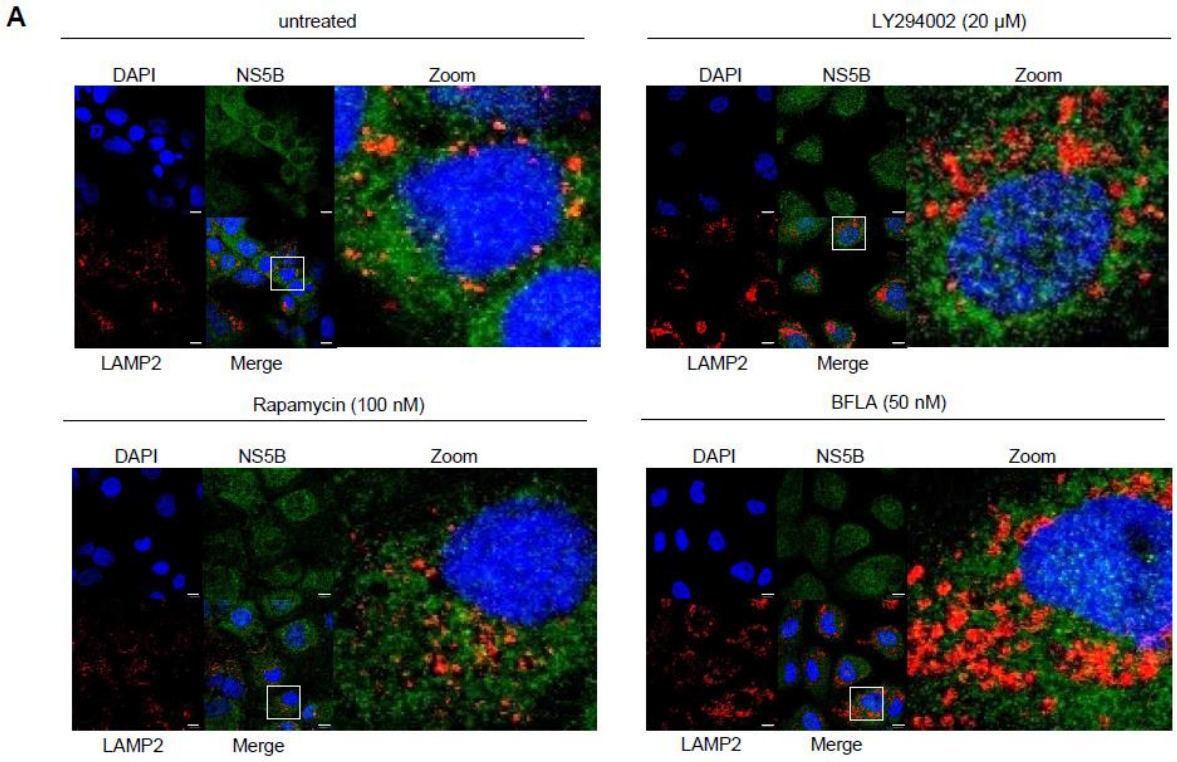

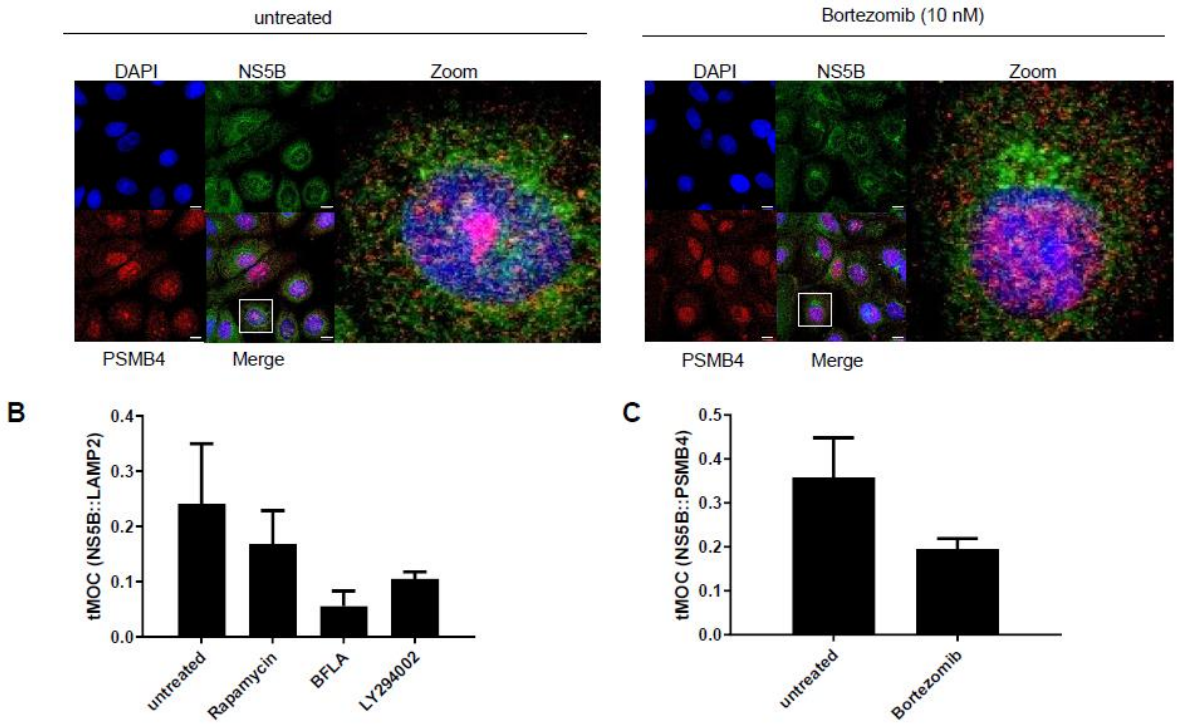

Figure 20 Colocalization of NS5B to LAMP2 and PSMB4 is decreased after modulation.
(**A**) CLSM analysis of HCV-positive Huh7.5 cells treated with modulators against autophagy and proteasome. The cells were stained using NS5B-(green), LAMP2-(red) and PSMB4-specific (red) antibodies. Nuclei were stained with DAPI (blue). Laser intensity was kept constant. Magnifications, x100. Higher magnification of indicated areas is marked with white squares. Scale bar represents 10 µM; (**B**) Colocalization of NS5B to LAMP2-positive structures by tMOC from a minimum of 7 cells (mean ± SEM); (**C**) Colocalization of NS5B to PSMB4-positive structures by tMOC from a minimum of 7 cells (mean ± SEM).

5.3.3 Inhibition of autophagy leads to stronger colocalization of NS4B with LAMP2

The hypothesis was, that autophagy is relevant in the fate of the nonstructural protein NS4B. To investigate the turnover of NS4B, the subgenomic replicon cells Huh9-13 were treated to modulate degradation pathways. Subsequent, the colocalization in fixed cells was investigated by immunofluorescence staining. For this, NS4B was stained as well as lysosomal marker protein LAMP2 or the proteasomal subunit PSMB4 and the colocalization or close proximity between NS4B and LAMP2 or NS4B and PSMB4 determined.

An altered colocalization between NS4B and LAMP2-positive structures was not observed in Rapamycin-treated and LY294002-treated cells when compared to the untreated. Yellow dots, indicating a colocalization to NS4B, were observed after

treatment with BFLA. The proximity of NS4B and PSMB4 was similar between untreated and Bortezomib-treated cells (Figure 21A).

To quantify colocalization, the threshold Mander's overlap coefficient (tMOC) was calculated. The tMOC of untreated Huh9-13 as well as after treatment with Rapamycin and LY294002 was about 17-18%, respectively. A higher tMOC of 26 % for NS4B and LAMP2 was obtained for BFLA-treated Huh9-13 (Figure 21B).

Calculated colocalization of NS4B and PSMB4 via tMOC was 28%, while less was analyzed for Bortezomib with 19 % (Figure 21C).

To sum it up, as a colocalization between NS4B and LAMP2 after BFLA treatment was observed and therefore autolysosomes seem to contain NS4B, autophagic degradation is assumed for this viral protein.

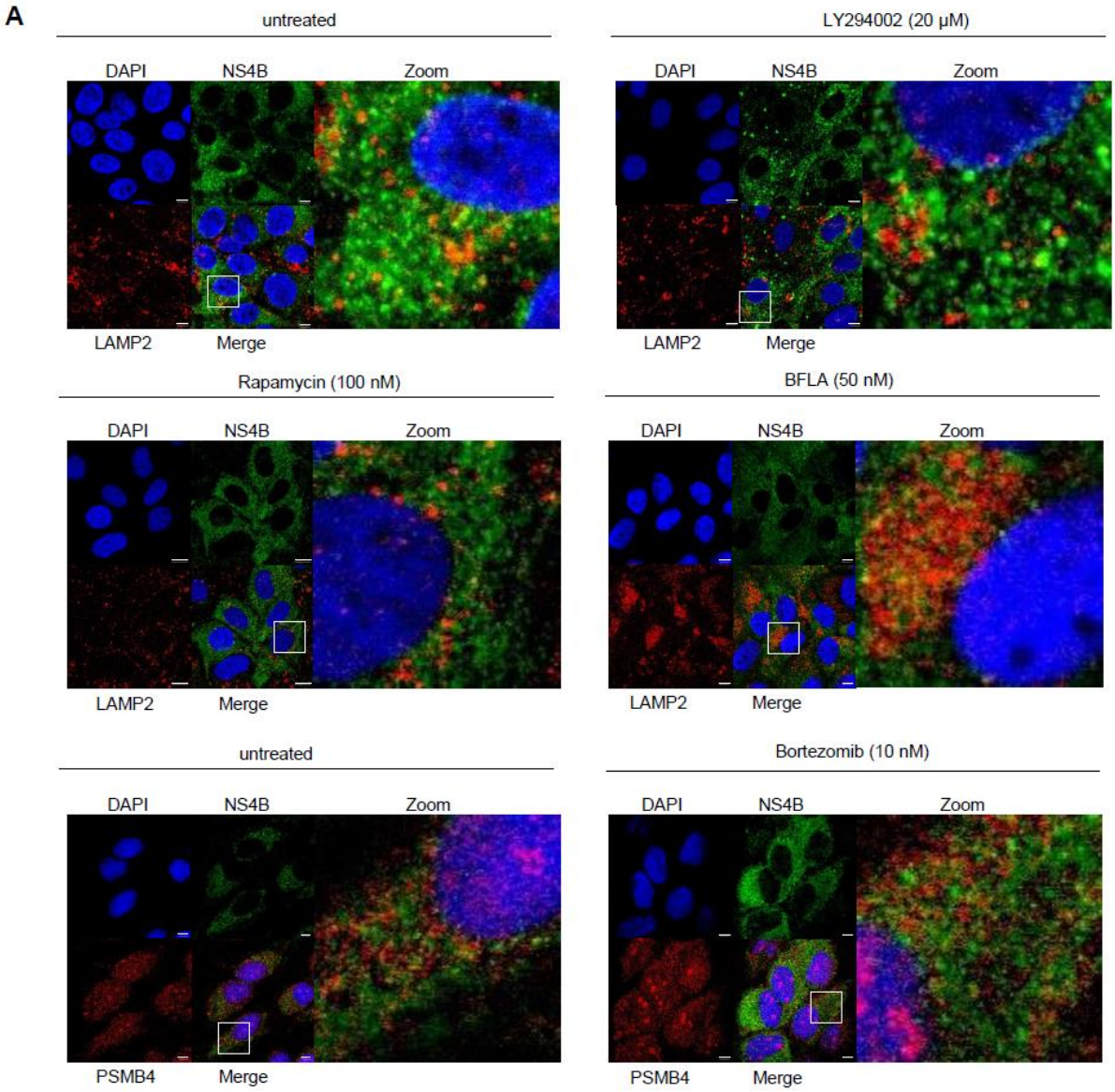

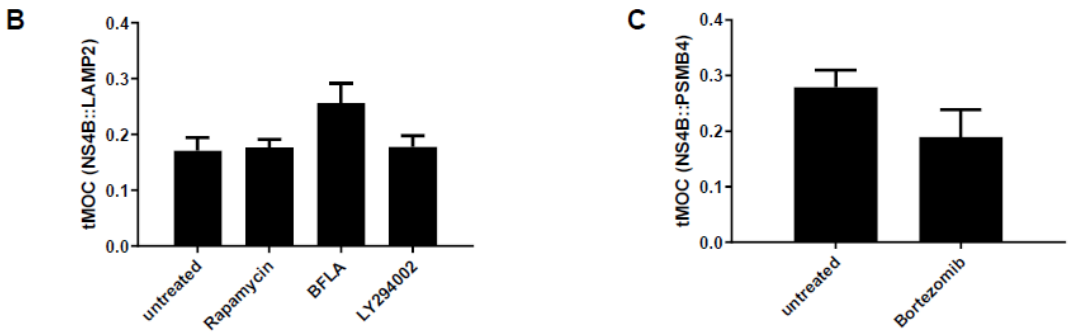

Figure 21 Stronger colocalization of NS4B to LAMP2 after inhibition of autophagy.
(**A**) CLSM analysis of Huh9-13 cells treated with modulators against autophagy and proteasome. The cells were stained using NS4B-(green), LAMP2-(red) and PSMB4-specific (red) antibodies. Nuclei were stained with DAPI (blue). Laser intensity was kept constant. Magnifications, x100 with Zoom-in 2.0. Higher magnification of indicated areas is marked with white squares. Scale bar represents 10 µM; (**B**) Colocalization of NS4B to LAMP2-positive structures by tMOC from a minimum of 7 cells (mean ± SEM); (**C**) Colocalization of NS4B to PSMB4-positive structures by tMOC from a minimum of 7 cells (mean ± SEM).

5.4 Transfection efficiency and duration restrict monitoring of autophagosomal turnover of NS proteins in transient LC3 modulation

A more specific approach to examine the fate of HCV NS proteins is to directly affect autophagy-related proteins by overexpression or knockout. Here, microtubule-associated protein 1A/1B light chain 3B (LC3) was selected for transient overexpression in Huh7.5-Jc1 cells. LC3 is a marker protein for autophagy, as it can be detected at autophagosomes. The transfection efficiency with the LC3 plasmid pcDNA3.1 LC3B was ~20% and can be considered as low. Furthermore, the pUC18 plasmid served as a control. Thereby, the protein signal of each protein of interest in pUC18 transfected cells was set to 1 to obtain the relative protein amount to the LC3 transfected cells.

Western blot analysis of transient LC3-transfected Huh7.5-Jc1 showed a stronger signal for the LC3 band and almost no changes for NS3, NS5A, LAMP2 and p62 bands when compared to the pUC18 control (Figure 22A).
After transfection with pCDNA3.1 LC3B, the amount of LC3 was 7-fold higher than in the control cells, LAMP2 and p62 were unchanged (Figure 22B).
In figure 22C, the detection signal of NS3 and NS5A in pUC18 transfected cells was set to 1, respectively, to obtain the relative protein amount. A significant increase of

quantified NS3 and NS5A up to 1.5-fold was observed after 72 h of transfection with LC3-DNA (Figure 22C).

In immunofluorescence stained Huh7.5-Jc1, cells with a transient overexpression of LC3 showed a strong LC3 signal, when compared to the pUC18 control cells, while no differences in the NS3 and NS5A signal can be observed after transfection (Figure 22D).

To quantify the fluorescence signals, the corrected total cell fluorescence (CTCF) values were determined for NS3 and NS5A. The quantification showed a lower signal for NS3 and a higher signal for NS5A in transient LC3-transfected cells (Figure 22E).

As direct and transient modulation of autophagy by LC3 was supposed to act as an inducer of the autophagic flux, decrease of NS3 and NS5A was expected. However, NS3 and NS5A increase in their protein amount, which can indicate that a transient LC3 transfection is not sufficient to enhance autophagosomal degradation of NS3 and NS5A. Transient LC3 transfection may rather affect viral replication than degradation. In addition, the observations of transient LC3 transfection did not correlate to those of Huh7.5-LC3 infected cells, which harbor exogenous LC3 with a stable long-term expression

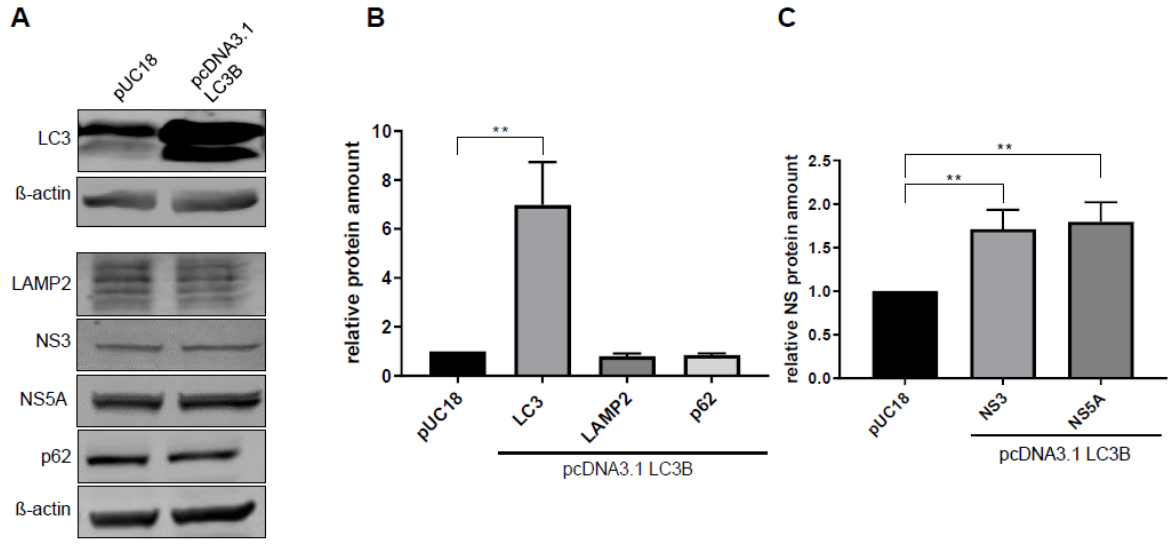

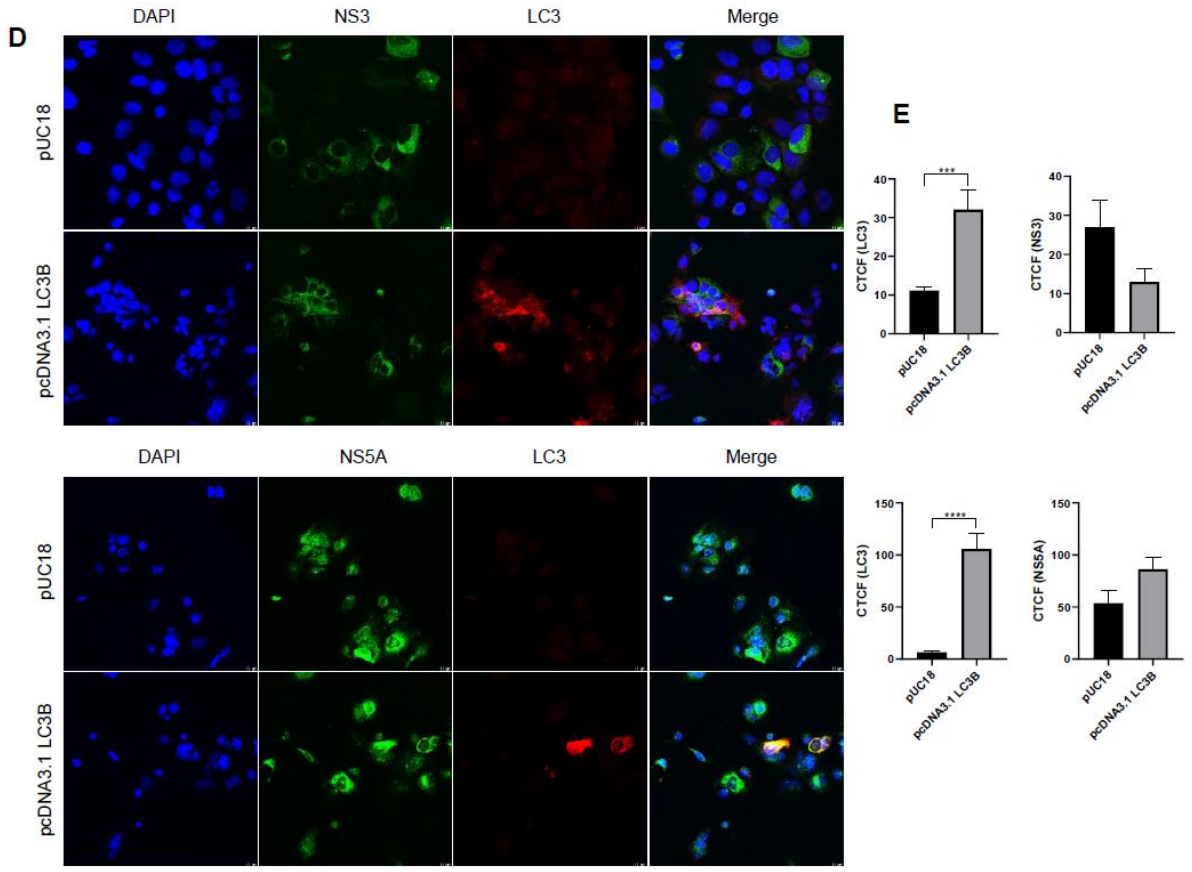

Figure 22 In Huh7.5-Jc1 NS3 and NS5A are increased after transient LC3 overexpression.
(**A**) Western blot analysis of cellular lysates derived from Huh7.5-Jc1 after transfection by PEI with pcDNA3.1 LC3B (1 µg) or pUC18 (1 µg) (control). The cells were analyzed 72 h after transfection using LC3-, LAMP2-, NS3-, NS5A- and p62-specific antibodies. ß-actin served as a loading control; (**B**) Densitometric quantification of LC3, LAMP2 and p62 from five independent experiments. pUC18 transfected cells served as a control and were set as 1 (n=5; mean ± SEM). Two-tailed unpaired *t*-test, **p<0.01; (**C**) Densitometric quantification of NS3 and NS5A from five independent experiments. pUC18 transfected cells served as a control and were set as 1 (n=5; mean ± SEM). Two-tailed unpaired *t*-test, **p<0.01; (**D**) CLSM analysis of HCV-positive Huh7.5 cells transfected with pcDNA3.1 LC3B or pUC18 (control). The cells were stained using NS3- (green) (Top) or NS5A-(green) (Bottom) and LC3-specific (red) antibodies. Nuclei were stained with DAPI (blue). Laser intensity was kept constant. Magnifications, x40. Scale bar represents 10 µM; (**E**) Total fluorescence per cell was calculated using ImageJ software and the following formula: Corrected total cell fluorescence (CTCF) = integrated density - (area of selected cell x mean fluorescence of background readings). In total, a minimum of 4 cells were measured (mean ± SEM). Two-tailed unpaired *t*-test, ***p<0.001, ****p < 0.0001.

5.5 In Huh7.5-LC3 degradation of NS3 and NS5A is enhanced

Transient overexpression of LC3 may be inconvenient to investigate the turnover of NS3 and NS5A due to transfection efficiency and short-term induction. Thus, Huh7.5 with a stable LC3 overexpression were generated and subsequent electroporated with

Jc1 RNA. As in the early stage of HCV infection the viral replication is predominant and in the late stage autophagic protein degradation is enhanced, cells were cultured up to three weeks until lysis (Wang et al. 2015; Shiode et al. 2020).

In Western blot analysis, a weaker signal for NS3 and NS5A was observed. Detected bands for LC3 were slightly stronger and p62 and LAMP2 weaker when compared to mock band (Figure 23A). Quantification of the bands showed a significant 2-fold higher amount of LC3 for Huh7.5-LC3 clone 6 and a significant 3-fold higher amount for Huh7.5-LC3 clone 18 (Figure 23B). The mean of quantified signal from NS3 and NS5A bands was about 60% significantly reduced when compared to the mock control cells (Figure 23C). Quantified LAMP2 and p62 showed a reduced signal in both Huh7.5-LC3 clones (Figure 23D).
To investigate the distribution of NS3 and NS5A and further quantification to the Western blot, Huh7.5-LC3 cells were stained for CLSM. Confocal fluorescence microscopy showed a more pronounced signal of LC3 in Huh7.5-LC3 and a perinuclear stained NS3, while in mock NS3 was found more distributed in the cytoplasm (Figure 23E). The quantified fluorescence by CTCF was higher for LC3 and lower for NS3 than in the mock control cells (Figure 23F).
For NS5A, Huh7.5-LC3 cells had a stronger signal for LC3 and a weaker for NS5A with a more perinuclear localization like NS3 (Figure 23G). CTCF of the cells showed for Huh7.5-LC3 clone 6 a high and for Huh7.5-LC3 clone 18 a slightly increase in LC3, while NS3 and NS5A were reduced (Figure 23H).

The conclusion from these results is, that first autophagy seems to be enhanced indicated by higher amounts of LC3 and lower amounts of LAMP2 and p62. And second, since NS3 and NS5A showed a significant strong decrease in the protein amount, autophagosomal degradation is assumed in the turnover of NS3 and NS5A.

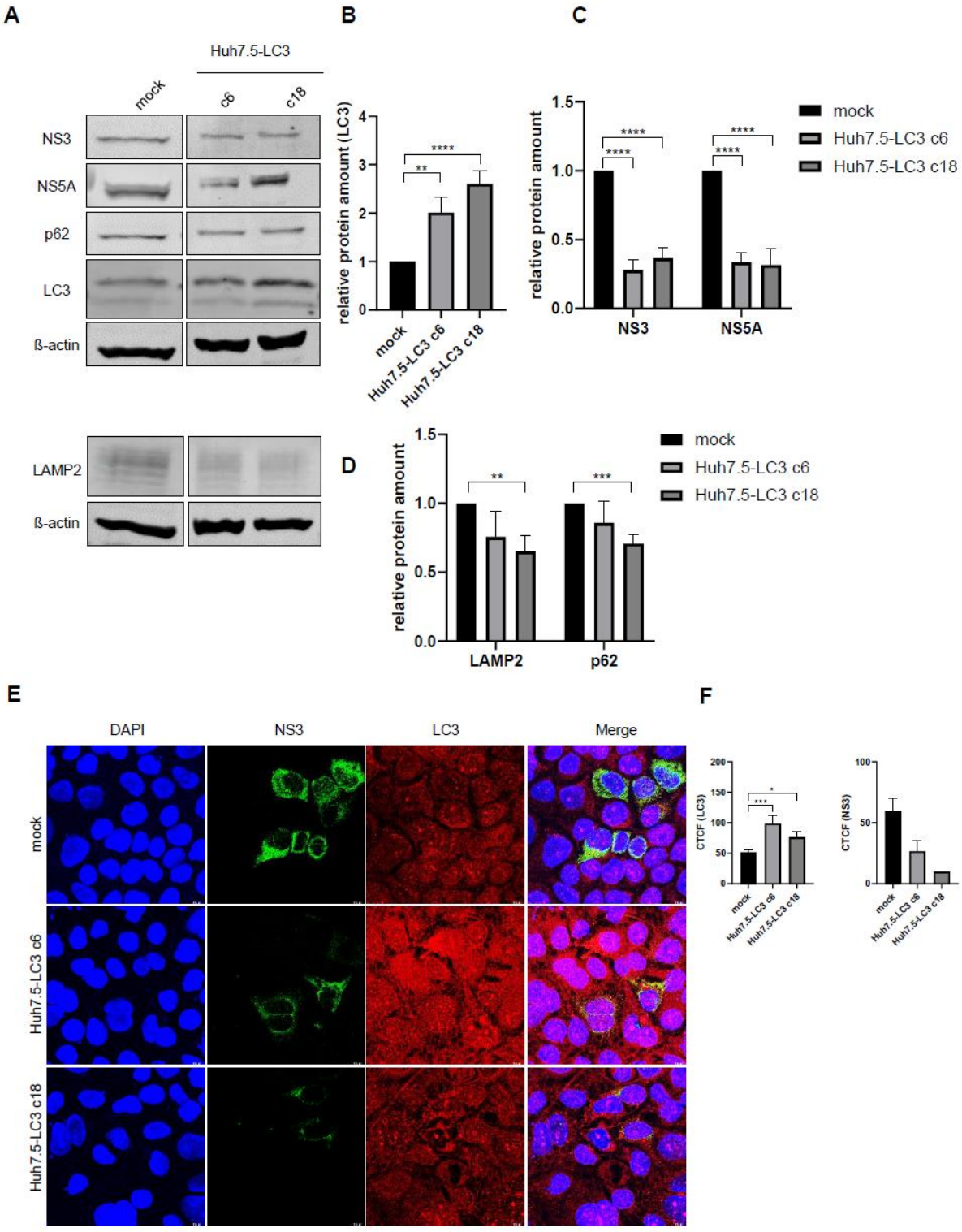
A
Huh7.5-LC3
mock
c6
c18
NS3
NS5A
p62
LC3
ß-actin
LAMP2
ß-actin
B
relative protein amount (LC3)
mock
Huh7.5-LC3 c6
Huh7.5-LC3 c18
C
relative protein amount
NS3
NS5A
mock
Huh7.5-LC3 c6
Huh7.5-LC3 c18
D
relative protein amount
LAMP2
p62
mock
Huh7.5-LC3 c6
Huh7.5-LC3 c18
E
DAPI
NS3
LC3
Merge
mock
Huh7.5-LC3 c6
Huh7.5-LC3 c18
F
CTCF (LC3)
CTCF (NS3)

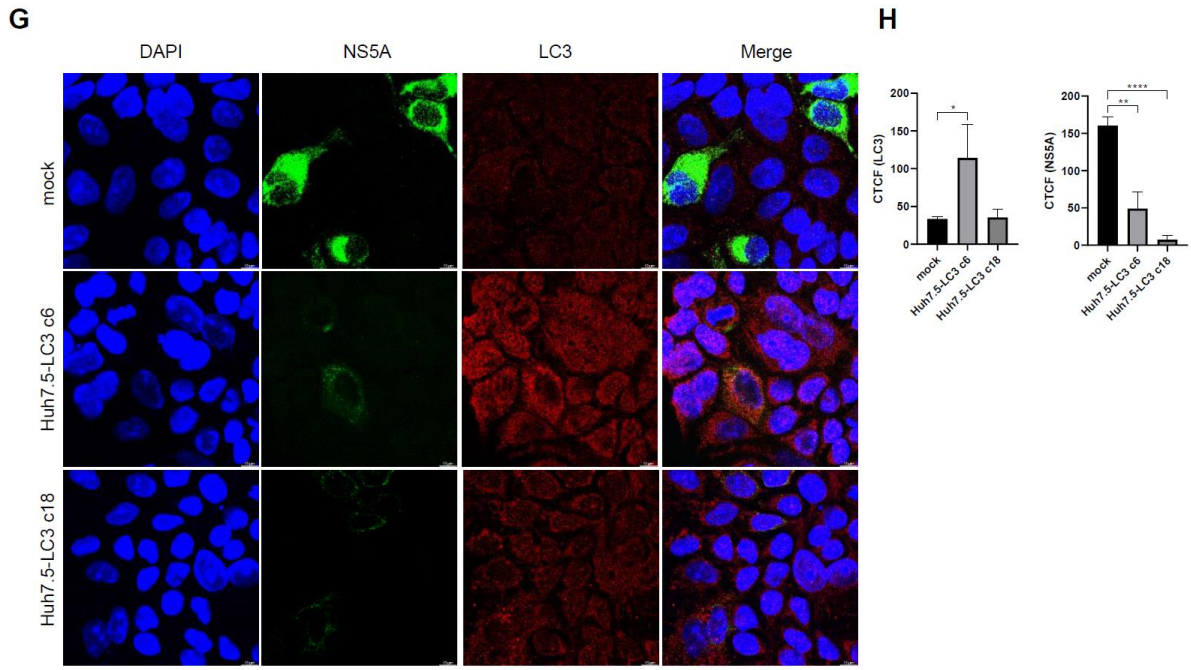

Figure 23 Stable LC3 overexpression leads to reduced amount of NS3 and NS5A. (**A**) Western blot analysis of cellular lysates derived from Huh7.5-LC3 electroporated with Jc1 RNA. The cells were kept in culture and analyzed one week after electroporation using LC3-, LAMP2-, NS3-, NS5A- and p62-specific antibodies. ß-actin served as a loading control; (**B**) Densitometric quantification of LC3 in Huh7.5-LC3 cells from five independent experiments. Mock-transfected cells served as a control and were set as 1 (n=5; mean ± SEM). Two-tailed unpaired *t*-test, **p<0.01, ****p<0.0001; (**C**) Densitometric quantification of NS3 and NS5A in Huh7.5-LC3 cells from five independent experiments. Mock-transfected cells served as a control and were set as 1 (n=5; mean ± SEM). Two-tailed unpaired *t*-test, ****p<0.0001; (**D**) Densitometric quantification of LAMP2 and p62 in Huh7.5-LC3 cells from five independent experiments. Mock-transfected cells served as a control and were set as 1 (n=5; mean ± SEM). Two-tailed unpaired *t*-test, **p<0.01, ***p<0.001; (**E**) CLSM analysis of Huh7.5-LC3 or mock-transfected cells (control) electroporated with Jc1. The cells were stained using NS3- (green) and LC3-specific (red) antibodies. Nuclei were stained with DAPI (blue). Laser intensity was kept constant. Magnifications, x100. Scale bar represents 10 µM; (**F**) Total fluorescence per cell was calculated using ImageJ software and the following formula: Corrected total cell fluorescence (CTCF) = integrated density - (area of selected cell x mean fluorescence of background readings). In total, a minimum of 2 cells were measured (mean ± SEM). Two-tailed unpaired *t*-test, *p<0.05, ***p<0.001; (**G**) CLSM analysis of Huh7.5-LC3 or mock-transfected cells (control) electroporated with Jc1. The cells were stained using NS5A- (green) and LC3-specific (red) antibodies. Nuclei were stained with DAPI (blue). Laser intensity was kept constant. Magnifications, x100. Scale bar represents 10 µM; (**H**) Total fluorescence per cell was calculated using ImageJ software and the following formula: Corrected total cell fluorescence (CTCF) = integrated density - (area of selected cell x mean fluorescence of background readings). In total, a minimum of 2 cells were measured (mean ± SEM). Two-tailed unpaired *t*-test, *p<0.05, **p<0.01, ****p<0.0001.

5.6 LAMP2 knockdown increases the amount of NS proteins

In return to an overexpression to examine the fate of HCV NS proteins, the lysosomal marker protein LAMP2 was used for a knockdown. Huh7.5 were electroporated with Jc1, kept in culture for three weeks and transfected with siRNA for LAMP2 or scrRNA as control. To obtain relative protein amounts between control and knockdown, the Western blot bands of scrRNA transfected cells were set to 1 for each protein.

Western blot analysis of cellular lysates revealed weaker bands for LAMP2 and slightly stronger bands for NS3 and NS5A in Huh7.5-Jc1 with LAMP2 siRNA (Figure 24A). A significant decrease of about 60% for LAMP2 and a 1.5-fold increase for NS3 and NS5A was observed after quantification of Western blot bands when compared to the scrRNA control (Figure 24B, C).
Fluorescence microscopy showed a decrease of LAMP2 in some Huh7.5-Jc1 cells after transfection with LAMP2 siRNA and localization of NS3 and NS5A seemed unchanged (Figure 24D). By calculation of CTCF fluorescence, intensity was reduced for LAMP2 and higher for NS3 and NS5A (Figure 24E).

These results indicate, that the autophagy machinery is relevant for the disposal of NS3 and NS5A, as a gene silencing of the autolysosomal/lysosomal marker protein LAMP2 resulted in a higher amount or an accumulation of the NS proteins in the autophagic flux.

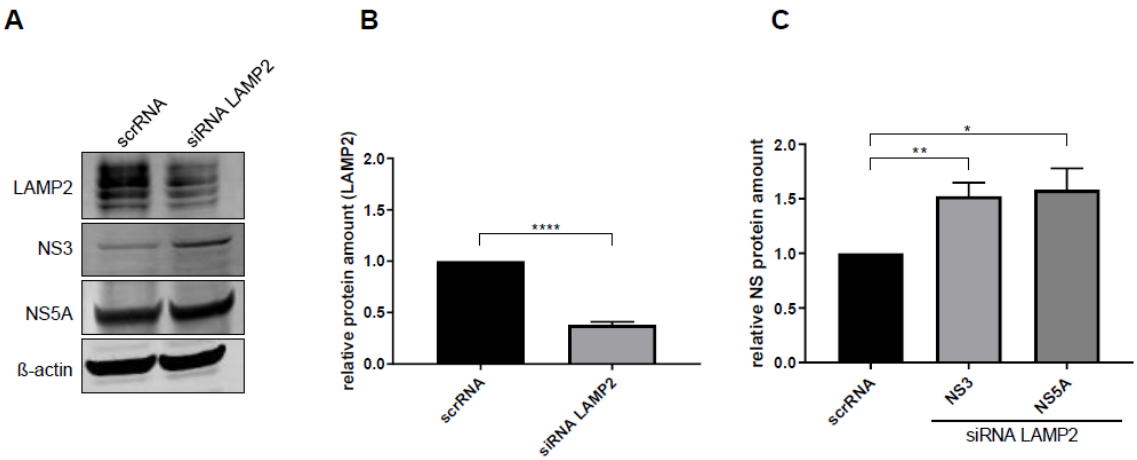

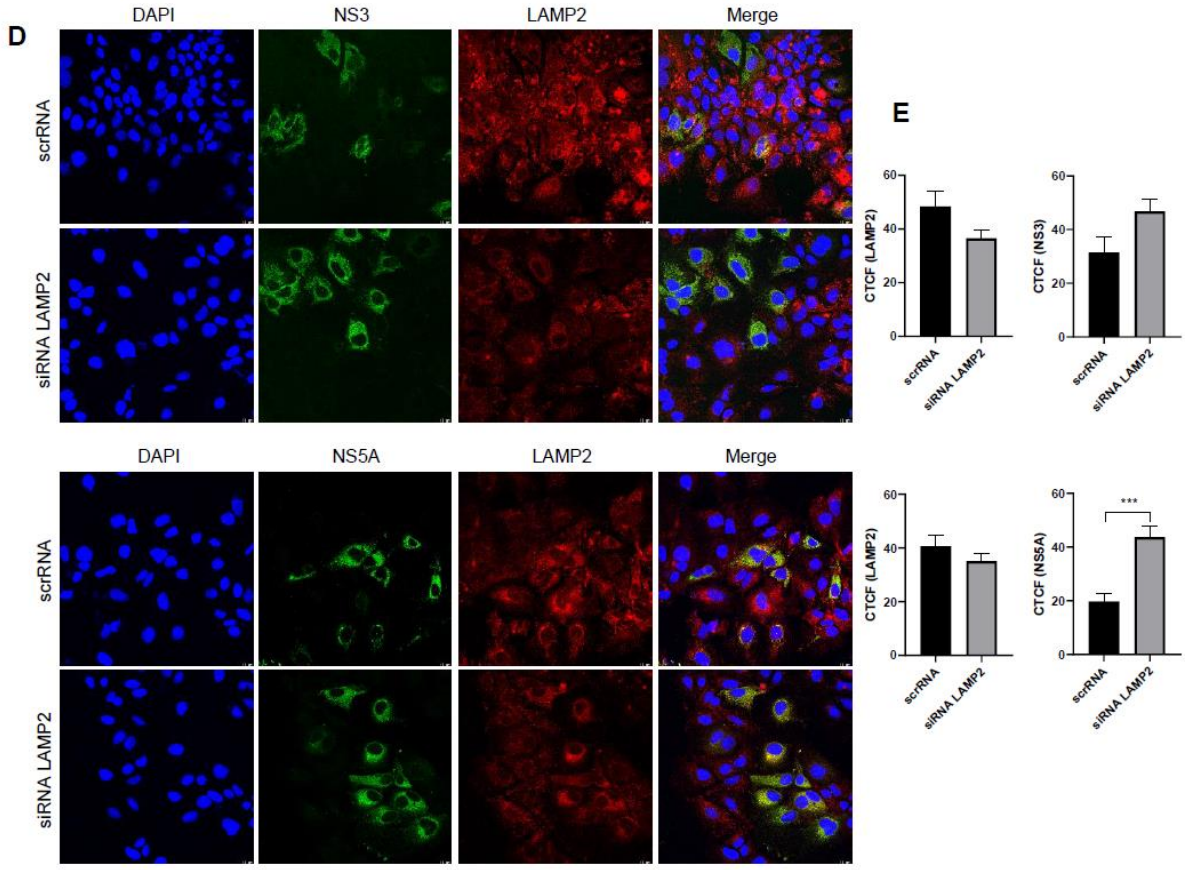

Figure 24 Increased amounts of NS3 and NS5A in LAMP2 knockdown cells. (**A**) Western blot lysates derived from Huh7.5-Jc1 cells transfected with a LAMP2-specific siRNA (50 nM) or scrRNA (50 nM) (control). Cells were harvested and analyzed 96 h after transfection using LAMP2-, NS3- and NS5A-specific antibodies. ß-actin served as a loading control; (**B**) Densitometric quantification of LAMP2 from four independent experiments. scrRNA transfected cells served as a control and were set as 1 (n=4; mean ± SEM). Two-tailed unpaired *t*-test, ****p<0.0001; (**C**) Densitometric quantification of NS3 and NS5A from four independent experiments. scrRNA transfected cells served as a control and were set as 1 (n=4; mean ± SEM). Two-tailed unpaired *t*-test, *p<0.05, **p<0.01; (**D**) CLSM analysis of HCV-positive Huh7.5 cells transfected with siRNA LAMP2 or scrRNA (control). The cells were stained using NS3-(green) (Top) or NS5A-(green) (Bottom) and LAMP2-specific (red) antibodies. Nuclei were stained with DAPI (blue). Laser intensity was kept constant. Magnifications, x40. Scale bar represents 10 µM; (**E**) Total fluorescence per cell was calculated using ImageJ software and the following formula: Corrected total cell fluorescence (CTCF) = integrated density - (area of selected cell x mean fluorescence of background readings). In total, a minimum of 8 cells were measured (mean ± SEM). Two-tailed unpaired *t*-test, ***p<0.001.

5.7 CRISPR-Cas9 knock out of LAMP2 reduces the degradation of NS3 and NS5A

To confirm the LAMP2 siRNA data, LAMP2 knock out by CRISPR-Cas9 in Huh7.5 cells was performed. Thereby, Huh7.5-LAMP2 KO cells have a stable KO in the LAMP2

gene. To investigate the relevance of autophagy on the turnover of NS3 and NS5A, Huh7.5-LAMP2 cells were then electroporated with the HCV Jc1 RNA. The relative protein amount of NS3 and NS5A in the KO cells was than compared with those in off target transfected cells. The off target represents an empty vector and therefore can serve as control.

Again, Western blot analysis showed a stronger signal for NS5A and in particular for NS3 bands in cells with a knock out and faint bands for LAMP2 (Figure 25A). The quantified bands showed almost no amount for LAMP2 (Figure 25B) and a significant increase of NS3 and NS5A up to 1.5-fold higher in the Huh7.5-LAMP2 KO clone 3 and clone 13 compared to Huh7.5-off target clone 4 as control (Figure 25C). Immunofluorescence staining was performed to examine distribution, localization and fluorescence intensity of HCV NS proteins. While LAMP2 staining was absent in Huh7.5-LAMP2 KO cells, the signal for NS3 was stronger and seemed to accumulate in Huh7.5-LAMP2 KO clone 18 (Figure 25D). Fluorescence intensity was quantified and showed higher amounts for NS3 in both Huh7.5-LAMP2 KO clone 3 and clone 13 when compared to the off target control (Figure 25E).
Like NS3, the fluorescence signal for NS5A was slightly stronger for each cell with LAMP2 KO and CTCF quantification showed an increase of fluorescence intensity for NS5A (Figure 25F, G).

According to the observations, reduced degradation of NS3 and NS5A in Huh7.5-LAMP2 KO cells clearly supports the hypothesis, in which the autophagosomal route is relevant for the turnover of NS3 and NS5A.

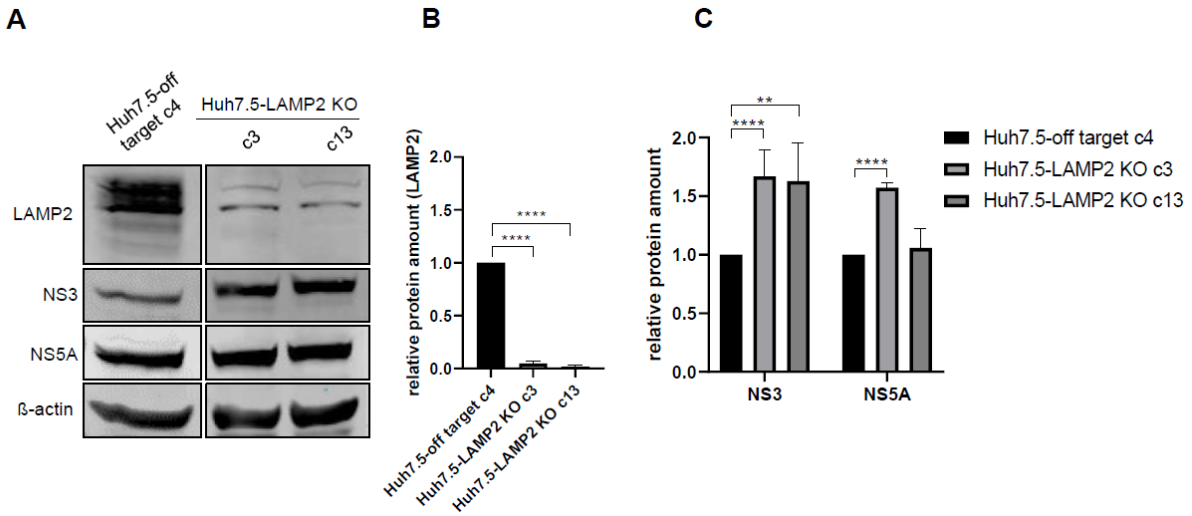

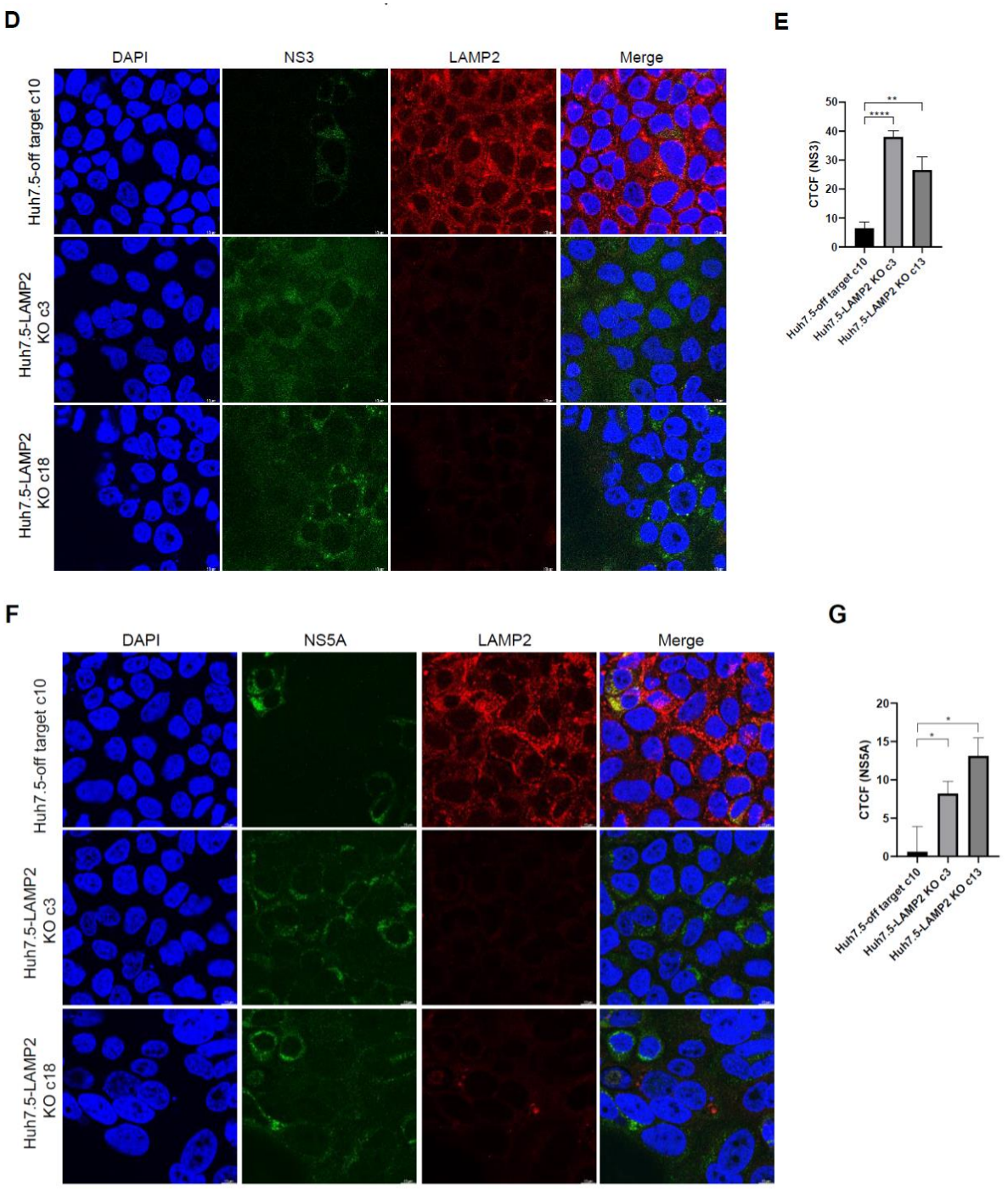

Figure 25 Stable LAMP2 KO leads to increased amount of NS3 and NS5A.
(**A**) Western blot analysis of cellular lysates derived from Huh7.5-LAMP2 KO electroporated with Jc1 RNA. The cells were kept in culture and analyzed one week after electroporation using LAMP2-, NS3-, and NS5A-specific antibodies. ß-actin served as a loading control; (**B**) Densitometric quantification of LAMP2 in Huh7.5-LAMP2 KO cells from six independent experiments. Huh7.5-off target clone 4 cells served as a control and were set as 1 (n=6; mean ± SEM). Two-tailed unpaired *t*-test, ****p<0.0001; (**C**) Densitometric quantification of NS3 and NS5A in Huh7.5-LAMP2 KO cells from six independent experiments. Huh7.5-off target clone 4 cells served as a control and were set as 1 (n=6; mean ± SEM). Two-tailed unpaired *t*-test, **p<0.01, ****p<0.0001; (**D**) CLSM analysis of Huh7.5-LAMP2 KO or Huh7.5-off target clone 10 cells (control) electroporated with Jc1. The cells were stained using NS3- (green) and LAMP2-specific (red) antibodies. Nuclei were stained with DAPI (blue). Laser intensity

was kept constant. Magnifications, x100. Scale bar represents 10 µM; (**E**) Total fluorescence per cell was calculated using ImageJ software and the following formula: Corrected total cell fluorescence (CTCF) = integrated density - (area of selected cell x mean fluorescence of background readings). In total, a minimum of 5 cells were measured (mean ± SEM). Two-tailed unpaired *t*-test, **p<0.01, ****p<0.0001; (**F**) CLSM analysis of Huh7.5-LAMP2 KO or Huh7.5-off target clone 10 cells (control) electroporated with Jc1. The cells were stained using NS5A- (green) and LAMP2-specific (red) antibodies. Nuclei were stained with DAPI (blue). Laser intensity was kept constant. Magnifications, x100. Scale bar represents 10 µM; (**G**) Total fluorescence per cell was calculated using ImageJ software and the following formula: Corrected total cell fluorescence (CTCF) = integrated density - (area of selected cell x mean fluorescence of background readings). In total, a minimum of 5 cells were measured (mean ± SEM). Two-tailed unpaired *t*-test, *p<0.05.

5.8 Isolated autolysosomes harboring NS proteins

To investigate whether NS proteins can be detected in isolated autolysosomes a density gradient ultracentrifugation with Iodixanol was performed. For this purpose, Huh7.5 were electroporated with Jc1 and cultivated three to four weeks until isolation of autolysosomes/lysosomes. To distinguish which host cell organelles beside lysosomes can be detected in the same fractions as NS proteins, several antibodies were used. Again, lysosomal marker protein LAMP2 was used as well as autophagosome marker LC3. EEA1 and Rab7a are markers against early endosomes/MVBs, which can fuse with autophagosomes to amphisomes and then a subsequent fusion with lysosomes to autolysosomes (Fader and Colombo 2009).

In Western blot analysis, fraction 2, 3 and 4 with a respective Iodixanol density of 1.055 g/ml, 1.085 g/ml and 1.094 g/ml were prominent for detection of lysosomal marker protein LAMP2. In the same fractions strong signals for NS3 and NS5A were detected (Figure 26A). The presence of autolysosomes in the isolated fractions were detected by antibodies against Rab7a and LC3. Proteasome subunit beta 5 (PSMB5) was used to exclude proteasome signal in fractions, which were supposed to contain autolysosomes. Iodixanol density was determined by refractive indices of all fractions with a steady increase from fraction 1 to 8 (Figure 26B). Relative protein amount of LAMP2 was the highest in fraction 3 with a density of 1.085 g/ml, while NS3 and NS5A had the highest amount in fractions with the density 1.055 g/ml, 1.085 g/ml and 1.094 g/ml (Figure 26C).

The detection of NS proteins in the same fractions where autolysosomes or precursors of autolysosomes are present is a further confirmation, that the fate of NS3 and NS5A is correlated to autophagy.

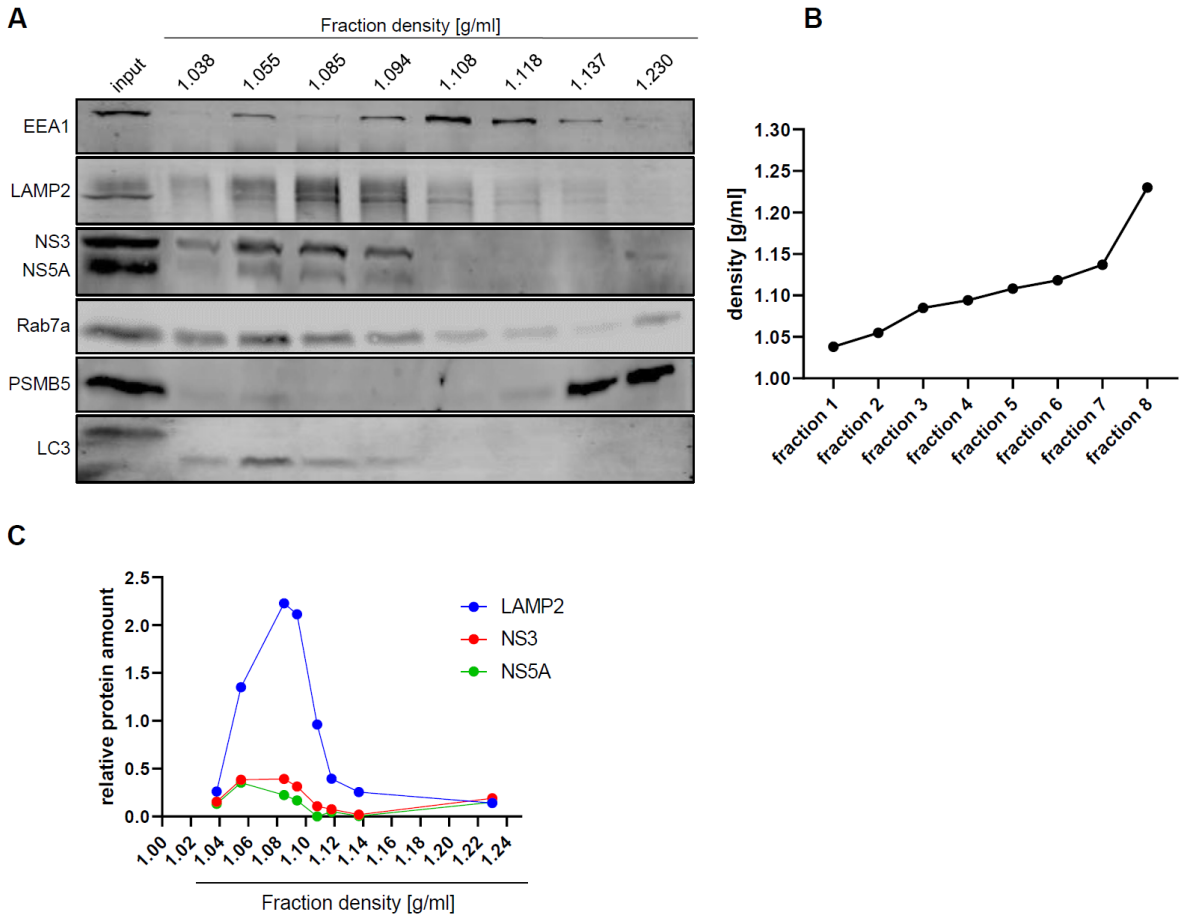

Figure 26 HCV NS proteins can be found in autolysosomes.
(**A**) Western blot analysis of separated cellular organelles in Huh7.5-Jc1. The cells were kept in culture for three weeks and harvested for isolation of autolysosomes by OptiPrep density gradient ultracentrifugation. Different fractions were taken and analyzed using EEA1-, LAMP2-, NS3-, NS5A-, Rab7a, PSMB5- and LC3-specific antibodies; (**B**) Calculated density of Iodixanol-containing fraction 1 to 8 by refractive indices with a standard curve after ultracentrifugation; (**C**) Densitometric quantification of LAMP2, NS3 and NS5A in different fractions of Huh7.5-Jc1 cells after autolysosome isolation. Input of Huh7.5-Jc1 cells served as a control and was set as 1.

5.9 NS proteins and HCV RNA correlate with host membrane proteins of autophagy

To investigate the fate of the excess NS proteins and the role of autophagy, a membrane flotation assay was used to separate cellular compartments, which contain viral NS proteins. The cellular compartments e.g., lysosomes, autolysosomes and HCV-associated membranes, were separated by their densities. The membrane

flotation assay can be performed by a subcellular fractionation with Iodixanol. The NS proteins NS3-NS5B belong to the HCV replicon complex (RC) and can be divided into active and involved in replication or inactive and targeted to autophagy for disposal. RC in different densities together with distinct host compartments after membrane flotation can indicate this active or inactive state of the RC. Then, a replicase assay can validate the activity of the RC (not performed). For this purpose, Huh7.5 cells were transfected by electroporation with Jc1 and several fractions taken after membrane flotation by ultracentrifugation. Beside antibodies against NS3 and NS5A, the lysosomal marker LAMP2 was used for detection of autolysosomes or precursors as well as p62, which is an autophagosome cargo protein. Furthermore, antibodies against the early endosome antigen 1 (EEA1) and Rab7a were used to detect early and late endosomes/MVBs, that can fuse with autophagosomes to amphisomes. Amphisomes then again fuse with lysosomes to autolysosomes (Fader and Colombo 2009). A direct fusion between autophagosomes and lysosomes can occur as well.

Western blot analysis of untreated Huh7.5-Jc1 cells showed weak signals of NS5A and Rab7a at the top of the gradient and strong signal for LAMP2, NS3, NS5A, p62 and Rab7a in lower densities. Moderate signal of EEA1, LAMP2, NS3, NS5A, p62 and Rab7a and faint signals for LAMP2 were found in the higher densities of the gradient. At the bottom of the gradient EEA1, Rab7a and PSMB5 signals were detected (Figure 27A). Refractive indices of iodixanol fractions were used to determine the respective density, which can be seen with three plateaus in Figure 27B. Isolated RNA from HCV positive-Huh7.5 supernatant was synthesized to cDNA to perform RT-qPCR. Values above 1.0 can be considered as positive for HCV RNA, the fold change in RNA amount is depicted on the y-axis. Small amounts of RNA were shown in fraction 2, 8 12 and 18 and high amounts of RNA in fraction 1, 10, 12, 16 and 17 (Figure 27C).

Hence, the NS proteins in untreated Huh7.5-Jc1 cells could be separated into three populations discriminated by their density, which correlated with the three plateaus observed in the measurements of the refractive indices. Moreover, HCV RNA correlate with the three populations, as RNA is present in each population. Thereby, it may can be distinguished between assembly of viral particles, autophagy-associated degradation and replication. In addition, NS3 and NS5A again were detected in the same fractions as LAMP2, suggesting the degradation.

The same experiment was performed with BFLA treatment. As an inhibitor of the vacuolar H^+-ATPase, the acidification of lysosomes and their fusion with autophagosomes/amphisomes is prevented. Through disruption of the autophagic flux, a shift in autophagosomal processes can be obtained e.g., accumulation of the RC.

Protein signals in fractions were more pronounced or shifted. Faint bands of LAMP2 in higher densities of untreated cells were in the BFLA-treated cells now detected at the top at the gradient as well as weak bands for NS5A, p62 and Rab7a. Signals for LAMP2, NS3, NS5A, p62 and Rab7a at lower densities are stronger after BFLA treatment when compared to untreated cells. Again, moderate signals for EEA1, NS3, NS5A, p62 and Rab7a can be observed in higher densities, while faint LAMP2 bands in BFLA-treated cells disappeared. EEA1, Rab7a and PSMB5 signals were detected at the bottom of the gradient (Figure 27D). For Huh7.5-Jc1 treated with BFLA, the measured refractive indices of the fractions were converted to the density and showed three plateaus similar to untreated cells (Figure 27E). In figure 27F, the fold change in the measured RNA amount is depicted on the y-axis, in which all values above the line can be considered as positive for HCV RNA. After treatment, high levels of HCV RNA were measured for fraction 1, 2, 3, 10, 12 and 16 and low levels of HCV RNA for fraction 17 (Figure 27F).

Signal distribution and intensities of the Western blot bands were compared between untreated and BFLA-treated cells and showed for NS3 higher signals in lower densities and weaker signals in higher densities for BFLA-treated cells. Additionally, NS3 signals disappeared in fraction 12 and 13 after use of BFLA (Figure 27G). For NS5A, the same tendency can be observed. In BFLA-treated cells, the NS5A signal is more pronounced in the lower densities and less in the higher densities compared to untreated. A shift can be observed since NS5A could be detected in fraction 2, 3, 12, 18 and 19 in untreated cells, but after treatment in fraction 1 and 2 and absent in fraction 3, 12, 18 and 19 (Figure 27H).

Indeed, a more pronounced RC was detected in lower densities with BFLA as well as a shift between untreated and BFLA-treated Huh7.5-Jc1 cells was observed. This may indicate a shift within the different RC population due to the interference in the autophagic flux.

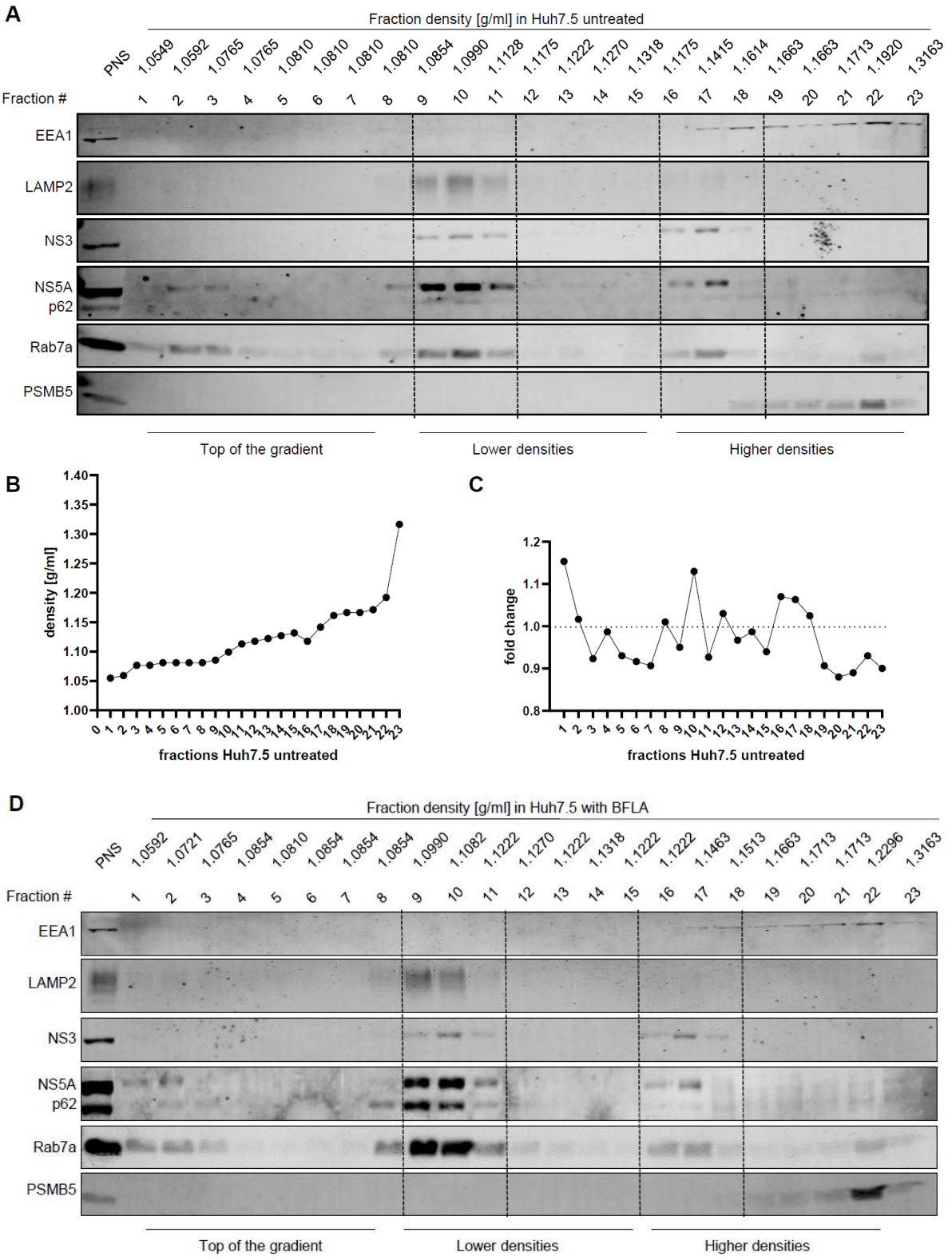
A
Fraction density [g/ml] in Huh7.5 untreated
PNS 1.0549 1.0592 1.0765 1.0765 1.0810 1.0810 1.0810 1.0810 1.0854 1.0990 1.1128 1.1175 1.1222 1.1270 1.1318 1.1175 1.1415 1.1614 1.1663 1.1663 1.1713 1.1920 1.3163
Fraction # 1 2 3 4 5 6 7 8 9 10 11 12 13 14 15 16 17 18 19 20 21 22 23
EEA1
LAMP2
NS3
NS5A
p62
Rab7a
PSMB5
Top of the gradient
Lower densities
Higher densities
B
density [g/ml]
1.40 1.35 1.30 1.25 1.20 1.15 1.10 1.05 1.00
0 1 2 3 4 5 6 7 8 9 10 11 12 13 14 15 16 17 18 19 20 21 22 23
fractions Huh7.5 untreated
C
fold change
1.2 1.1 1.0 0.9 0.8
1 2 3 4 5 6 7 8 9 10 11 12 13 14 15 16 17 18 19 20 21 22 23
fractions Huh7.5 untreated
D
Fraction density [g/ml] in Huh7.5 with BFLA
PNS 1.0592 1.0721 1.0765 1.0854 1.0810 1.0854 1.0854 1.0854 1.0990 1.1082 1.1222 1.1270 1.1222 1.1318 1.1222 1.1222 1.1463 1.1513 1.1663 1.1713 1.1713 1.2296 1.3163
Fraction # 1 2 3 4 5 6 7 8 9 10 11 12 13 14 15 16 17 18 19 20 21 22 23
EEA1
LAMP2
NS3
NS5A
p62
Rab7a
PSMB5
Top of the gradient
Lower densities
Higher densities

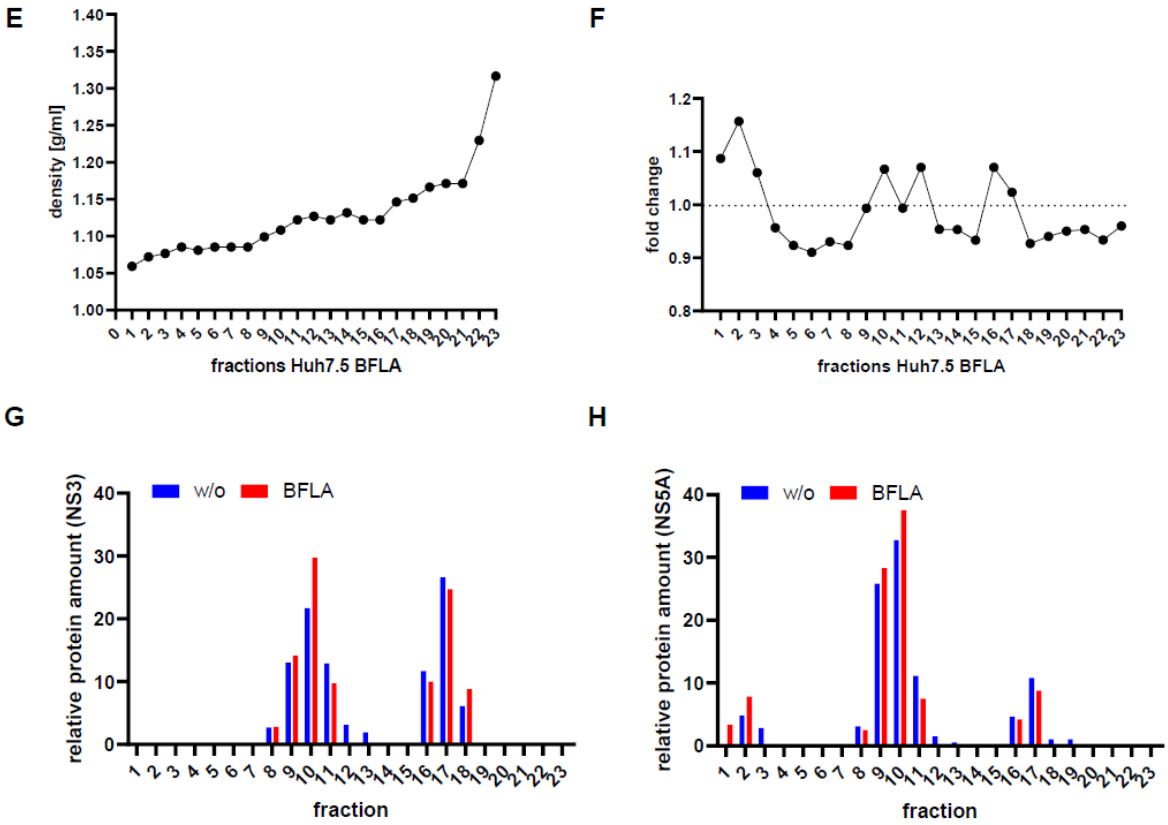

Figure 27 Isolated HCV replicon complex proteins and HCV RNA correlate with autophagy marker proteins.
(**A**) Western blot analysis of untreated Huh7.5-Jc1 after subcellular fractionation in a membrane flotation assay by using EEA1-, LAMP2-, NS3, NS5A-, p62-, Rab7a and PSMB5-specific antibodies. Post-nuclear supernatant (PNS) served as loading control; (**B**) Calculated density of Iodixanol-containing fraction 1 to 23 by refractive indices with a standard curve after ultracentrifugation of untreated cells; (**C**) RT-qPCR analysis of HCV RNA in the supernatant of each fraction from three independent experiments (n=3). HCV qPCR standard served as a control and set to 1; (**D**) Western blot analysis of BFLA-treated Huh7.5-Jc1 after subcellular fractionation in a membrane flotation assay by using EEA1-, LAMP2-, NS3-, NS5A-, p62-, Rab7a and PSMB5-specific antibodies. Post-nuclear supernatant (PNS) served as loading control; (**E**) Calculated density of Iodixanol containing fraction 1 to 23 by refractive indices with a standard curve after ultracentrifugation of BFLA-treated cells; (**F**) RT-qPCR analysis of HCV RNA in the supernatant of each fraction from three independent experiments (n=3). HCV qPCR standard served as a control and set to 1; (**G**) Densitometric quantification and signal distribution of NS3 in untreated and BFLA-treated cells in each fraction related to total NS3 signal in the blot from fraction 1 to 23; (**H**) Densitometric quantification and signal distribution of NS5A in untreated and BFLA-treated cells in each fraction related to total NS5A000 signal in the blot from fraction 1 to 23.

To sum all results up, the different half-lives of NS3, NS5A, NS5B and NS4B after the use of different modulators against autophagy and the UPS gave the first hint on the turnover of the viral nonstructural proteins and the relevance of autophagy for this. The data roughly speaking for autophagy for NS5A and NS4B as half-life was prolonged when autophagy was inhibited. However, for NS3 and NS5B the UPS is involved in degradation as well, or rather an equilibrium between these two pathways, as half-life is altered according to inhibition or activation of each pathway. Regarding NS5A, the two phosphorylation states seem to act different as hyperphosphorylated NS5A may underlying a strong time-dependent degradation.

Immunofluorescence staining of NS proteins and LAMP2 showed LAMP2-positive structures containing NS proteins, which was more pronounced when using inhibitors for autophagy, suggesting a targeting to autolysosomal organelles for disposal.

The transient LC3 overexpression was not sufficient to enhance the autophagic flux and the degradation of NS3 and NS5A, which might be due to the low transfection efficiency and the importance of the duration in overexpressing the LC3 protein.

However, Huh7.5-LC3 cells with a stable and long-term LC3 overexpression resulted in a strong decrease of NS3 and NS5A and reflect an enhanced turnover regarding enhanced autophagosomal degradation.

Vice versa to the overexpression, a gene silencing and a CRISPR-Cas9 KO of LAMP2 was performed, that clearly disrupted the degradation of NS3 and NS5A and underpin the hypothesis in which autophagy is crucial for the disposal.

A stronger focus on autolysosomes/lysosomes by their isolation showed NS3 and NS5A to be correlated with LAMP2-positive compartments. Here, it clearly shows autolysosomes, which originate from one of the two different maturation routes: The fusion between autophagosomes and EE/MVBs to amphisomes due to detection of LC3, EEA1 and Rab7a, followed by fusion with lysosomes (detection of LAMP2).

The last validation to confirm the relevance of autophagy on the turnover of NS proteins was the membrane flotation assay. Here, cellular compartments containing NS proteins could be separated and revealed three different populations of the viral RC in close correlation with autophagy-associated organelles. By interrupting the autophagic flux through inhibition, the relation between replication and degradation in HCV-associated membranes was reflected due to a shift of NS proteins and RNA towards degradation.

6 Discussion

The nonstructural proteins of HCV play an essential role for the processing of the polyprotein and the viral RNA replication. At the so-called membranous web, which is composed of ER-derived membranes, LDs and double-membrane vesicles, the RNA replication takes place (Egger et al. 2002; Romero-Brey et al. 2012; Ferraris et al. 2010). With the need of autophagic membranes and proteins, the virus exploits the cellular autophagy machinery for its replication. The HCV RNA genome is replicated by the replicon complex, which is composed of the nonstructural proteins NS3 to NS5B (Bartenschlager et al. 2010). Quantitative analysis of the replicon complex showed a major intracellular excess of NS proteins compared to viral RNA and led to the assumption that the majority of NS proteins is not involved in replication (Quinkert et al. 2005). Second aspect is the release of structural proteins as viral particles, but no accumulation of nonstructural proteins occurs in the host cell. The close association of HCV to autophagy raises the question if the disposal of excess NS proteins is implemented by the autophagosomal machinery.

The nonstructural proteins of the replicon complex NS5B, NS4B, but mainly NS3 and NS5A were chosen in this work. NS4B plays an important role in the formation of the membranous web and the replicon complex, while NS5B represents the RNA-dependent RNA polymerase. NS3 is required for the cleavage of the viral polyprotein and NS5A is involved in viral assembly. Both NS3 and NS5A are important for viral replication and impair the host immunity (Ashfaq et al. 2011). The idea of autophagosomal degradation, especially for NS5A, is not a new concept. The data provides the relevance of this crucial cell process to the life cycle of HCV with focus on the fate of the NS proteins.

6.1 NS3 degradation is balanced, but NS5A favors autophagy

Under nutrient-rich conditions the serine/threonine kinase mechanistic target of rapamycin (mTOR kinase) represses autophagy through phosphorylation of the Unc-like kinase 1 and 2 (ULK1/2-complex) (Alers et al. 2012). Beside events like starvation or oxidative stress, the kinase activity of mTOR can be inhibited by Rapamycin. Short half-life of NS3, NS5A and basally phosphorylated NS5A can be a result by enhanced autophagy. Less calculated colocalization of NS3 and NS5A to LAMP2 in immunostained cells verifies enhanced autolysosomal degradation.

In the late stage of autophagy, Bafilomycin A1 (BFLA) impairs acidification of lysosomes by the vacuolar H+-ATPase and therefore blocks the fusion of autophagosomes and lysosomes. NS3 has been shown to be quite pH-sensitive and more stable in an acidic environment under a pH of 6.4 where a more open conformation contributes to the helicase function (Ventura et al. 2014). Therefore, under pH-neutral conditions NS3 could lose stability and can be targeted to degradation, which leads to a short half-life and an equal colocalization to LAMP2 with BFLA as for untreated and DMSO-treated cells. Prolonged half-life of NS5A and basally phosphorylated NS5A with BFLA assume an accumulation and reduced degradation by the autophagosomal pathway.

The inhibition of the phosphatidylinositol-3-kinase (PI3K) prevents autophagosome formation in the early stage of autophagy. The two reagents Wortmannin and LY294002 inhibit the PI3K, but differ in their target spectrum of inhibition. Wortmannin is an irreversible, covalent inhibitor with little specificity to the members of PI3K family and can inhibit mitogen-activated protein kinase (MAPK) in high concentrations. The reagent LY294002 is a reversible, more specific inhibitor of class I PI3K subunit p110 with three isoforms α/δ/β and more stable in solution than Wortmannin. Less stability and low specificity of Wortmannin to the isoforms of the PI3K subunits could explain a less strong increase of half-life for NS3, NS5A and basally phosphorylated NS5A after treatment, while in cells treated with LY294002 the half-life was shown to be even more extended. Furthermore, the ability of Wortmannin to inhibit the p38 MAPK in high concentrations can enhance proteasomal degradation and cause shorter half-lives and less colocalization to LAMP2-positive structures as seen for NS5A.

Since proteasomal degradation is assumed to play a role in the turnover of NS proteins as well, modulation of the ubiquitin-proteasome (UPS) was included in this work. The half-life and colocalization to LAMP2 for NS3, NS5A and NS5A phosphorylation states in cells treated with Bortezomib and PD169316 was examined. Bortezomib is a well-known 20S proteasome inhibitor and PD169316 enhances proteasomal degradation via inhibition of the p38 MAPK (Leestemaker et al. 2017). The data showed an increase of half-life for NS3, NS5A and basally phosphorylated NS5A after use of Bortezomib and a slight decrease for PD169316-treated cells, suggesting an involvement of the UPS in the turnover of NS proteins.

The results showed a similar extension of the half-life for NS3, NS5A and basally phosphorylated NS5A between inhibition of autophagy and the UPS. The activation of

endoplasmic reticulum (ER)-stress induces unfolded protein response (UPR) where misfolded proteins are usually degraded through the UPS. It has been found that during UPR, a cross-talk between autophagy and the UPS is prevalent (Korolchuk et al. 2010). Degradation by UPS is restricted to soluble proteins and autophagy to insoluble like aggregates or protein complexes (Ding and Yin 2008). Furthermore, previous studies showed an induction of ER-stress and the resulting UPR by the hepatitis C virus (Tardif et al. 2002). This leads to the assumption that autophagy is involved in the turnover of NS proteins in an equilibrium with the UPS.

However, colocalization of NS3 and NS5A to LAMP2 is quite low when the proteasome is inhibited with Bortezomib. Hence, autolysosomal degradation is speculated to be more distinct than proteasomal. Furthermore, treatment with the same modulators but stained *vice versa* with the proteasome subunit beta type 4 (PSMB4) showed in Bortezomib-treated cells not a higher but an equal colocalization to PSMB4 when compared to BFLA (data not shown). These observations may reflect a stronger influence of autophagy in the turnover of NS3 and NS5A, but still a high probability of the pH-sensitive NS3 to be targeted to the proteasome as well.

6.2 Delayed degradation of hyperphosphorylated NS5A

A prolonged half-life of hyperphosphorylated NS5A in special with autophagy-inducing Rapamycin was observed. Beside HCV replication, autophagy is required for the release of viral particles (Ploen and Hildt 2015). Previous data showed that hyperphosphorylated NS5A takes part in viral assembly and release, while basally phosphorylated NS5A is required for HCV replication (Masaki et al. 2014; Goonawardane et al. 2017). Since treatment with Rapamycin was performed 16 h before Cycloheximide was added to prevent *de novo* protein translation, elevated levels of autophagosomal processes could have an effect on the hyperphosphorylation of NS5A. Higher half-life with Rapamycin may result from accumulated hyperphosphorylated NS5A from the assembly site. Another fact that supports this assumption of accumulation is the increased release of viral particle, while RNA replication levels stay the same, like it is a hallmark for the Jc1 construct (Pietschmann et al. 2006).

As an inhibitor for the p38 MAPK, PD169316 can not only lead to the activation of proteasomal degradation, but to a down-regulated autophagy. A previous study showed a phosphorylation of Atg5 by p38 MAPK, which inhibits the function of Atg5

and prevents the insertion of LC3 into autophagosomal membranes (Keil et al. 2013). Further on, p38 MAPK phosphorylates ULK1, preventing it from binding to Atg13 and reduces autophagy (He et al. 2018). Stronger colocalization of LAMP2 and NS5A by using PD169316 could reflect the hyperphosphorylated state of NS5A, as half-life is slightly increased for hyperphosphorylated NS5A. The ratio of hyperphosphorylated to basal phosphorylated NS5A was mainly unaffected after incubation with proteasome modulators and CHX. However, cells incubated with Rapamycin showed a decreased quotient from hyper to basal, suggesting disposal of hyperphosphorylated NS5A via autophagy. Therefore, in addition to a potential accumulation by Rapamycin and PD169316, a delayed degradation of hyperphosphorylated NS5A is suggested. NS5A exists as free protein in the cytoplasm or bound in membranes. Hence, hyperphosphorylated NS5A may occur more in the bounded form and the high phosphorylation prevents it from degradation, while basal phosphorylated NS5A represents the majority of the free NS5A and is degraded first. To further examine the difference in degradation for both populations, the phosphorylation site at the serine residue, e.g. S225 or S235, can be manipulated (Ross-Thriepland et al. 2015; Lee et al. 2016b). For this purpose, phosphomimetic mutations can be performed as shown in further studies The NS5A phosphorylation occurs at the serine residue, but the replacement with aspartic acid acts as a mimicry for the phosphorylation form of NS5A, while exchange with alanine keeps the unphosphorylated form (Ross-Thriepland et al. 2015). Furthermore, hypo- and hyperphosphorylated NS5A could be monitored indirect by detection of the phosphorylation state of serine 229, since this residue balances the NS5A phosphorylation forms (Tsai et al. 2019).

6.3 Autophagy and UPS is assumed for NS5B turnover

Since the half-life of NS5B was prolonged after inhibition of autophagy and shortened after induction, the autolysosomal degradation seemed to be involved. Half-life was slightly increased with Bortezomib and lower after use of PD169316. However, colocalization of NS5B and proteasomal subunit beta type 4 (PSMB4) was less compared to the control. This effect can arise from the ability of Bortezomib to induce ER stress and therefore autophagosomal degradation of NS5B (Boccadoro et al. 2005; Kroemer et al. 2010). By the use of BFLA, an inhibition of viral infection can occur, which could explain the low tMOC of NS5B and LAMP2 (Meertens et al. 2006). Viral particles enter the cell via clathrin-mediated endocytosis, followed by a fusion between

the viral and the endosomal membrane through acidification (Dubuisson and Cosset 2014). The v-ATPase is required for acidification, but inhibited by BFLA resulting in the inhibition of the viral infection. Furthermore, BFLA is known to inhibit the viral replication, which can be an explanation for the low effect on half-life and decreased colocalization between RNA-dependent RNA polymerase NS5B and LAMP2 (Meertens et al. 2006).

In further studies in which the proteasomal pathway is implied, the RRM2 (ribonucleotide reductase M2) was found to protect NS5B from its degradation via hPLIC1 (human homolog 1 of protein linking integrin-associated protein and cytoskeleton) (Kitab et al. 2019). Probably, other approaches are necessary to suppress cellular and viral protection against disposal and to target NS5B to degradation.

6.4 Degradation of NS4B is strongly affected by autophagy

In Huh9-13 cells incubated with BFLA, the half-life was strongly prolonged and localization to LAMP2-structures increased, indicating an accumulation in the blocked autolysosomal pathway. Moreover, induction of autophagy by Rapamycin showed a lower half-life. Therefore, NS4B seems to favor the autophagosomal-lysosomal degradation, which is further underpinned by the use of Bortezomib. No stronger colocalization of NS4B with PSMB4 was found with Bortezomib and half-life was slightly altered after the incubation with proteasomal modulators. This indicates less impact of the UPS on the turnover of NS4B.

The membrane localization of NS3 is mediated by a small α-helix and its interaction with NS4A (Bartenschlager et al. 2013). In addition, the proteasome favors soluble proteins, which can contribute to the turnover of NS3 by both degradation pathways (Ding and Yin 2008). On the contrary, the hydrophobic NS4B protein contains four transmembrane domains, suggesting a stronger membrane insertion (Lundin et al. 2006; Gouttenoire et al. 2010a). NS4B was shown to form oligomers, which further strengthen the hypothesis of an autophagosomal pathway (Yu et al. 2006; Gouttenoire et al. 2010a).

The weak effect of Wortmannin and LY294002 on half-life may arise from the early interaction of NS4B with autophagosomal structures. The membrane-associated protein induces distinct membrane alterations to form the membranous web (Egger et al. 2002). NS4B interacts with Rab5 and Vps34 in the early stage of autophagy and

can be sufficient to induce it (Su et al. 2011). Therefore, an inhibition of the PI3K by Wortmannin or LY294002 might be less effective in case of NS4B.

6.5 LC3 and LAMP2 are required for degradation of NS3 and NS5A

To confirm the findings from chemical inhibition and to focus more on autophagy, overexpression and downmodulation of autophagosomal and lysosomal proteins as a more specific approach was used. The data showed that a transient transfection of LC3 for 3 days may have not the same impact on the degradation like a stable overexpression. A simple explanation could be the low transfection efficiency and the short duration of the LC3 transfection.

A more complex explanation is the balance between replication and degradation during autophagy. Probably, this approach is more suitable to monitor the relation between autophagy and HCV replication than to degradation. Since the LC3-level was 7-fold higher in transient transfected cells but only up to 2-fold higher in the Huh7.5-LC3, it is assumed that strongly pronounced autophagy-related proteins may have more influence on replication than degradation and therefore lead to the higher amount of new replicated NS3 and NS5A. A decrease of p62 or LAMP2 was not observed, which indicates no enhancement of autophagy. Conversely, a transient LAMP2 KO for 5 days with the CRISPR-Cas9 LAMP2 KO-plasmid led to a strong decline for NS3 and NS5A and suppose a higher use of autophagy in modified replication again than on degradation, which was confirmed by an affected Core formation in Bodipy-stained LDs (data not shown). It is assumed that short-term gene modulation by plasmid transfection first affects HCV replication and with long-term a switch to the degradation is executed, where the protection for disposal of HCV proteins by replication or host cell factors is no longer given. In addition, multiple studies have indicated a delay in autophagosomal-lysosomal fusion in HCV infected cells and thereby an accumulation of autophagosomes in the early stage of infection (Chu and Ou 2021). The delayed maturation of autophagosomes was found to be due to different induction of Rubicon and UVRAG (UV radiation resistance-associated gene protein) proteins by HCV (Wang et al. 2015; Shiode et al. 2020). In the early stage of infection, Rubicon was upregulated, which inhibited the fusion, while in the late stage UVRAG was upregulated to overcome the inhibitory effect of Rubicon. Therefore, completion of the autophagic flux is may in a late stage of infection and a longer duration of LC3 overexpression is needed to monitor the turnover.

In the generated Huh7.5-LC3, overexpression of LC3 seemed to be more established and indeed leads to significant decreased amounts of NS3 and NS5A. Besides, reduction of p62 and LAMP2 suppose an enhanced autolysosomal pathway.
To approach a downregulation of lysosomal marker protein LAMP2, gene silencing by siRNA was performed. This method was more efficient to reduce LAMP2 than transient transfection with the LAMP2 KO plasmid. LAMP2 was decreased about 60% whereas NS3 and NS5A levels were elevated in Western blot and fluorescence intensity analysis. These results suggest an impaired lysosomal degradation by the gene silencing of LAMP2 in the need of autophagy for the fate of NS proteins.
Due to CRISPR-Cas9 knock out and long-term cultivation, LAMP2 could be further reduced in the Huh7.5-LAMP2 KO cell line. Characterization of both KO clones revealed a missense mutation and two deletions for clone 3 as well as nucleotide insertion for clone 13 in the LAMP2 gene with altered amino acids as a result (data not shown). Thus, signals for LAMP2 in the analysis can be considered as left-over of glycosylation, but principally as unfunctional LAMP2. However, accumulation of NS3 and NS5A could not be enhanced when compared to the gene silencing and a potentially limit of turnover seemed to be reached.
With additional inhibition of viral replication more insights into the autolysosomal degradation process in HCV-infected cells could be gained.

6.6 Autolysosomes are involved in the turnover of NS3 and NS5A

To exclude modulated replication in investigating the turnover, autolysosomes were isolated and *vice versa* the HCV replicon complex. Interestingly, NS3 and NS5A were observed to be prominent in the same specific densities where autolysosomal proteins like LAMP2, Rab7a and LC3 were detected. Rab7 GTPase together with Rab5 regulate the maturation of EE to LE by a conversion of the Rab proteins, which results in the loss of Rab5 and transfer of Rab7a to LEs (Hyttinen et al. 2013; Kucera et al. 2016; Guerra and Bucci 2016). Small amounts of EEA1 as well as Rab7a suggest early endosomes or amphisomes fused with autophagosomes, as an intermediate before merging with lysosomes. Since LAMP2 is restricted to lysosomes and endosomes, which are required for disposal and recycling of proteins, it can be proven that degradation occurs here without doubts to impact the replication.

6.7 Inactive RC is degraded by autolysosomes

Similar results were observed when autophagy-associated membranes together with the replicon complex and RNA were isolated and fractions in a broad range were taken from the OptiPrep gradient. Again, NS3 and NS5A could be detected in an iodixanol density of about 1.08 g/ml and 1.09 g/ml together with LAMP2.

Treatment with BFLA led to a stronger signal of NS3 and NS5A along with LAMP2 and revealed reduced autolysosomal degradation. Furthermore, HCV RNA is less and split in two peaks in low density fractions. According to this, here, an inactive replicon complex could be displayed and targeted to degradation. In the higher densities, NS3 and NS5A as well as HCV RNA was found, but absence of LAMP2. This indicates RNA to be processed in active replication complex. A second hint is the loss of RNA in fraction 18 when autophagy is inhibited by BFLA, since autophagy is required for viral replication. In addition to the supposed replication in higher densities, EEA1 and Rab7a were reported to play a role in the membranous web and its trafficking of the required proteins (Romero-Brey et al. 2012). In HCV replication, Rab7 is relevant for the formation of the replicon complex, while during release Rab7a is associated with MVBs (Elgner et al. 2018).

Moreover, inhibition through BFLA led to a slight shift of the NS3 and NS5A bands from the higher to the lower densities regarding signal presence and intensity. This means in the higher densities NS3 and NS5A were less pronounced, but in the lower more when compared to untreated cells. These findings may reflect the shift from active to an inactive RC to the lower density and subsequent targeting for degradation.

No bands for NS3 and faint bands of NS5A were detected in the top of the gradient, but HCV RNA had the highest peak and Rab7a was prevalent. Here, isolated infectious viral particles are assumed. In previous studies, accumulation of lipoviral particles was found at densities of 1.01–1.12 g/ml and 1.13–1.14 g/ml with higher infectivity at lower densities (Bartenschlager et al. 2004).

To further confirm this theory and to better distinguish between active and inactive RC, a cell-free *in-vitro* replicase activity assays could be performed. As an alternative to the treatment with BFLA, a knockdown of Stx17 could inhibit autophagosome-lysosome fusion without having cumulated effects of BFLA, while waste cargo is trapped in autophagosomes and degradation is prevented.

Taken together, these data strengthen the relevance of autophagy for the life cycle of HCV in addition to its well-known crucial role for replication and release. The autolysosomal degradation of NS3, NS5A, NS5B and NS4B in accordance with the UPS, gene modulation, and a rough distinction of the different populations of NS3 and NS5A between the active and inactive replicon complex regarding disposal were described for the first time.

Further studies in addressing the question about the autophagy-relevant turnover of the remaining HCV proteins, especially the nonstructural proteins, could be of interest to gain a better understanding of the viral proteins and the life cycle of HCV.

7 Summary

Hepatitis C virus (HCV) causes acute and chronic liver diseases. According to the World Health Organization (WHO) currently about 58 million people suffer from chronic HCV infection and approximately 290.000 people die each year due to liver cirrhosis and hepatocellular carcinoma. Despite the ability to treat a chronic infection with high priced direct-acting antivirals that allows a cure rate over 97%, there is no prophylactic vaccine available so far.

After infection of the host cell, the HCV RNA is translated to the polyprotein followed by cleavage into the structural and nonstructural proteins. The structural proteins are released as viral particles from the host cell, while the same amount of produced nonstructural proteins remain in the cell. Since there is no accumulation observed, a degradation of excess nonstructural proteins is suggested. Autophagy is an important machinery for HCV replication and release. In this study, the focus was on autolysosomal degradation to investigate the fate of the HCV nonstructural proteins NS5B and NS4B and mainly NS3 and NS5A with consideration of protein turnover by the proteasome.

Treatment with Cycloheximide and modulators for autophagy as well as for proteasome were used to determine the half-life of NS3, NS5A, NS5B and NS4B and CLSM analysis for a potential colocalization with lysosomal marker protein LAMP2. The turnover was monitored in cells with a LAMP2 CRISPR-Cas9 knockout as well as knockdown and in return by overexpression of LC3. For further analysis of NS proteins, autolysosomes and the HCV replicon complex (RC) were isolated with subcellular fractionation by gradient centrifugation.

Along with increased half-life after inhibition of proteasomal degradation in HCV-positive cells, nonstructural proteins had a higher half-life when autophagy was inhibited. NS3, NS5A, NS5B and NS4B were found to colocalize with LAMP2-positive structures. In cells with a stable LC3 overexpression, NS3 and NS5A were decreased, while a knockdown and knock out of LAMP2 showed an increase of NS proteins. In isolated autolysosomes and HCV replicon complex, NS3 and NS5A were detected together with LAMP2 in the same fractions.

While NS3 and NS5B were mainly affected by the crosstalk between autophagy and UPS, degradation of NS5A and NS4B favors the autolysosomal pathway. The two populations of NS5A, distinguished in their phosphorylation form, are speculated for a distinct turnover of each form by autophagy in a time-dependent manner.

Therefore, beside HCV replication and release the autophagosomal machinery plays a crucial role in the turnover of excess HCV nonstructural proteins.

8 Zusammenfassung

Weltweit leiden etwa 58 Millionen Menschen unter einer chronischen Hepatitis C Infektion und jährlich sterben ca. 290 000 Menschen an den Folgen der Leberzirrhose und des hepatozellulären Leberkarzinoms. Die Therapie mit sogenannten DAAs verspricht zwar eine Heilungsrate von bis zu 97%, ist aber aufgrund der hohen Kosten hauptsächlich in den Industrieländern möglich. Bis heute ist keine prophylaktische Impfung gegen HCV verfügbar.

In der infizierten Wirtszelle wird zunächst das virale RNA Genom in ein Polyprotein translatiert und dann in Struktur- und Nichtstrukturproteine gespalten. Während die Strukturproteine als virale Partikel die Zelle verlassen, verbleiben die Nichtstrukturproteine in der Zelle. Da die Nichtstrukturproteine in gleichen Maßen synthetisiert wurden, könnte man eine Akkumulierung in der Zelle erwarten, welche aber bisher nicht beobachtet wurde. Autophagie ist ein Prozess zum Abbau und Recycling zellulärer Bestandteile und wird von HCV für die Replikation und Freisetzung induziert. Um den Abbau der Nichtstrukturproteine NS3, NS4B, NS5A und NS5B zu untersuchen, wurde zwar der proteasomale Abbau zum Teil mit in Betracht gezogen, der Hauptfokus lag jedoch auf dem autophagosomalen Abbau.

Mithilfe von Cycloheximid wurde die Halbwertszeit der Proteine bestimmt, deren Abbau mit Modulatoren verstärkt oder gehemmt wurde. Immunfluoreszenzfärbungen sollten über die Kolokalisation zwischen Nichtstrukturproteinen und dem lysosomalen Markerprotein LAMP2 aufklären. Die direkte Regulierung von Autophagie-assoziierten Proteinen wurde mittels Knock out und Knockdown von LAMP2 sowie Überexpression von LC3 durchgeführt. Des Weiteren wurden mit subzellulärer Fraktionierung autolysosomale Strukturen und der virale Replikonkomplex isoliert und analysiert.

Eine verlängerte Halbwertszeit der Nichtstrukturproteine trat vor allem nach Inhibition von Autophagie auf. Zusätzlich waren einige wenige bis viele Kolokalisationen mit LAMP2 in mikroskopischen Aufnahmen zu beobachten. Wirtszellen, die eine Überexpression von LC3 hatten, neigten zu einer geringeren Menge an NS3 und NS5A, während LAMP2 Defizite eine höhere Menge aufzeigten. Interessanterweise wurden nach Isolierung der Autolysosomen und des Replikonkomplexes NS3 und NS5A in denselben Fraktionen gefunden wie autophagosomale und lysosomale Strukturen. Diese Ergebnisse führen zu der Schlussfolgerung, dass der Abbau von NS3 und NS5B von dem Wechselspiel der Autophagie mit dem Proteasom betroffen ist, während NS5A und NS4B bevorzugt über Autophagie abgebaut werden. Weiterhin

scheinen sich die zwei Phosphorylierungsformen von NS5A durch einen zeitabhängigen autophagsomalen Abbau zu unterscheiden.
Autophagie scheint daher nicht nur für die virale Replikation und die Partikelfreisetzung von Bedeutung, sondern ist auch erforderlich für den Abbau von überschüssigen Nichtstrukturproteinen in der Wirtszelle.

9 References

1. Agnello, V.; Abel, G.; Elfahal, M.; Knight, G. B.; Zhang, Q. X. (1999): Hepatitis C virus and other flaviviridae viruses enter cells via low density lipoprotein receptor. In *Proceedings of the National Academy of Sciences of the United States of America* 96 (22), pp. 12766–12771. DOI: 10.1073/pnas.96.22.12766.

2. Albecka, Anna; Belouzard, Sandrine; Beeck, Anne op de; Descamps, Véronique; Goueslain, Lucie; Bertrand-Michel, Justine et al. (2012): Role of low-density lipoprotein receptor in the hepatitis C virus life cycle. In *Hepatology (Baltimore, Md.)* 55 (4), pp. 998–1007. DOI: 10.1002/hep.25501.

3. Alers, Sebastian; Löffler, Antje S.; Wesselborg, Sebastian; Stork, Björn (2012): Role of AMPK-mTOR-Ulk1/2 in the regulation of autophagy. Cross talk, shortcuts, and feedbacks. In *Molecular and cellular biology* 32 (1), pp. 2–11. DOI: 10.1128/MCB.06159-11.

4. Alter, M. J. (1997): Epidemiology of hepatitis C. In *Hepatology (Baltimore, Md.)* 26 (3 Suppl 1), 62S-65S. DOI: 10.1002/hep.510260711.

5. Alter, Miriam J. (2007): Epidemiology of hepatitis C virus infection. In *World journal of gastroenterology* 13 (17), pp. 2436–2441. DOI: 10.3748/wjg.v13.i17.2436.

6. André, P.; Komurian-Pradel, F.; Deforges, S.; Perret, M.; Berland, J. L.; Sodoyer, M. et al. (2002): Characterization of low- and very-low-density hepatitis C virus RNA-containing particles. In *Journal of virology* 76 (14), pp. 6919–6928. DOI: 10.1128/jvi.76.14.6919-6928.2002.

7. Appel, Nicole; Zayas, Margarita; Miller, Sven; Krijnse-Locker, Jacomine; Schaller, Torsten; Friebe, Peter et al. (2008): Essential role of domain III of nonstructural protein 5A for hepatitis C virus infectious particle assembly. In *PLoS pathogens* 4 (3), e1000035. DOI: 10.1371/journal.ppat.1000035.

8. Arias, Esperanza; Cuervo, Ana Maria (2011): Chaperone-mediated autophagy in protein quality control. In *Current opinion in cell biology* 23 (2), pp. 184–189. DOI: 10.1016/j.ceb.2010.10.009.

9. Arora, Payal; Basu, Amartya; Schmidt, M. Lee; Clark, Geoffrey J.; Donninger, Howard; Nichols, Daniel B. et al. (2017): Nonstructural protein 5B promotes degradation of the NORE1A tumor suppressor to facilitate hepatitis C virus replication. In *Hepatology (Baltimore, Md.)* 65 (5), pp. 1462–1477. DOI: 10.1002/hep.29049.

10. Ashfaq, Usman A.; Javed, Tariq; Rehman, Sidra; Nawaz, Zafar; Riazuddin, Sheikh (2011): An overview of HCV molecular biology, replication and immune responses. In *Virology journal* 8, p. 161. DOI: 10.1186/1743-422X-8-161.

11. Asselah, Tarik; Bièche, Ivan; Mansouri, Abdellah; Laurendeau, Ingrid; Cazals-Hatem, Dominique; Feldmann, Gérard et al. (2010): In vivo hepatic endoplasmic reticulum stress in patients with chronic hepatitis C. In *The Journal of pathology* 221 (3), pp. 264–274. DOI: 10.1002/path.2703.

12. Axe, Elizabeth L.; Walker, Simon A.; Manifava, Maria; Chandra, Priya; Roderick, H. Llewelyn; Habermann, Anja et al. (2008): Autophagosome formation from membrane compartments enriched in phosphatidylinositol 3-phosphate and

dynamically connected to the endoplasmic reticulum. In *The Journal of cell biology* 182 (4), pp. 685–701. DOI: 10.1083/jcb.200803137.

13. Bankwitz, Dorothea; Steinmann, Eike; Bitzegeio, Julia; Ciesek, Sandra; Friesland, Martina; Herrmann, Eva et al. (2010): Hepatitis C virus hypervariable region 1 modulates receptor interactions, conceals the CD81 binding site, and protects conserved neutralizing epitopes. In *Journal of virology* 84 (11), pp. 5751–5763. DOI: 10.1128/JVI.02200-09.
14. Barba, G.; Harper, F.; Harada, T.; Kohara, M.; Goulinet, S.; Matsuura, Y. et al. (1997): Hepatitis C virus core protein shows a cytoplasmic localization and associates to cellular lipid storage droplets. In *Proceedings of the National Academy of Sciences of the United States of America* 94 (4), pp. 1200–1205. DOI: 10.1073/pnas.94.4.1200.
15. Bartenschlager, R.; Ahlborn-Laake, L.; Mous, J.; Jacobsen, H. (1993): Nonstructural protein 3 of the hepatitis C virus encodes a serine-type proteinase required for cleavage at the NS3/4 and NS4/5 junctions. In *Journal of virology* 67 (7), pp. 3835–3844. DOI: 10.1128/JVI.67.7.3835-3844.1993.
16. Bartenschlager, R.; Ahlborn-Laake, L.; Mous, J.; Jacobsen, H. (1994): Kinetic and structural analyses of hepatitis C virus polyprotein processing. In *Journal of virology* 68 (8), pp. 5045–5055. DOI: 10.1128/JVI.68.8.5045-5055.1994.
17. Bartenschlager, Ralf; Cosset, Francois-Loic; Lohmann, Volker (2010): Hepatitis C virus replication cycle. In *Journal of hepatology* 53 (3), pp. 583–585. DOI: 10.1016/j.jhep.2010.04.015.
18. Bartenschlager, Ralf; Frese, Michael; Pietschmann, Thomas (2004): Novel Insights into Hepatitis C Virus Replication and Persistence. In : Advances in Virus Research, vol. 63: Academic Press, pp. 71–180.
19. Bartenschlager, Ralf; Lohmann, Volker; Penin, Francois (2013): The molecular and structural basis of advanced antiviral therapy for hepatitis C virus infection. In *Nature reviews. Microbiology* 11 (7), pp. 482–496. DOI: 10.1038/nrmicro3046.
20. Bartenschlager, Ralf; Penin, Francois; Lohmann, Volker; André, Patrice (2011): Assembly of infectious hepatitis C virus particles. In *Trends in microbiology* 19 (2), pp. 95–103. DOI: 10.1016/j.tim.2010.11.005.
21. Bartosch, Birke; Dubuisson, Jean; Cosset, François-Loïc (2003): Infectious hepatitis C virus pseudo-particles containing functional E1-E2 envelope protein complexes. In *The Journal of experimental medicine* 197 (5), pp. 633–642. DOI: 10.1084/jem.20021756.
22. Bartosch, Birke; Thimme, Robert; Blum, Hubert E.; Zoulim, Fabien (2009): Hepatitis C virus-induced hepatocarcinogenesis. In *Journal of hepatology* 51 (4), pp. 810–820. DOI: 10.1016/j.jhep.2009.05.008.
23. Baumert, T. F.; Ito, S.; Wong, D. T.; Liang, T. J. (1998): Hepatitis C virus structural proteins assemble into viruslike particles in insect cells. In *Journal of virology* 72 (5), pp. 3827–3836. DOI: 10.1128/JVI.72.5.3827-3836.1998.
24. Bayer, Karen; Banning, Carina; Bruss, Volker; Wiltzer-Bach, Linda; Schindler, Michael (2016): Hepatitis C Virus Is Released via a Noncanonical Secretory Route. In *Journal of virology* 90 (23), pp. 10558–10573. DOI: 10.1128/JVI.01615-16.

25. Bender, Daniela; Hildt, Eberhard (2019): Effect of Hepatitis Viruses on the Nrf2/Keap1-Signaling Pathway and Its Impact on Viral Replication and Pathogenesis. In *International journal of molecular sciences* 20 (18). DOI: 10.3390/ijms20184659.

26. Benedicto, Ignacio; Molina-Jiménez, Francisca; Bartosch, Birke; Cosset, François-Loïc; Lavillette, Dimitri; Prieto, Jesús et al. (2009): The tight junction-associated protein occludin is required for a postbinding step in hepatitis C virus entry and infection. In *Journal of virology* 83 (16), pp. 8012–8020. DOI: 10.1128/JVI.00038-09.

27. Berggren, Keith A.; Suzuki, Saori; Ploss, Alexander (2020): Animal Models Used in Hepatitis C Virus Research. In *International journal of molecular sciences* 21 (11). DOI: 10.3390/ijms21113869.

28. Blanchard, Emmanuelle; Belouzard, Sandrine; Goueslain, Lucie; Wakita, Takaji; Dubuisson, Jean; Wychowski, Czeslaw; Rouillé, Yves (2006): Hepatitis C virus entry depends on clathrin-mediated endocytosis. In *Journal of virology* 80 (14), pp. 6964–6972. DOI: 10.1128/JVI.00024-06.

29. Blázquez, Ana-Belén; Escribano-Romero, Estela; Merino-Ramos, Teresa; Saiz, Juan-Carlos; Martín-Acebes, Miguel A. (2014): Stress responses in flavivirus-infected cells. Activation of unfolded protein response and autophagy. In *Frontiers in microbiology* 5, p. 266. DOI: 10.3389/fmicb.2014.00266.

30. Blight, K. J.; Kolykhalov, A. A.; Rice, C. M. (2000): Efficient initiation of HCV RNA replication in cell culture. In *Science (New York, N.Y.)* 290 (5498), pp. 1972–1974. DOI: 10.1126/science.290.5498.1972.

31. Blight, Keril J.; McKeating, Jane A.; Rice, Charles M. (2002): Highly permissive cell lines for subgenomic and genomic hepatitis C virus RNA replication. In *Journal of virology* 76 (24), pp. 13001–13014. DOI: 10.1128/jvi.76.24.13001-13014.2002.

32. Boccadoro, Mario; Morgan, Gareth; Cavenagh, Jamie (2005): Preclinical evaluation of the proteasome inhibitor bortezomib in cancer therapy. In *Cancer cell international* 5 (1), p. 18. DOI: 10.1186/1475-2867-5-18.

33. Boulant, Steeve; Montserret, Roland; Hope, R. Graham; Ratinier, Maxime; Targett-Adams, Paul; Lavergne, Jean-Pierre et al. (2006): Structural determinants that target the hepatitis C virus core protein to lipid droplets. In *The Journal of biological chemistry* 281 (31), pp. 22236–22247. DOI: 10.1074/jbc.M601031200.

34. Brass, Volker; Berke, Jan Martin; Montserret, Roland; Blum, Hubert E.; Penin, François; Moradpour, Darius (2008): Structural determinants for membrane association and dynamic organization of the hepatitis C virus NS3-4A complex. In *Proceedings of the National Academy of Sciences of the United States of America* 105 (38), pp. 14545–14550. DOI: 10.1073/pnas.0807298105.

35. Brass, Volker; Bieck, Elke; Montserret, Roland; Wölk, Benno; Hellings, Jan Albert; Blum, Hubert E. et al. (2002): An amino-terminal amphipathic alpha-helix mediates membrane association of the hepatitis C virus nonstructural protein 5A. In *The Journal of biological chemistry* 277 (10), pp. 8130–8139. DOI: 10.1074/jbc.M111289200.

36. Brazzoli, Michela; Bianchi, Alessia; Filippini, Sara; Weiner, Amy; Zhu, Qing; Pizza, Mariagrazia; Crotta, Stefania (2008): CD81 is a central regulator of cellular events required for hepatitis C virus infection of human hepatocytes. In *Journal of virology* 82 (17), pp. 8316–8329. DOI: 10.1128/JVI.00665-08.

37. Bruening, Janina; Lasswitz, Lisa; Banse, Pia; Kahl, Sina; Marinach, Carine; Vondran, Florian W. et al. (2018): Hepatitis C virus enters liver cells using the CD81 receptor complex proteins calpain-5 and CBLB. In *PLoS pathogens* 14 (7), e1007111. DOI: 10.1371/journal.ppat.1007111.

38. Bürckstümmer, T.; Kriegs, M.; Lupberger, J.; Pauli, E. K.; Schmittel, S.; Hildt, E. (2006): Raf-1 kinase associates with Hepatitis C virus NS5A and regulates viral replication. In *FEBS letters* 580 (2), pp. 575–580. DOI: 10.1016/j.febslet.2005.12.071.

39. Carlsson, Sven R.; Simonsen, Anne (2015): Membrane dynamics in autophagosome biogenesis. In *Journal of cell science* 128 (2), pp. 193–205. DOI: 10.1242/jcs.141036.

40. Carvajal-Yepes, Monica; Himmelsbach, Kiyoshi; Schaedler, Stephanie; Ploen, Daniela; Krause, Janis; Ludwig, Leopold et al. (2011): Hepatitis C virus impairs the induction of cytoprotective Nrf2 target genes by delocalization of small Maf proteins. In *The Journal of biological chemistry* 286 (11), pp. 8941–8951. DOI: 10.1074/jbc.M110.186684.

41. Catanese, Maria Teresa; Dorner, Marcus (2015): Advances in experimental systems to study hepatitis C virus in vitro and in vivo. In *Virology* 479-480, pp. 221–233. DOI: 10.1016/j.virol.2015.03.014.

42. Chan, Stephanie T.; Ou, Jing-Hsiung James (2017): Hepatitis C Virus-Induced Autophagy and Host Innate Immune Response. In *Viruses* 9 (8). DOI: 10.3390/v9080224.

43. Chang, Ming-Ling; Hu, Jing-Hong; Yen, Ching-Hao; Chen, Kuan-Hsing; Kuo, Chia-Jung; Lin, Ming-Shyan et al. (2020): Evolution of ferritin levels in hepatitis C patients treated with antivirals. In *Scientific reports* 10 (1), p. 19744. DOI: 10.1038/s41598-020-76871-z.

44. Chaudhari, Rahul; Fouda, Sherouk; Sainu, Ashik; Pappachan, Joseph M. (2021): Metabolic complications of hepatitis C virus infection. In *World journal of gastroenterology* 27 (13), pp. 1267–1282. DOI: 10.3748/wjg.v27.i13.1267.

45. Chevaliez, Stéphane; Pawlotsky, Jean-Michel (2008): Diagnosis and management of chronic viral hepatitis. Antigens, antibodies and viral genomes. In *Best practice & research. Clinical gastroenterology* 22 (6), pp. 1031–1048. DOI: 10.1016/j.bpg.2008.11.004.

46. Chiang, Cho-Han; Lai, Yen-Ling; Huang, Yu-Ning; Yu, Chun-Chiao; Lu, Christine C.; Yu, Guann-Yi; Yu, Ming-Jiun (2020): Sequential Phosphorylation of the Hepatitis C Virus NS5A Protein Depends on NS3-Mediated Autocleavage between NS3 and NS4A. In *Journal of virology* 94 (19). DOI: 10.1128/JVI.00420-20.

47. Choo, Q. L.; Kuo, G.; Weiner, A. J.; Overby, L. R.; Bradley, D. W.; Houghton, M. (1989): Isolation of a cDNA clone derived from a blood-borne non-A, non-B viral hepatitis genome. In *Science (New York, N.Y.)* 244 (4902), pp. 359–362. DOI: 10.1126/science.2523562.

48. Choudhary, Vineet; Ojha, Namrata; Golden, Andy; Prinz, William A. (2015): A conserved family of proteins facilitates nascent lipid droplet budding from the ER. In *The Journal of cell biology* 211 (2), pp. 261–271. DOI: 10.1083/jcb.201505067.

49. Choukhi, A.; Ung, S.; Wychowski, C.; Dubuisson, J. (1998): Involvement of endoplasmic reticulum chaperones in the folding of hepatitis C virus glycoproteins. In *Journal of virology* 72 (5), pp. 3851–3858. DOI: 10.1128/JVI.72.5.3851-3858.1998.

50. Chu, Ja Yeon Kim; Ou, Jing-Hsiung James (2021): Autophagy in HCV Replication and Protein Trafficking. In *International journal of molecular sciences* 22 (3). DOI: 10.3390/ijms22031089.

51. Ciechanover, A. (1994): The ubiquitin-proteasome proteolytic pathway. In *Cell* 79 (1), pp. 13–21. DOI: 10.1016/0092-8674(94)90396-4.

52. Ciesek, Sandra; Friesland, Martina; Steinmann, Jörg; Becker, Britta; Wedemeyer, Heiner; Manns, Michael P. et al. (2010): How stable is the hepatitis C virus (HCV)? Environmental stability of HCV and its susceptibility to chemical biocides. In *The Journal of infectious diseases* 201 (12), pp. 1859–1866. DOI: 10.1086/652803.

53. Clarke, A.; Kulasegaram, R. (2006): Hepatitis C transmission -- where are we now? In *International journal of STD & AIDS* 17 (2), 74-80; quiz 80. DOI: 10.1258/095646206775455685.

54. Cohen-Kaplan, Victoria; Livneh, Ido; Avni, Noa; Cohen-Rosenzweig, Chen; Ciechanover, Aaron (2016): The ubiquitin-proteasome system and autophagy. Coordinated and independent activities. In *The international journal of biochemistry & cell biology* 79, pp. 403–418. DOI: 10.1016/j.biocel.2016.07.019.

55. Coller, Kelly E.; Berger, Kristi L.; Heaton, Nicholas S.; Cooper, Jacob D.; Yoon, Rosa; Randall, Glenn (2009): RNA interference and single particle tracking analysis of hepatitis C virus endocytosis. In *PLoS pathogens* 5 (12), e1000702. DOI: 10.1371/journal.ppat.1000702.

56. Coller, Kelly E.; Heaton, Nicholas S.; Berger, Kristi L.; Cooper, Jacob D.; Saunders, Jessica L.; Randall, Glenn (2012): Molecular determinants and dynamics of hepatitis C virus secretion. In *PLoS pathogens* 8 (1), e1002466. DOI: 10.1371/journal.ppat.1002466.

57. Counihan, Natalie A.; Rawlinson, Stephen M.; Lindenbach, Brett D. (2011): Trafficking of hepatitis C virus core protein during virus particle assembly. In *PLoS pathogens* 7 (10), e1002302. DOI: 10.1371/journal.ppat.1002302.

58. Cox, Andrea L. (2020): Challenges and Promise of a Hepatitis C Virus Vaccine. In *Cold Spring Harbor perspectives in medicine* 10 (2). DOI: 10.1101/cshperspect.a036947.

59. Dao Thi, Viet Loan; Granier, Christelle; Zeisel, Mirjam B.; Guérin, Maryse; Mancip, Jimmy; Granio, Ophélia et al. (2012): Characterization of hepatitis C virus particle subpopulations reveals multiple usage of the scavenger receptor BI for entry steps. In *The Journal of biological chemistry* 287 (37), pp. 31242–31257. DOI: 10.1074/jbc.M112.365924.

60. Deleersnyder, V.; Pillez, A.; Wychowski, C.; Blight, K.; Xu, J.; Hahn, Y. S. et al. (1997): Formation of native hepatitis C virus glycoprotein complexes. In *Journal of virology* 71 (1), pp. 697–704. DOI: 10.1128/JVI.71.1.697-704.1997.

61. Deng, Libin; Jiang, Wang; Wang, Xiaoning; Merz, Andreas; Hiet, Marie-Sophie; Chen, Yujie et al. (2019): Syntenin regulates hepatitis C virus sensitivity to neutralizing antibody by promoting E2 secretion through exosomes. In *Journal of hepatology* 71 (1), pp. 52–61. DOI: 10.1016/j.jhep.2019.03.006.

62. DGVS (2020): DGVS. S3 guidelines chronic hepatits C. Available online at https://www.dgvs.de/wissen/leitlinien/leitlinien-dgvs/hepatitis-c/.

63. Diamond, Deborah L.; Syder, Andrew J.; Jacobs, Jon M.; Sorensen, Christina M.; Walters, Kathie-Anne; Proll, Sean C. et al. (2010): Temporal proteome and lipidome profiles reveal hepatitis C virus-associated reprogramming of hepatocellular metabolism and bioenergetics. In *PLoS pathogens* 6 (1), e1000719. DOI: 10.1371/journal.ppat.1000719.

64. Ding, Wen-Xing; Yin, Xiao-Ming (2008): Sorting, recognition and activation of the misfolded protein degradation pathways through macroautophagy and the proteasome. In *Autophagy* 4 (2), pp. 141–150. DOI: 10.4161/auto.5190.

65. Dubuisson, Jean; Cosset, François-Loïc (2014): Virology and cell biology of the hepatitis C virus life cycle. An update. In *Journal of hepatology* 61 (1 Suppl), S3-S13. DOI: 10.1016/j.jhep.2014.06.031.

66. Egger, Denise; Wölk, Benno; Gosert, Rainer; Bianchi, Leonardo; Blum, Hubert E.; Moradpour, Darius; Bienz, Kurt (2002): Expression of hepatitis C virus proteins induces distinct membrane alterations including a candidate viral replication complex. In *Journal of virology* 76 (12), pp. 5974–5984. DOI: 10.1128/jvi.76.12.5974-5984.2002.

67. Elgner, Fabian (2016): Charakterisierung des endosomalen Freisetzungsweges von Hepatitis-C-Virionen. Dissertation. Goethe-Universität, Frankfurt am Main.

68. Elgner, Fabian; Donnerhak, Christian; Ren, Huimei; Medvedev, Regina; Schreiber, André; Weber, Lorenz et al. (2016a): Characterization of α-taxilin as a novel factor controlling the release of hepatitis C virus. In *The Biochemical journal* 473 (2), pp. 145–155. DOI: 10.1042/BJ20150717.

69. Elgner, Fabian; Hildt, Eberhard; Bender, Daniela (2018): Relevance of Rab Proteins for the Life Cycle of Hepatitis C Virus. In *Frontiers in cell and developmental biology* 6, p. 166. DOI: 10.3389/fcell.2018.00166.

70. Elgner, Fabian; Ren, Huimei; Medvedev, Regina; Ploen, Daniela; Himmelsbach, Kiyoshi; Boller, Klaus; Hildt, Eberhard (2016b): The Intracellular Cholesterol Transport Inhibitor U18666A Inhibits the Exosome-Dependent Release of Mature Hepatitis C Virus. In *Journal of virology* 90 (24), pp. 11181–11196. DOI: 10.1128/JVI.01053-16.

71. Eskelinen, Eeva-Liisa (2006): Roles of LAMP-1 and LAMP-2 in lysosome biogenesis and autophagy. In *Molecular aspects of medicine* 27 (5-6), pp. 495–502. DOI: 10.1016/j.mam.2006.08.005.

72. Eskelinen, Eeva-Liisa; Illert, Anna Lena; Tanaka, Yoshitaka; Schwarzmann, Günter; Blanz, Judith; Figura, Kurt von; Saftig, Paul (2002): Role of LAMP-2 in lysosome biogenesis and autophagy. In *Molecular biology of the cell* 13 (9), pp. 3355–3368. DOI: 10.1091/mbc.e02-02-0114.

73. Eskelinen, Eeva-Liisa; Saftig, Paul (2009): Autophagy. A lysosomal degradation pathway with a central role in health and disease. In *Biochimica et biophysica acta* 1793 (4), pp. 664–673. DOI: 10.1016/j.bbamcr.2008.07.014.

74. Evans, Matthew J.; Hahn, Thomas von; Tscherne, Donna M.; Syder, Andrew J.; Panis, Maryline; Wölk, Benno et al. (2007): Claudin-1 is a hepatitis C virus co-receptor required for a late step in entry. In *Nature* 446 (7137), pp. 801–805. DOI: 10.1038/nature05654.

75. Fader, C. M.; Colombo, M. I. (2009): Autophagy and multivesicular bodies. Two closely related partners. In *Cell death and differentiation* 16 (1), pp. 70–78. DOI: 10.1038/cdd.2008.168.

76. Fahmy, Ahmed M.; Labonté, Patrick (2017): The autophagy elongation complex (ATG5-12/16L1) positively regulates HCV replication and is required for wild-type membranous web formation. In *Scientific reports* 7, p. 40351. DOI: 10.1038/srep40351.

77. Farci, P.; Purcell, R. H. (2000): Clinical significance of hepatitis C virus genotypes and quasispecies. In *Seminars in liver disease* 20 (1), pp. 103–126.

78. Farquhar, M. J.; McKeating, J. A. (2008): Primary hepatocytes as targets for hepatitis C virus replication. In *Journal of viral hepatitis* 15 (12), pp. 849–854. DOI: 10.1111/j.1365-2893.2008.01051.x.

79. Farquhar, Michelle J.; Harris, Helen J.; Diskar, Mandy; Jones, Sarah; Mee, Christopher J.; Nielsen, Søren U. et al. (2008): Protein kinase A-dependent step(s) in hepatitis C virus entry and infectivity. In *Journal of virology* 82 (17), pp. 8797–8811. DOI: 10.1128/JVI.00592-08.

80. Farquhar, Michelle J.; Hu, Ke; Harris, Helen J.; Davis, Christopher; Brimacombe, Claire L.; Fletcher, Sarah J. et al. (2012): Hepatitis C virus induces CD81 and claudin-1 endocytosis. In *Journal of virology* 86 (8), pp. 4305–4316. DOI: 10.1128/JVI.06996-11.

81. Feinstone, S. M.; Kapikian, A. Z.; Purcell, R. H.; Alter, H. J.; Holland, P. V. (1975): Transfusion-associated hepatitis not due to viral hepatitis type A or B. In *The New England journal of medicine* 292 (15), pp. 767–770. DOI: 10.1056/NEJM197504102921502.

82. Feng, Yuchen; He, Ding; Yao, Zhiyuan; Klionsky, Daniel J. (2014): The machinery of macroautophagy. In *Cell research* 24 (1), pp. 24–41. DOI: 10.1038/cr.2013.168.

83. Ferraris, Pauline; Blanchard, Emmanuelle; Roingeard, Philippe (2010): Ultrastructural and biochemical analyses of hepatitis C virus-associated host cell membranes. In *The Journal of general virology* 91 (Pt 9), pp. 2230–2237. DOI: 10.1099/vir.0.022186-0.

84. Finley, Daniel (2009): Recognition and processing of ubiquitin-protein conjugates by the proteasome. In *Annual review of biochemistry* 78, pp. 477–513. DOI: 10.1146/annurev.biochem.78.081507.101607.

85. Foreman, Kyle J.; Marquez, Neal; Dolgert, Andrew; Fukutaki, Kai; Fullman, Nancy; McGaughey, Madeline et al. (2018): Forecasting life expectancy, years of life lost, and all-cause and cause-specific mortality for 250 causes of death. Reference and alternative scenarios for 2016-40 for 195 countries and territories. In *Lancet (London, England)* 392 (10159), pp. 2052–2090. DOI: 10.1016/S0140-6736(18)31694-5.

86. Fortmann, Karen T.; Lewis, Russell D.; Ngo, Kim A.; Fagerlund, Riku; Hoffmann, Alexander (2015): A Regulated, Ubiquitin-Independent Degron in IκBα. In *Journal of molecular biology* 427 (17), pp. 2748–2756. DOI: 10.1016/j.jmb.2015.07.008.

87. Foy, Eileen; Li, Kui; Sumpter, Rhea; Loo, Yueh-Ming; Johnson, Cynthia L.; Wang, Chunfu et al. (2005): Control of antiviral defenses through hepatitis C virus disruption of retinoic acid-inducible gene-I signaling. In *Proceedings of the National Academy of Sciences of the United States of America* 102 (8), pp. 2986–2991. DOI: 10.1073/pnas.0408707102.

88. Frank, C.; Mohamed, M. K.; Strickland, G. T.; Lavanchy, D.; Arthur, R. R.; Magder, L. S. et al. (2000): The role of parenteral antischistosomal therapy in the spread of hepatitis C virus in Egypt. In *Lancet (London, England)* 355 (9207), pp. 887–891. DOI: 10.1016/s0140-6736(99)06527-7.

89. Fujita, Naonobu; Itoh, Takashi; Omori, Hiroko; Fukuda, Mitsunori; Noda, Takeshi; Yoshimori, Tamotsu (2008): The Atg16L complex specifies the site of LC3 lipidation for membrane biogenesis in autophagy. In *Molecular biology of the cell* 19 (5), pp. 2092–2100. DOI: 10.1091/mbc.e07-12-1257.

90. Fujiwara, Yuuki; Furuta, Akiko; Kikuchi, Hisae; Aizawa, Shu; Hatanaka, Yusuke; Konya, Chiho et al. (2013): Discovery of a novel type of autophagy targeting RNA. In *Autophagy* 9 (3), pp. 403–409. DOI: 10.4161/auto.23002.

91. Gale, M. J.; Korth, M. J.; Tang, N. M.; Tan, S. L.; Hopkins, D. A.; Dever, T. E. et al. (1997): Evidence that hepatitis C virus resistance to interferon is mediated through repression of the PKR protein kinase by the nonstructural 5A protein. In *Virology* 230 (2), pp. 217–227. DOI: 10.1006/viro.1997.8493.

92. Gallastegui, Nerea; Groll, Michael (2010): The 26S proteasome. Assembly and function of a destructive machine. In *Trends in biochemical sciences* 35 (11), pp. 634–642. DOI: 10.1016/j.tibs.2010.05.005.

93. Gastaminza, Pablo; Cheng, Guofeng; Wieland, Stefan; Zhong, Jin; Liao, Wei; Chisari, Francis V. (2008): Cellular determinants of hepatitis C virus assembly, maturation, degradation, and secretion. In *Journal of virology* 82 (5), pp. 2120–2129. DOI: 10.1128/JVI.02053-07.

94. Gastaminza, Pablo; Dryden, Kelly A.; Boyd, Bryan; Wood, Malcolm R.; Law, Mansun; Yeager, Mark; Chisari, Francis V. (2010): Ultrastructural and biophysical characterization of hepatitis C virus particles produced in cell culture. In *Journal of virology* 84 (21), pp. 10999–11009. DOI: 10.1128/JVI.00526-10.

95. Gastaminza, Pablo; Kapadia, Sharookh B.; Chisari, Francis V. (2006): Differential biophysical properties of infectious intracellular and secreted hepatitis C virus particles. In *Journal of virology* 80 (22), pp. 11074–11081. DOI: 10.1128/JVI.01150-06.

96. Gentzsch, Juliane; Brohm, Christiane; Steinmann, Eike; Friesland, Martina; Menzel, Nicolas; Vieyres, Gabrielle et al. (2013): hepatitis c Virus p7 is critical for capsid assembly and envelopment. In *PLoS pathogens* 9 (5), e1003355. DOI: 10.1371/journal.ppat.1003355.

97. Ghany, Marc G.; Nelson, David R.; Strader, Doris B.; Thomas, David L.; Seeff, Leonard B. (2011): An update on treatment of genotype 1 chronic hepatitis C virus infection. 2011 practice guideline by the American Association for the Study

of Liver Diseases. In *Hepatology (Baltimore, Md.)* 54 (4), pp. 1433–1444. DOI: 10.1002/hep.24641.

98. Goonawardane, Niluka; Gebhardt, Anna; Bartlett, Christopher; Pichlmair, Andreas; Harris, Mark (2017): Phosphorylation of Serine 225 in Hepatitis C Virus NS5A Regulates Protein-Protein Interactions. In *Journal of virology* 91 (17). DOI: 10.1128/JVI.00805-17.

99. Gouttenoire, Jérôme; Penin, François; Moradpour, Darius (2010a): Hepatitis C virus nonstructural protein 4B. A journey into unexplored territory. In *Reviews in medical virology* 20 (2), pp. 117–129. DOI: 10.1002/rmv.640.

100. Gouttenoire, Jérôme; Roingeard, Philippe; Penin, François; Moradpour, Darius (2010b): Amphipathic alpha-helix AH2 is a major determinant for the oligomerization of hepatitis C virus nonstructural protein 4B. In *Journal of virology* 84 (24), pp. 12529–12537. DOI: 10.1128/JVI.01798-10.

101. Grégoire, Isabel Pombo; Richetta, Clémence; Meyniel-Schicklin, Laurène; Borel, Sophie; Pradezynski, Fabrine; Diaz, Olivier et al. (2011): IRGM is a common target of RNA viruses that subvert the autophagy network. In *PLoS pathogens* 7 (12), e1002422. DOI: 10.1371/journal.ppat.1002422.

102. Griffin, Stephen D. C.; Beales, Lucy P.; Clarke, Dean S.; Worsfold, Oliver; Evans, Stephen D.; Jaeger, Joachim et al. (2003): The p7 protein of hepatitis C virus forms an ion channel that is blocked by the antiviral drug, Amantadine. In *FEBS letters* 535 (1-3), pp. 34–38. DOI: 10.1016/s0014-5793(02)03851-6.

103. Gu, Meigang; Rice, Charles M. (2013): Structures of hepatitis C virus nonstructural proteins required for replicase assembly and function. In *Current opinion in virology* 3 (2), pp. 129–136. DOI: 10.1016/j.coviro.2013.03.013.

104. Guerra, Flora; Bucci, Cecilia (2016): Multiple Roles of the Small GTPase Rab7. In *Cells* 5 (3). DOI: 10.3390/cells5030034.

105. Gupta, Ekta; Bajpai, Meenu; Choudhary, Aashish (2014): Hepatitis C virus. Screening, diagnosis, and interpretation of laboratory assays. In *Asian journal of transfusion science* 8 (1), pp. 19–25. DOI: 10.4103/0973-6247.126683.

106. Harris, Helen J.; Davis, Christopher; Mullins, Jonathan G. L.; Hu, Ke; Goodall, Margaret; Farquhar, Michelle J. et al. (2010): Claudin association with CD81 defines hepatitis C virus entry. In *The Journal of biological chemistry* 285 (27), pp. 21092–21102. DOI: 10.1074/jbc.M110.104836.

107. Harris, Helen J.; Farquhar, Michelle J.; Mee, Christopher J.; Davis, Christopher; Reynolds, Gary M.; Jennings, Adam et al. (2008): CD81 and claudin 1 coreceptor association. Role in hepatitis C virus entry. In *Journal of virology* 82 (10), pp. 5007–5020. DOI: 10.1128/JVI.02286-07.

108. He, Yingli; She, Hua; Zhang, Ting; Xu, Haidong; Cheng, Lihong; Yepes, Manuel et al. (2018): p38 MAPK inhibits autophagy and promotes microglial inflammatory responses by phosphorylating ULK1. In *The Journal of cell biology* 217 (1), pp. 315–328. DOI: 10.1083/jcb.201701049.

109. Hegedűs, Krisztina; Takáts, Szabolcs; Kovács, Attila L.; Juhász, Gábor (2013): Evolutionarily conserved role and physiological relevance of a STX17/Syx17 (syntaxin 17)-containing SNARE complex in autophagosome fusion with endosomes and lysosomes. In *Autophagy* 9 (10), pp. 1642–1646. DOI: 10.4161/auto.25684.

110. Heinemeyer, W.; Fischer, M.; Krimmer, T.; Stachon, U.; Wolf, D. H. (1997): The active sites of the eukaryotic 20 S proteasome and their involvement in subunit precursor processing. In *The Journal of biological chemistry* 272 (40), pp. 25200–25209. DOI: 10.1074/jbc.272.40.25200.

111. Herker, Eva; Harris, Charles; Hernandez, Céline; Carpentier, Arnaud; Kaehlcke, Katrin; Rosenberg, Arielle R. et al. (2010): Efficient hepatitis C virus particle formation requires diacylglycerol acyltransferase-1. In *Nature medicine* 16 (11), pp. 1295–1298. DOI: 10.1038/nm.2238.

112. Himmelsbach, K.; Sauter, D.; Baumert, T. F.; Ludwig, L.; Blum, H. E.; Hildt, E. (2009): New aspects of an anti-tumour drug. Sorafenib efficiently inhibits HCV replication. In *Gut* 58 (12), pp. 1644–1653. DOI: 10.1136/gut.2009.182212.

113. Hirano, Junki; Yoshio, Sachiyo; Sakai, Yusuke; Songling, Li; Suzuki, Tatsuya; Itoh, Yumi et al. (2021): Hepatitis C virus modulates signal peptide peptidase to alter host protein processing. In *Proceedings of the National Academy of Sciences of the United States of America* 118 (22). DOI: 10.1073/pnas.2026184118.

114. Hope, R. Graham; Murphy, Denis J.; McLauchlan, John (2002): The domains required to direct core proteins of hepatitis C virus and GB virus-B to lipid droplets share common features with plant oleosin proteins. In *The Journal of biological chemistry* 277 (6), pp. 4261–4270. DOI: 10.1074/jbc.M108798200.

115. Hubert, Virginie; Peschel, Andrea; Langer, Brigitte; Gröger, Marion; Rees, Andrew; Kain, Renate (2016): LAMP-2 is required for incorporating syntaxin-17 into autophagosomes and for their fusion with lysosomes. In *Biology open* 5 (10), pp. 1516–1529. DOI: 10.1242/bio.018648.

116. Hügle, T.; Fehrmann, F.; Bieck, E.; Kohara, M.; Kräusslich, H. G.; Rice, C. M. et al. (2001): The hepatitis C virus nonstructural protein 4B is an integral endoplasmic reticulum membrane protein. In *Virology* 284 (1), pp. 70–81. DOI: 10.1006/viro.2001.0873.

117. Hyttinen, Juha M. T.; Niittykoski, Minna; Salminen, Antero; Kaarniranta, Kai (2013): Maturation of autophagosomes and endosomes. A key role for Rab7. In *Biochimica et biophysica acta* 1833 (3), pp. 503–510. DOI: 10.1016/j.bbamcr.2012.11.018.

118. Ichimura, Yoshinobu; Waguri, Satoshi; Sou, Yu-Shin; Kageyama, Shun; Hasegawa, Jun; Ishimura, Ryosuke et al. (2013): Phosphorylation of p62 activates the Keap1-Nrf2 pathway during selective autophagy. In *Molecular cell* 51 (5), pp. 618–631. DOI: 10.1016/j.molcel.2013.08.003.

119. Irshad, M.; Ansari, M. A.; Singh, Akanksha; Nag, Prashant; Raghvendra, L.; Singh, Shiwani; Badhal, Sukhbir Singh (2010): HCV-genotypes. A review on their origin, global status, assay system, pathogenecity and response to treatment. In *Hepato-gastroenterology* 57 (104), pp. 1529–1538.

120. Irshad, Mohammad; Mankotia, Dhananjay Singh; Irshad, Khushboo (2013): An insight into the diagnosis and pathogenesis of hepatitis C virus infection. In *World journal of gastroenterology* 19 (44), pp. 7896–7909. DOI: 10.3748/wjg.v19.i44.7896.

121. Itakura, Eisuke; Kishi-Itakura, Chieko; Mizushima, Noboru (2012): The hairpin-type tail-anchored SNARE syntaxin 17 targets to autophagosomes for fusion with

endosomes/lysosomes. In *Cell* 151 (6), pp. 1256–1269. DOI: 10.1016/j.cell.2012.11.001.

122. Itakura, Eisuke; Mizushima, Noboru (2010): Characterization of autophagosome formation site by a hierarchical analysis of mammalian Atg proteins. In *Autophagy* 6 (6), pp. 764–776. DOI: 10.4161/auto.6.6.12709.

123. Itakura, Eisuke; Mizushima, Noboru (2013): Syntaxin 17. The autophagosomal SNARE. In *Autophagy* 9 (6), pp. 917–919. DOI: 10.4161/auto.24109.

124. Janiak, Maciej; Caraballo Cortes, Kamila; Demkow, Urszula; Radkowski, Marek (2018): Spontaneous Elimination of Hepatitis C Virus Infection. In *Advances in experimental medicine and biology* 1039, pp. 45–54. DOI: 10.1007/5584_2017_76.

125. Jirasko, Vlastimil; Montserret, Roland; Lee, Ji Young; Gouttenoire, Jérôme; Moradpour, Darius; Penin, Francois; Bartenschlager, Ralf (2010): Structural and functional studies of nonstructural protein 2 of the hepatitis C virus reveal its key role as organizer of virion assembly. In *PLoS pathogens* 6 (12), e1001233. DOI: 10.1371/journal.ppat.1001233.

126. Johansen, Terje; Lamark, Trond (2011): Selective autophagy mediated by autophagic adapter proteins. In *Autophagy* 7 (3), pp. 279–296. DOI: 10.4161/auto.7.3.14487.

127. Johri, Manish Kumar; Lashkari, Hiren Vasantrai; Gupta, Divya; Vedagiri, Dhiviya; Harshan, Krishnan Harinivas (2020): mTORC1 restricts hepatitis C virus RNA replication through ULK1-mediated suppression of miR-122 and facilitates post-replication events. In *The Journal of general virology* 101 (1), pp. 86–95. DOI: 10.1099/jgv.0.001356.

128. Kabeya, Y.; Mizushima, N.; Ueno, T.; Yamamoto, A.; Kirisako, T.; Noda, T. et al. (2000): LC3, a mammalian homologue of yeast Apg8p, is localized in autophagosome membranes after processing. In *The EMBO journal* 19 (21), pp. 5720–5728. DOI: 10.1093/emboj/19.21.5720.

129. Kamili, Saleem; Krawczynski, Kris; McCaustland, Karen; Li, Xiaofang; Alter, Miriam J. (2007): Infectivity of hepatitis C virus in plasma after drying and storing at room temperature. In *Infection control and hospital epidemiology* 28 (5), pp. 519–524. DOI: 10.1086/513727.

130. Ke, Po-Yuan; Chen, Steve S-L (2011a): Activation of the unfolded protein response and autophagy after hepatitis C virus infection suppresses innate antiviral immunity in vitro. In *The Journal of clinical investigation* 121 (1), pp. 37–56. DOI: 10.1172/JCI41474.

131. Ke, Po-Yuan; Chen, Steve S-L (2011b): Autophagy. A novel guardian of HCV against innate immune response. In *Autophagy* 7 (5), pp. 533–535. DOI: 10.4161/auto.7.5.14732.

132. Keil, E.; Höcker, R.; Schuster, M.; Essmann, F.; Ueffing, N.; Hoffman, B. et al. (2013): Phosphorylation of Atg5 by the Gadd45β-MEKK4-p38 pathway inhibits autophagy. In *Cell death and differentiation* 20 (2), pp. 321–332. DOI: 10.1038/cdd.2012.129.

133. Kensler, Thomas W.; Wakabayashi, Nobunao (2010): Nrf2. Friend or foe for chemoprevention? In *Carcinogenesis* 31 (1), pp. 90–99. DOI: 10.1093/carcin/bgp231.

134. Kensler, Thomas W.; Wakabayashi, Nobunao; Biswal, Shyam (2007): Cell survival responses to environmental stresses via the Keap1-Nrf2-ARE pathway. In *Annual review of pharmacology and toxicology* 47, pp. 89–116. DOI: 10.1146/annurev.pharmtox.46.120604.141046.

135. Khaliq, Saba; Jahan, Shah; Pervaiz, Asim (2011): Sequence variability of HCV Core region. Important predictors of HCV induced pathogenesis and viral production. In *Infection, genetics and evolution : journal of molecular epidemiology and evolutionary genetics in infectious diseases* 11 (3), pp. 543–556. DOI: 10.1016/j.meegid.2011.01.017.

136. Khan, Abdul Ghafoor; Miller, Matthew T.; Marcotrigiano, Joseph (2015): HCV glycoprotein structures. What to expect from the unexpected. In *Current opinion in virology* 12, pp. 53–58. DOI: 10.1016/j.coviro.2015.02.004.

137. Kim, J. L.; Morgenstern, K. A.; Lin, C.; Fox, T.; Dwyer, M. D.; Landro, J. A. et al. (1996): Crystal structure of the hepatitis C virus NS3 protease domain complexed with a synthetic NS4A cofactor peptide. In *Cell* 87 (2), pp. 343–355. DOI: 10.1016/s0092-8674(00)81351-3.

138. Kim, Ja Yeon; Wang, Linya; Lee, Jiyoung; Ou, Jing-Hsiung James (2017): Hepatitis C Virus Induces the Localization of Lipid Rafts to Autophagosomes for Its RNA Replication. In *Journal of virology* 91 (20). DOI: 10.1128/JVI.00541-17.

139. Kim, Peter Kijun; Hailey, Dale Warren; Mullen, Robert Thomas; Lippincott-Schwartz, Jennifer (2008): Ubiquitin signals autophagic degradation of cytosolic proteins and peroxisomes. In *Proceedings of the National Academy of Sciences of the United States of America* 105 (52), pp. 20567–20574. DOI: 10.1073/pnas.0810611105.

140. Kitab, Bouchra; Satoh, Masaaki; Ohmori, Yusuke; Munakata, Tsubasa; Sudoh, Masayuki; Kohara, Michinori; Tsukiyama-Kohara, Kyoko (2019): Ribonucleotide reductase M2 promotes RNA replication of hepatitis C virus by protecting NS5B protein from hPLIC1-dependent proteasomal degradation. In *The Journal of biological chemistry* 294 (15), pp. 5759–5773. DOI: 10.1074/jbc.RA118.004397.

141. Koegl, M.; Hoppe, T.; Schlenker, S.; Ulrich, H. D.; Mayer, T. U.; Jentsch, S. (1999): A novel ubiquitination factor, E4, is involved in multiubiquitin chain assembly. In *Cell* 96 (5), pp. 635–644. DOI: 10.1016/s0092-8674(00)80574-7.

142. Kolykhalov, A. A.; Feinstone, S. M.; Rice, C. M. (1996): Identification of a highly conserved sequence element at the 3' terminus of hepatitis C virus genome RNA. In *Journal of virology* 70 (6), pp. 3363–3371. DOI: 10.1128/JVI.70.6.3363-3371.1996.

143. Korolchuk, Viktor I.; Menzies, Fiona M.; Rubinsztein, David C. (2010): Mechanisms of cross-talk between the ubiquitin-proteasome and autophagy-lysosome systems. In *FEBS letters* 584 (7), pp. 1393–1398. DOI: 10.1016/j.febslet.2009.12.047.

144. Koutsoudakis, George; Kaul, Artur; Steinmann, Eike; Kallis, Stephanie; Lohmann, Volker; Pietschmann, Thomas; Bartenschlager, Ralf (2006): Characterization of the early steps of hepatitis C virus infection by using luciferase reporter viruses. In *Journal of virology* 80 (11), pp. 5308–5320. DOI: 10.1128/JVI.02460-05.

145. Kroemer, Guido; Mariño, Guillermo; Levine, Beth (2010): Autophagy and the integrated stress response. In *Molecular cell* 40 (2), pp. 280–293. DOI: 10.1016/j.molcel.2010.09.023.

146. Kryston, Thomas B.; Georgiev, Anastassiya B.; Pissis, Polycarpos; Georgakilas, Alexandros G. (2011): Role of oxidative stress and DNA damage in human carcinogenesis. In *Mutation research* 711 (1-2), pp. 193–201. DOI: 10.1016/j.mrfmmm.2010.12.016.

147. Kucera, Ana; Bakke, Oddmund; Progida, Cinzia (2016): The multiple roles of Rab9 in the endolysosomal system. In *Communicative & integrative biology* 9 (4), e1204498. DOI: 10.1080/19420889.2016.1204498.

148. Kuiken, Carla; Simmonds, Peter (2009): Nomenclature and numbering of the hepatitis C virus. In *Methods in molecular biology (Clifton, N.J.)* 510, pp. 33–53. DOI: 10.1007/978-1-59745-394-3_4.

149. Kukhanova, Marina K.; Tunitskaya, Vera L.; Smirnova, Olga A.; Khomich, Olga A.; Zakirova, Natalia F.; Ivanova, Olga N. et al. (2019): Hepatitis C Virus RNA-Dependent RNA Polymerase Is Regulated by Cysteine S-Glutathionylation. In *Oxidative medicine and cellular longevity* 2019, p. 3196140. DOI: 10.1155/2019/3196140.

150. Kwak, Juri; Tiwari, Indira; Jang, Kyung Lib (2017): Hepatitis C virus core activates proteasomal activator 28γ expression via upregulation of p53 levels to control virus propagation. In *The Journal of general virology* 98 (1), pp. 56–67. DOI: 10.1099/jgv.0.000655.

151. Kwak, Mi-Kyoung; Kensler, Thomas W. (2006): Induction of 26S proteasome subunit PSMB5 by the bifunctional inducer 3-methylcholanthrene through the Nrf2-ARE, but not the AhR/Arnt-XRE, pathway. In *Biochemical and biophysical research communications* 345 (4), pp. 1350–1357. DOI: 10.1016/j.bbrc.2006.05.043.

152. Lai, Chao-Kuen; Jeng, King-Song; Machida, Keigo; Lai, Michael M. C. (2010): Hepatitis C virus egress and release depend on endosomal trafficking of core protein. In *Journal of virology* 84 (21), pp. 11590–11598. DOI: 10.1128/JVI.00587-10.

153. Le Cong; Ran, F. Ann; Cox, David; Lin, Shuailiang; Barretto, Robert; Habib, Naomi et al. (2013): Multiplex genome engineering using CRISPR/Cas systems. In *Science (New York, N.Y.)* 339 (6121), pp. 819–823. DOI: 10.1126/science.1231143.

154. Lee, Gi Young; Lee, Sora; Lee, Hye-Ra; Yoo, Young Do (2016a): Hepatitis C virus p7 mediates membrane-to-membrane adhesion. In *Biochimica et biophysica acta* 1861 (9 Pt A), pp. 1096–1101. DOI: 10.1016/j.bbalip.2016.06.011.

155. Lee, Hye-Ra; Lee, Gi Young; You, Deok-Gyun; Kim, Hong Kyu; Yoo, Young Do (2020): Hepatitis C Virus p7 Induces Membrane Permeabilization by Interacting with Phosphatidylserine. In *International journal of molecular sciences* 21 (3). DOI: 10.3390/ijms21030897.

156. Lee, Kuan-Ying; Chen, Yi-Hung; Hsu, Shih-Chin; Yu, Ming-Jiun (2016b): Phosphorylation of Serine 235 of the Hepatitis C Virus Non-Structural Protein

NS5A by Multiple Kinases. In *PloS one* 11 (11), e0166763. DOI: 10.1371/journal.pone.0166763.

157. Leestemaker, Yves; Jong, Annemieke de; Witting, Katharina F.; Penning, Renske; Schuurman, Karianne; Rodenko, Boris et al. (2017): Proteasome Activation by Small Molecules. In *Cell chemical biology* 24 (6), 725-736.e7. DOI: 10.1016/j.chembiol.2017.05.010.

158. Lefèvre, Mathieu; Felmlee, Daniel J.; Parnot, Marie; Baumert, Thomas F.; Schuster, Catherine (2014): Syndecan 4 is involved in mediating HCV entry through interaction with lipoviral particle-associated apolipoprotein E. In *PloS one* 9 (4), e95550. DOI: 10.1371/journal.pone.0095550.

159. Li, Kui; Foy, Eileen; Ferreon, Josephine C.; Nakamura, Mitsuyasu; Ferreon, Allan C. M.; Ikeda, Masanori et al. (2005): Immune evasion by hepatitis C virus NS3/4A protease-mediated cleavage of the Toll-like receptor 3 adaptor protein TRIF. In *Proceedings of the National Academy of Sciences of the United States of America* 102 (8), pp. 2992–2997. DOI: 10.1073/pnas.0408824102.

160. Li, Li; Kim, Eunjung; Yuan, Haixin; Inoki, Ken; Goraksha-Hicks, Pankuri; Schiesher, Rachel L. et al. (2010): Regulation of mTORC1 by the Rab and Arf GTPases. In *The Journal of biological chemistry* 285 (26), pp. 19705–19709. DOI: 10.1074/jbc.C110.102483.

161. Liang, Yisha; Zhang, Guigen; Li, Qiheng; Han, Lin; Hu, Xiaoyou; Guo, Yu et al. (2021): TRIM26 is a critical host factor for HCV replication and contributes to host tropism. In *Science advances* 7 (2). DOI: 10.1126/sciadv.abd9732.

162. Lindenbach, Brett D.; Evans, Matthew J.; Syder, Andrew J.; Wölk, Benno; Tellinghuisen, Timothy L.; Liu, Christopher C. et al. (2005): Complete replication of hepatitis C virus in cell culture. In *Science (New York, N.Y.)* 309 (5734), pp. 623–626. DOI: 10.1126/science.1114016.

163. Lindenbach, Brett D.; Meuleman, Philip; Ploss, Alexander; Vanwolleghem, Thomas; Syder, Andrew J.; McKeating, Jane A. et al. (2006): Cell culture-grown hepatitis C virus is infectious in vivo and can be recultured in vitro. In *Proceedings of the National Academy of Sciences of the United States of America* 103 (10), pp. 3805–3809. DOI: 10.1073/pnas.0511218103.

164. Lindenbach, Brett D.; Prágai, Béla M.; Montserret, Roland; Beran, Rudolf K. F.; Pyle, Anna M.; Penin, François; Rice, Charles M. (2007): The C terminus of hepatitis C virus NS4A encodes an electrostatic switch that regulates NS5A hyperphosphorylation and viral replication. In *Journal of virology* 81 (17), pp. 8905–8918. DOI: 10.1128/JVI.00937-07.

165. Lindenbach, Brett D.; Rice, Charles M. (2005): Unravelling hepatitis C virus replication from genome to function. In *Nature* 436 (7053), pp. 933–938. DOI: 10.1038/nature04077.

166. Lindenbach, Brett D.; Rice, Charles M. (2013): The ins and outs of hepatitis C virus entry and assembly. In *Nature reviews. Microbiology* 11 (10), pp. 688–700. DOI: 10.1038/nrmicro3098.

167. Livneh, Ido; Cohen-Kaplan, Victoria; Cohen-Rosenzweig, Chen; Avni, Noa; Ciechanover, Aaron (2016): The life cycle of the 26S proteasome. From birth, through regulation and function, and onto its death. In *Cell research* 26 (8), pp. 869–885. DOI: 10.1038/cr.2016.86.

168. Lohmann, V.; Körner, F.; Dobierzewska, A.; Bartenschlager, R. (2001): Mutations in hepatitis C virus RNAs conferring cell culture adaptation. In *Journal of virology* 75 (3), pp. 1437–1449. DOI: 10.1128/JVI.75.3.1437-1449.2001.

169. Lohmann, V.; Körner, F.; Koch, J.; Herian, U.; Theilmann, L.; Bartenschlager, R. (1999): Replication of subgenomic hepatitis C virus RNAs in a hepatoma cell line. In *Science (New York, N.Y.)* 285 (5424), pp. 110–113. DOI: 10.1126/science.285.5424.110.

170. Lohmann, Volker (2013): Hepatitis C virus RNA replication. In *Current topics in microbiology and immunology* 369, pp. 167–198. DOI: 10.1007/978-3-642-27340-7_7.

171. Lundin, Marika; Lindström, Hannah; Grönwall, Caroline; Persson, Mats A. A. (2006): Dual topology of the processed hepatitis C virus protein NS4B is influenced by the NS5A protein. In *The Journal of general virology* 87 (Pt 11), pp. 3263–3272. DOI: 10.1099/vir.0.82211-0.

172. Lupberger, Joachim; Zeisel, Mirjam B.; Xiao, Fei; Thumann, Christine; Fofana, Isabel; Zona, Laetitia et al. (2011): EGFR and EphA2 are host factors for hepatitis C virus entry and possible targets for antiviral therapy. In *Nature medicine* 17 (5), pp. 589–595. DOI: 10.1038/nm.2341.

173. Lynch, Shaina M.; Wu, George Y. (2016): Hepatitis C Virus. A Review of Treatment Guidelines, Cost-effectiveness, and Access to Therapy. In *Journal of clinical and translational hepatology* 4 (4), pp. 310–319. DOI: 10.14218/JCTH.2016.00027.

174. Ma, Yinghong; Anantpadma, Manu; Timpe, Jennifer M.; Shanmugam, Saravanabalaji; Singh, Sher M.; Lemon, Stanley M.; Yi, Minkyung (2011): Hepatitis C virus NS2 protein serves as a scaffold for virus assembly by interacting with both structural and nonstructural proteins. In *Journal of virology* 85 (1), pp. 86–97. DOI: 10.1128/JVI.01070-10.

175. Macdonald, Andrew; Crowder, Katherine; Street, Andrew; McCormick, Christopher; Harris, Mark (2004): The hepatitis C virus NS5A protein binds to members of the Src family of tyrosine kinases and regulates kinase activity. In *The Journal of general virology* 85 (Pt 3), pp. 721–729. DOI: 10.1099/vir.0.19691-0.

176. Madan, Vanesa; Bartenschlager, Ralf (2015): Structural and Functional Properties of the Hepatitis C Virus p7 Viroporin. In *Viruses* 7 (8), pp. 4461–4481. DOI: 10.3390/v7082826.

177. Mankouri, Jamel; Walter, Cheryl; Stewart, Hazel; Bentham, Matthew; Park, Wei Sun; Heo, Won Do et al. (2016): Release of Infectious Hepatitis C Virus from Huh7 Cells Occurs via a trans-Golgi Network-to-Endosome Pathway Independent of Very-Low-Density Lipoprotein Secretion. In *Journal of virology* 90 (16), pp. 7159–7170. DOI: 10.1128/JVI.00826-16.

178. Martell, M.; Esteban, J. I.; Quer, J.; Genescà, J.; Weiner, A.; Esteban, R. et al. (1992): Hepatitis C virus (HCV) circulates as a population of different but closely related genomes. Quasispecies nature of HCV genome distribution. In *Journal of virology* 66 (5), pp. 3225–3229. DOI: 10.1128/JVI.66.5.3225-3229.1992.

179. Martin, Danyelle N.; Uprichard, Susan L. (2013): Identification of transferrin receptor 1 as a hepatitis C virus entry factor. In *Proceedings of the National*

Academy of Sciences of the United States of America 110 (26), pp. 10777–10782. DOI: 10.1073/pnas.1301764110.

180. Marwaha, Neelam; Sachdev, Suchet (2014): Current testing strategies for hepatitis C virus infection in blood donors and the way forward. In *World journal of gastroenterology* 20 (11), pp. 2948–2954. DOI: 10.3748/wjg.v20.i11.2948.

181. Masaki, Takahiro; Matsunaga, Satoko; Takahashi, Hirotaka; Nakashima, Kenji; Kimura, Yayoi; Ito, Masahiko et al. (2014): Involvement of hepatitis C virus NS5A hyperphosphorylation mediated by casein kinase I-α in infectious virus production. In *Journal of virology* 88 (13), pp. 7541–7555. DOI: 10.1128/JVI.03170-13.

182. McLauchlan, J. (2000): Properties of the hepatitis C virus core protein. A structural protein that modulates cellular processes. In *Journal of viral hepatitis* 7 (1), pp. 2–14. DOI: 10.1046/j.1365-2893.2000.00201.x.

183. Medvedev, Regina; Hildt, Eberhard; Ploen, Daniela (2017a): Look who's talking-the crosstalk between oxidative stress and autophagy supports exosomal-dependent release of HCV particles. In *Cell biology and toxicology* 33 (3), pp. 211–231. DOI: 10.1007/s10565-016-9376-3.

184. Medvedev, Regina; Ploen, Daniela; Hildt, Eberhard (2016): HCV and Oxidative Stress. Implications for HCV Life Cycle and HCV-Associated Pathogenesis. In *Oxidative medicine and cellular longevity* 2016, p. 9012580. DOI: 10.1155/2016/9012580.

185. Medvedev, Regina; Ploen, Daniela; Spengler, Catrina; Elgner, Fabian; Ren, Huimei; Bunten, Sarah; Hildt, Eberhard (2017b): HCV-induced oxidative stress by inhibition of Nrf2 triggers autophagy and favors release of viral particles. In *Free radical biology & medicine* 110, pp. 300–315. DOI: 10.1016/j.freeradbiomed.2017.06.021.

186. Meertens, Laurent; Bertaux, Claire; Dragic, Tatjana (2006): Hepatitis C virus entry requires a critical postinternalization step and delivery to early endosomes via clathrin-coated vesicles. In *Journal of virology* 80 (23), pp. 11571–11578. DOI: 10.1128/JVI.01717-06.

187. Menzel, Nicolas; Fischl, Wolfgang; Hueging, Kathrin; Bankwitz, Dorothea; Frentzen, Anne; Haid, Sibylle et al. (2012): MAP-kinase regulated cytosolic phospholipase A2 activity is essential for production of infectious hepatitis C virus particles. In *PLoS pathogens* 8 (7), e1002829. DOI: 10.1371/journal.ppat.1002829.

188. Merz, Andreas; Long, Gang; Hiet, Marie-Sophie; Brügger, Britta; Chlanda, Petr; Andre, Patrice et al. (2011): Biochemical and morphological properties of hepatitis C virus particles and determination of their lipidome. In *The Journal of biological chemistry* 286 (4), pp. 3018–3032. DOI: 10.1074/jbc.M110.175018.

189. Messina, Jane P.; Humphreys, Isla; Flaxman, Abraham; Brown, Anthony; Cooke, Graham S.; Pybus, Oliver G.; Barnes, Eleanor (2015): Global distribution and prevalence of hepatitis C virus genotypes. In *Hepatology (Baltimore, Md.)* 61 (1), pp. 77–87. DOI: 10.1002/hep.27259.

190. Mindell, Joseph A. (2012): Lysosomal acidification mechanisms. In *Annual review of physiology* 74, pp. 69–86. DOI: 10.1146/annurev-physiol-012110-142317.

191. Miyanari, Yusuke; Atsuzawa, Kimie; Usuda, Nobuteru; Watashi, Koichi; Hishiki, Takayuki; Zayas, Margarita et al. (2007): The lipid droplet is an important organelle for hepatitis C virus production. In *Nature cell biology* 9 (9), pp. 1089–1097. DOI: 10.1038/ncb1631.

192. Mizushima, Noboru; Levine, Beth; Cuervo, Ana Maria; Klionsky, Daniel J. (2008): Autophagy fights disease through cellular self-digestion. In *Nature* 451 (7182), pp. 1069–1075. DOI: 10.1038/nature06639.

193. Mizushima, Noboru; Yoshimori, Tamotsu; Ohsumi, Yoshinori (2011): The role of Atg proteins in autophagosome formation. In *Annual review of cell and developmental biology* 27, pp. 107–132. DOI: 10.1146/annurev-cellbio-092910-154005.

194. Moradpour, Darius; Evans, Matthew J.; Gosert, Rainer; Yuan, Zhenghong; Blum, Hubert E.; Goff, Stephen P. et al. (2004): Insertion of green fluorescent protein into nonstructural protein 5A allows direct visualization of functional hepatitis C virus replication complexes. In *Journal of virology* 78 (14), pp. 7400–7409. DOI: 10.1128/JVI.78.14.7400-7409.2004.

195. Moradpour, Darius; Penin, François; Rice, Charles M. (2007): Replication of hepatitis C virus. In *Nature reviews. Microbiology* 5 (6), pp. 453–463. DOI: 10.1038/nrmicro1645.

196. Mori, Hiroyuki; Fukuhara, Takasuke; Ono, Chikako; Tamura, Tomokazu; Sato, Asuka; Fauzyah, Yuzy et al. (2018): Induction of selective autophagy in cells replicating hepatitis C virus genome. In *The Journal of general virology* 99 (12), pp. 1643–1657. DOI: 10.1099/jgv.0.001161.

197. Moriishi, Kohji; Shoji, Ikuo; Mori, Yoshio; Suzuki, Ryosuke; Suzuki, Tetsuro; Kataoka, Chikako; Matsuura, Yoshiharu (2010): Involvement of PA28gamma in the propagation of hepatitis C virus. In *Hepatology (Baltimore, Md.)* 52 (2), pp. 411–420. DOI: 10.1002/hep.23680.

198. Morikawa, K.; Lange, C. M.; Gouttenoire, J.; Meylan, E.; Brass, V.; Penin, F.; Moradpour, D. (2011): Nonstructural protein 3-4A. The Swiss army knife of hepatitis C virus. In *Journal of viral hepatitis* 18 (5), pp. 305–315. DOI: 10.1111/j.1365-2893.2011.01451.x.

199. Moustafa, Rehab I.; Haddad, Juliano G.; Linna, Lydia; Hanoulle, Xavier; Descamps, Véronique; Mesalam, Ahmed Atef et al. (2018): Functional Study of the C-Terminal Part of the Hepatitis C Virus E1 Ectodomain. In *Journal of virology* 92 (20). DOI: 10.1128/JVI.00939-18.

200. Munakata, Tsubasa; Liang, Yuqiong; Kim, Seungtaek; McGivern, David R.; Huibregtse, Jon; Nomoto, Akio; Lemon, Stanley M. (2007): Hepatitis C virus induces E6AP-dependent degradation of the retinoblastoma protein. In *PLoS pathogens* 3 (9), pp. 1335–1347. DOI: 10.1371/journal.ppat.0030139.

201. Munakata, Tsubasa; Nakamura, Mitsuyasu; Liang, Yuqiong; Li, Kui; Lemon, Stanley M. (2005): Down-regulation of the retinoblastoma tumor suppressor by the hepatitis C virus NS5B RNA-dependent RNA polymerase. In *Proceedings of the National Academy of Sciences of the United States of America* 102 (50), pp. 18159–18164. DOI: 10.1073/pnas.0505605102.

202. Nawaz, Allah; Zaidi, Syed Faisal; Usmanghani, Khan; Ahmad, Irshad (2015): Concise review on the insight of hepatitis C. In *Journal of Taibah University Medical Sciences* 10 (2), pp. 132–139. DOI: 10.1016/j.jtumed.2014.08.004.

203. Neufeldt, Christopher J.; Cortese, Mirko; Acosta, Eliana G.; Bartenschlager, Ralf (2018): Rewiring cellular networks by members of the Flaviviridae family. In *Nature reviews. Microbiology* 16 (3), pp. 125–142. DOI: 10.1038/nrmicro.2017.170.

204. Nishino, I.; Fu, J.; Tanji, K.; Yamada, T.; Shimojo, S.; Koori, T. et al. (2000): Primary LAMP-2 deficiency causes X-linked vacuolar cardiomyopathy and myopathy (Danon disease). In *Nature* 406 (6798), pp. 906–910. DOI: 10.1038/35022604.

205. Nishino, Ichizo (2003): Autophagic vacuolar myopathies. In *Current neurology and neuroscience reports* 3 (1), pp. 64–69. DOI: 10.1007/s11910-003-0040-y.

206. Nogami, Satoru; Satoh, Sachie; Nakano, Michiko; Shimizu, Hiroaki; Fukushima, Hiromichi; Maruyama, Ayumi et al. (2003a): Taxilin; a novel syntaxin-binding protein that is involved in Ca2+-dependent exocytosis in neuroendocrine cells. In *Genes to cells : devoted to molecular & cellular mechanisms* 8 (1), pp. 17–28. DOI: 10.1046/j.1365-2443.2003.00612.x.

207. Nogami, Satoru; Satoh, Sachie; Nakano, Michiko; Terano, Akira; Shirataki, Hiromichi (2003b): Interaction of taxilin with syntaxin which does not form the SNARE complex. In *Biochemical and biophysical research communications* 311 (4), pp. 797–802. DOI: 10.1016/j.bbrc.2003.10.069.

208. Oh, In Soo; Textoris-Taube, Kathrin; Sung, Pil Soo; Kang, Wonseok; Gorny, Xenia; Kähne, Thilo et al. (2016): Immunoproteasome induction is suppressed in hepatitis C virus-infected cells in a protein kinase R-dependent manner. In *Experimental & molecular medicine* 48 (11), e270. DOI: 10.1038/emm.2016.98.

209. Olzmann, James A.; Li, Lian; Chudaev, Maksim V.; Chen, Jue; Perez, Francisco A.; Palmiter, Richard D.; Chin, Lih-Shen (2007): Parkin-mediated K63-linked polyubiquitination targets misfolded DJ-1 to aggresomes via binding to HDAC6. In *The Journal of cell biology* 178 (6), pp. 1025–1038. DOI: 10.1083/jcb.200611128.

210. Orlowski, M. (1990): The multicatalytic proteinase complex, a major extralysosomal proteolytic system. In *Biochemistry* 29 (45), pp. 10289–10297. DOI: 10.1021/bi00497a001.

211. Orlowski, Marian; Wilk, Sherwin (2003): Ubiquitin-independent proteolytic functions of the proteasome. In *Archives of biochemistry and biophysics* 415 (1), pp. 1–5. DOI: 10.1016/s0003-9861(03)00197-8.

212. Parzych, Katherine R.; Klionsky, Daniel J. (2014): An overview of autophagy. Morphology, mechanism, and regulation. In *Antioxidants & redox signaling* 20 (3), pp. 460–473. DOI: 10.1089/ars.2013.5371.

213. Pascual, Sonia; Herrera, Iván; Irurzun, Javier (2016): New advances in hepatocellular carcinoma. In *World journal of hepatology* 8 (9), pp. 421–438. DOI: 10.4254/wjh.v8.i9.421.

214. Pascut, Devis; Hoang, Minh; Nguyen, Nhu N. Q.; Pratama, Muhammad Yogi; Tiribelli, Claudio (2021): HCV Proteins Modulate the Host Cell miRNA Expression

Contributing to Hepatitis C Pathogenesis and Hepatocellular Carcinoma Development. In *Cancers* 13 (10). DOI: 10.3390/cancers13102485.

215. Paul, David; Hoppe, Simone; Saher, Gesine; Krijnse-Locker, Jacomine; Bartenschlager, Ralf (2013): Morphological and biochemical characterization of the membranous hepatitis C virus replication compartment. In *Journal of virology* 87 (19), pp. 10612–10627. DOI: 10.1128/JVI.01370-13.

216. Pawlotsky, Jean-Michel; Feld, Jordan J.; Zeuzem, Stefan; Hoofnagle, Jay H. (2015): From non-A, non-B hepatitis to hepatitis C virus cure. In *Journal of hepatology* 62 (1 Suppl), S87-99. DOI: 10.1016/j.jhep.2015.02.006.

217. Penin, François; Dubuisson, Jean; Rey, Felix A.; Moradpour, Darius; Pawlotsky, Jean-Michel (2004): Structural biology of hepatitis C virus. In *Hepatology (Baltimore, Md.)* 39 (1), pp. 5–19. DOI: 10.1002/hep.20032.

218. Petruzziello, Arnolfo; Marigliano, Samantha; Loquercio, Giovanna; Cozzolino, Anna; Cacciapuoti, Carmela (2016): Global epidemiology of hepatitis C virus infection. An up-date of the distribution and circulation of hepatitis C virus genotypes. In *World journal of gastroenterology* 22 (34), pp. 7824–7840. DOI: 10.3748/wjg.v22.i34.7824.

219. Pickart, C. M. (2000): Ubiquitin in chains. In *Trends in biochemical sciences* 25 (11), pp. 544–548. DOI: 10.1016/s0968-0004(00)01681-9.

220. Pietschmann, Thomas; Kaul, Artur; Koutsoudakis, George; Shavinskaya, Anna; Kallis, Stephanie; Steinmann, Eike et al. (2006): Construction and characterization of infectious intragenotypic and intergenotypic hepatitis C virus chimeras. In *Proceedings of the National Academy of Sciences of the United States of America* 103 (19), pp. 7408–7413. DOI: 10.1073/pnas.0504877103.

221. Pileri, P.; Uematsu, Y.; Campagnoli, S.; Galli, G.; Falugi, F.; Petracca, R. et al. (1998): Binding of hepatitis C virus to CD81. In *Science (New York, N.Y.)* 282 (5390), pp. 938–941. DOI: 10.1126/science.282.5390.938.

222. Ploen, Daniela; Hafirassou, Mohamed Lamine; Himmelsbach, Kiyoshi; Sauter, Daniel; Biniossek, Martin L.; Weiss, Thomas S. et al. (2013a): TIP47 plays a crucial role in the life cycle of hepatitis C virus. In *Journal of hepatology* 58 (6), pp. 1081–1088. DOI: 10.1016/j.jhep.2013.01.022.

223. Ploen, Daniela; Hafirassou, Mohamed Lamine; Himmelsbach, Kiyoshi; Schille, Stefan A.; Biniossek, Martin L.; Baumert, Thomas F. et al. (2013b): TIP47 is associated with the hepatitis C virus and its interaction with Rab9 is required for release of viral particles. In *European journal of cell biology* 92 (12), pp. 374–382. DOI: 10.1016/j.ejcb.2013.12.003.

224. Ploen, Daniela; Hildt, Eberhard (2015): Hepatitis C virus comes for dinner. How the hepatitis C virus interferes with autophagy. In *World journal of gastroenterology* 21 (28), pp. 8492–8507. DOI: 10.3748/wjg.v21.i28.8492.

225. Ploss, Alexander; Evans, Matthew J.; Gaysinskaya, Valeriya A.; Panis, Maryline; You, Hana; Jong, Ype P. de; Rice, Charles M. (2009): Human occludin is a hepatitis C virus entry factor required for infection of mouse cells. In *Nature* 457 (7231), pp. 882–886. DOI: 10.1038/nature07684.

226. Ploss, Alexander; Khetani, Salman R.; Jones, Christopher T.; Syder, Andrew J.; Trehan, Kartik; Gaysinskaya, Valeriya A. et al. (2010): Persistent hepatitis C virus infection in microscale primary human hepatocyte cultures. In *Proceedings of the*

National Academy of Sciences of the United States of America 107 (7), pp. 3141–3145. DOI: 10.1073/pnas.0915130107.

227. Podevin, Philippe; Carpentier, Arnaud; Pène, Véronique; Aoudjehane, Lynda; Carrière, Matthieu; Zaïdi, Sakina et al. (2010): Production of infectious hepatitis C virus in primary cultures of human adult hepatocytes. In *Gastroenterology* 139 (4), pp. 1355–1364. DOI: 10.1053/j.gastro.2010.06.058.

228. Popescu, Costin-Ioan; Callens, Nathalie; Trinel, Dave; Roingeard, Philippe; Moradpour, Darius; Descamps, Véronique et al. (2011): NS2 protein of hepatitis C virus interacts with structural and non-structural proteins towards virus assembly. In *PLoS pathogens* 7 (2), e1001278. DOI: 10.1371/journal.ppat.1001278.

229. Popescu, Costin-Ioan; Riva, Laura; Vlaicu, Ovidiu; Farhat, Rayan; Rouillé, Yves; Dubuisson, Jean (2014): Hepatitis C virus life cycle and lipid metabolism. In *Biology* 3 (4), pp. 892–921. DOI: 10.3390/biology3040892.

230. Quinkert, Doris; Bartenschlager, Ralf; Lohmann, Volker (2005): Quantitative analysis of the hepatitis C virus replication complex. In *Journal of virology* 79 (21), pp. 13594–13605. DOI: 10.1128/JVI.79.21.13594-13605.2005.

231. Ran, F. Ann; Hsu, Patrick D.; Wright, Jason; Agarwala, Vineeta; Scott, David A.; Zhang, Feng (2013): Genome engineering using the CRISPR-Cas9 system. In *Nature protocols* 8 (11), pp. 2281–2308. DOI: 10.1038/nprot.2013.143.

232. Rao, Varsha; Guan, Bin; Mutton, Laura N.; Bieberich, Charles J. (2012): Proline-mediated proteasomal degradation of the prostate-specific tumor suppressor NKX3.1. In *The Journal of biological chemistry* 287 (43), pp. 36331–36340. DOI: 10.1074/jbc.M112.352823.

233. Ravikumar, Brinda; Moreau, Kevin; Jahreiss, Luca; Puri, Claudia; Rubinsztein, David C. (2010): Plasma membrane contributes to the formation of pre-autophagosomal structures. In *Nature cell biology* 12 (8), pp. 747–757. DOI: 10.1038/ncb2078.

234. Reggiori, Fulvio; Shintani, Takahiro; Nair, Usha; Klionsky, Daniel J. (2005): Atg9 cycles between mitochondria and the pre-autophagosomal structure in yeasts. In *Autophagy* 1 (2), pp. 101–109. DOI: 10.4161/auto.1.2.1840.

235. Reiss, Simon; Rebhan, Ilka; Backes, Perdita; Romero-Brey, Ines; Erfle, Holger; Matula, Petr et al. (2011): Recruitment and activation of a lipid kinase by hepatitis C virus NS5A is essential for integrity of the membranous replication compartment. In *Cell host & microbe* 9 (1), pp. 32–45. DOI: 10.1016/j.chom.2010.12.002.

236. Ren, Huimei; Elgner, Fabian; Himmelsbach, Kiyoshi; Akhras, Sami; Jiang, Bingfu; Medvedev, Regina et al. (2017): Identification of syntaxin 4 as an essential factor for the hepatitis C virus life cycle. In *European journal of cell biology* 96 (6), pp. 542–552. DOI: 10.1016/j.ejcb.2017.06.002.

237. Ren, Huimei; Elgner, Fabian; Jiang, Bingfu; Himmelsbach, Kiyoshi; Medvedev, Regina; Ploen, Daniela; Hildt, Eberhard (2016): The Autophagosomal SNARE Protein Syntaxin 17 Is an Essential Factor for the Hepatitis C Virus Life Cycle. In *Journal of virology* 90 (13), pp. 5989–6000. DOI: 10.1128/JVI.00551-16.

238. Reynolds, Gary M.; Harris, Helen J.; Jennings, Adam; Hu, Ke; Grove, Joe; Lalor, Patricia F. et al. (2008): Hepatitis C virus receptor expression in normal and

diseased liver tissue. In *Hepatology (Baltimore, Md.)* 47 (2), pp. 418–427. DOI: 10.1002/hep.22028.

239. Ríos-Ocampo, W. Alfredo; Daemen, Toos; Buist-Homan, Manon; Faber, Klaas Nico; Navas, María-Cristina; Moshage, Han (2019): Hepatitis C virus core or NS3/4A protein expression preconditions hepatocytes against oxidative stress and endoplasmic reticulum stress. In *Redox report : communications in free radical research* 24 (1), pp. 17–26. DOI: 10.1080/13510002.2019.1596431.

240. Rivett, A. J. (1989): The Multicatalytic Proteinase. In *The Journal of biological chemistry* 264 (21), pp. 12215–12219. DOI: 10.1016/S0021-9258(18)63843-8.

241. Roberts, Eve A.; Yeung, Latifa (2002): Maternal-infant transmission of hepatitis C virus infection. In *Hepatology (Baltimore, Md.)* 36 (5 Suppl 1), S106-13. DOI: 10.1053/jhep.2002.36792.

242. Rockey, Don C.; Bissell, D. Montgomery (2006): Noninvasive measures of liver fibrosis. In *Hepatology (Baltimore, Md.)* 43 (2 Suppl 1), S113-20. DOI: 10.1002/hep.21046.

243. Romero-Brey, Inés; Bartenschlager, Ralf (2014): Membranous replication factories induced by plus-strand RNA viruses. In *Viruses* 6 (7), pp. 2826–2857. DOI: 10.3390/v6072826.

244. Romero-Brey, Inés; Merz, Andreas; Chiramel, Abhilash; Lee, Ji-Young; Chlanda, Petr; Haselman, Uta et al. (2012): Three-dimensional architecture and biogenesis of membrane structures associated with hepatitis C virus replication. In *PLoS pathogens* 8 (12), e1003056. DOI: 10.1371/journal.ppat.1003056.

245. Ross-Thriepland, Douglas; Amako, Yutaka; Harris, Mark (2013): The C terminus of NS5A domain II is a key determinant of hepatitis C virus genome replication, but is not required for virion assembly and release. In *The Journal of general virology* 94 (Pt 5), pp. 1009–1018. DOI: 10.1099/vir.0.050633-0.

246. Ross-Thriepland, Douglas; Mankouri, Jamel; Harris, Mark (2015): Serine phosphorylation of the hepatitis C virus NS5A protein controls the establishment of replication complexes. In *Journal of virology* 89 (6), pp. 3123–3135. DOI: 10.1128/JVI.02995-14.

247. Sabahi, Ali; Marsh, Katherine A.; Dahari, Harel; Corcoran, Peter; Lamora, Jennifer M.; Yu, Xuemei et al. (2010): The rate of hepatitis C virus infection initiation in vitro is directly related to particle density. In *Virology* 407 (1), pp. 110–119. DOI: 10.1016/j.virol.2010.07.026.

248. Sainz, Bruno; Barretto, Naina; Martin, Danyelle N.; Hiraga, Nobuhiko; Imamura, Michio; Hussain, Snawar et al. (2012): Identification of the Niemann-Pick C1-like 1 cholesterol absorption receptor as a new hepatitis C virus entry factor. In *Nature medicine* 18 (2), pp. 281–285. DOI: 10.1038/nm.2581.

249. Sakai, Akito; Claire, Marisa St; Faulk, Kristina; Govindarajan, Sugantha; Emerson, Suzanne U.; Purcell, Robert H.; Bukh, Jens (2003): The p7 polypeptide of hepatitis C virus is critical for infectivity and contains functionally important genotype-specific sequences. In *Proceedings of the National Academy of Sciences of the United States of America* 100 (20), pp. 11646–11651. DOI: 10.1073/pnas.1834545100.

250. Saleh, Maged; Rüschenbaum, Sabrina; Welsch, Christoph; Zeuzem, Stefan; Moradpour, Darius; Gouttenoire, Jérôme; Lange, Christian M. (2018): Glycogen

Synthase Kinase 3β Enhances Hepatitis C Virus Replication by Supporting miR-122. In *Frontiers in microbiology* 9, p. 2949. DOI: 10.3389/fmicb.2018.02949.

251. Salloum, Shadi; Wang, Hongliang; Ferguson, Charles; Parton, Robert G.; Tai, Andrew W. (2013): Rab18 binds to hepatitis C virus NS5A and promotes interaction between sites of viral replication and lipid droplets. In *PLoS pathogens* 9 (8), e1003513. DOI: 10.1371/journal.ppat.1003513.

252. Scarselli, Elisa; Ansuini, Helenia; Cerino, Raffaele; Roccasecca, Rosa Maria; Acali, Stefano; Filocamo, Gessica et al. (2002): The human scavenger receptor class B type I is a novel candidate receptor for the hepatitis C virus. In *The EMBO journal* 21 (19), pp. 5017–5025. DOI: 10.1093/emboj/cdf529.

253. Schulze, Heike; Kolter, Thomas; Sandhoff, Konrad (2009): Principles of lysosomal membrane degradation. Cellular topology and biochemistry of lysosomal lipid degradation. In *Biochimica et biophysica acta* 1793 (4), pp. 674–683. DOI: 10.1016/j.bbamcr.2008.09.020.

254. Seme, Katja; Poljak, Mario; Babic, Dunja Z.; Mocilnik, Tina; Vince, Adriana (2005): The role of core antigen detection in management of hepatitis C. A critical review. In *Journal of clinical virology : the official publication of the Pan American Society for Clinical Virology* 32 (2), pp. 92–101. DOI: 10.1016/j.jcv.2004.10.005.

255. Shao, Run-Xuan; Zhang, Leiliang; Peng, Lee F.; Sun, Eileen; Chung, Woo Jin; Jang, Jae Yong et al. (2010): Suppressor of cytokine signaling 3 suppresses hepatitis C virus replication in an mTOR-dependent manner. In *Journal of virology* 84 (12), pp. 6060–6069. DOI: 10.1128/JVI.02484-09.

256. Shi, Guoli; Suzuki, Tetsuro (2018): Molecular Basis of Encapsidation of Hepatitis C Virus Genome. In *Frontiers in microbiology* 9, p. 396. DOI: 10.3389/fmicb.2018.00396.

257. Shi, Qing; Jiang, Jieyun; Luo, Guangxiang (2013): Syndecan-1 serves as the major receptor for attachment of hepatitis C virus to the surfaces of hepatocytes. In *Journal of virology* 87 (12), pp. 6866–6875. DOI: 10.1128/JVI.03475-12.

258. Shiode, Yuto; Hikita, Hayato; Tanaka, Satoshi; Shirai, Kumiko; Doi, Akira; Sakane, Sadatsugu et al. (2020): Hepatitis C virus enhances Rubicon expression, leading to autophagy inhibition and intracellular innate immune activation. In *Scientific reports* 10 (1), p. 15290. DOI: 10.1038/s41598-020-72294-y.

259. Shoji, Ikuo (2012): Roles of the two distinct proteasome pathways in hepatitis C virus infection. In *World journal of virology* 1 (2), pp. 44–50. DOI: 10.5501/wjv.v1.i2.44.

260. Shrivastava, Shubham; Bhanja Chowdhury, Joydip; Steele, Robert; Ray, Ranjit; Ray, Ratna B. (2012): Hepatitis C virus upregulates Beclin1 for induction of autophagy and activates mTOR signaling. In *Journal of virology* 86 (16), pp. 8705–8712. DOI: 10.1128/JVI.00616-12.

261. Shrivastava, Shubham; Devhare, Pradip; Sujijantarat, Nanthiya; Steele, Robert; Kwon, Young-Chan; Ray, Ranjit; Ray, Ratna B. (2016): Knockdown of Autophagy Inhibits Infectious Hepatitis C Virus Release by the Exosomal Pathway. In *Journal of virology* 90 (3), pp. 1387–1396. DOI: 10.1128/JVI.02383-15.

262. Simmonds, Peter (2004): Genetic diversity and evolution of hepatitis C virus--15 years on. In *The Journal of general virology* 85 (Pt 11), pp. 3173–3188. DOI: 10.1099/vir.0.80401-0.

263. Sir, Donna; Chen, Wen-Ling; Choi, Jinah; Wakita, Takaji; Yen, T. S. Benedict; Ou, Jing-Hsiung James (2008): Induction of incomplete autophagic response by hepatitis C virus via the unfolded protein response. In *Hepatology (Baltimore, Md.)* 48 (4), pp. 1054–1061. DOI: 10.1002/hep.22464.

264. Siu, Gavin Ka Yu; Zhou, Fan; Yu, Mei Kuen; Zhang, Leiliang; Wang, Tuanlao; Liang, Yongheng et al. (2016): Hepatitis C virus NS5A protein cooperates with phosphatidylinositol 4-kinase IIIα to induce mitochondrial fragmentation. In *Scientific reports* 6, p. 23464. DOI: 10.1038/srep23464.

265. Stapleford, Kenneth A.; Lindenbach, Brett D. (2011): Hepatitis C virus NS2 coordinates virus particle assembly through physical interactions with the E1-E2 glycoprotein and NS3-NS4A enzyme complexes. In *Journal of virology* 85 (4), pp. 1706–1717. DOI: 10.1128/JVI.02268-10.

266. Steinmann, Eike; Penin, Francois; Kallis, Stephanie; Patel, Arvind H.; Bartenschlager, Ralf; Pietschmann, Thomas (2007): Hepatitis C virus p7 protein is crucial for assembly and release of infectious virions. In *PLoS pathogens* 3 (7), e103. DOI: 10.1371/journal.ppat.0030103.

267. Stoeck, Ina Karen; Lee, Ji-Young; Tabata, Keisuke; Romero-Brey, Inés; Paul, David; Schult, Philipp et al. (2018): Hepatitis C Virus Replication Depends on Endosomal Cholesterol Homeostasis. In *Journal of virology* 92 (1). DOI: 10.1128/JVI.01196-17.

268. Su, Wen-Chi; Chao, Ti-Chun; Huang, Yih-Leh; Weng, Shih-Che; Jeng, King-Song; Lai, Michael M. C. (2011): Rab5 and class III phosphoinositide 3-kinase Vps34 are involved in hepatitis C virus NS4B-induced autophagy. In *Journal of virology* 85 (20), pp. 10561–10571. DOI: 10.1128/JVI.00173-11.

269. Sumpter, Rhea; Loo, Yueh-Ming; Foy, Eileen; Li, Kui; Yoneyama, Mitsutoshi; Fujita, Takashi et al. (2005): Regulating intracellular antiviral defense and permissiveness to hepatitis C virus RNA replication through a cellular RNA helicase, RIG-I. In *Journal of virology* 79 (5), pp. 2689–2699. DOI: 10.1128/JVI.79.5.2689-2699.2005.

270. Suzuki, Ryosuke; Matsuda, Mami; Watashi, Koichi; Aizaki, Hideki; Matsuura, Yoshiharu; Wakita, Takaji; Suzuki, Tetsuro (2013): Signal peptidase complex subunit 1 participates in the assembly of hepatitis C virus through an interaction with E2 and NS2. In *PLoS pathogens* 9 (8), e1003589. DOI: 10.1371/journal.ppat.1003589.

271. Sy, Theodore; Jamal, M. Mazen (2006): Epidemiology of hepatitis C virus (HCV) infection. In *International journal of medical sciences* 3 (2), pp. 41–46. DOI: 10.7150/ijms.3.41.

272. Tabata, Keisuke; Neufeldt, Christopher J.; Bartenschlager, Ralf (2020): Hepatitis C Virus Replication. In *Cold Spring Harbor perspectives in medicine* 10 (3). DOI: 10.1101/cshperspect.a037093.

273. Takasugi, Toshiyuki; Minegishi, Seiji; Asada, Akiko; Saito, Taro; Kawahara, Hiroyuki; Hisanaga, Shin-ichi (2016): Two Degradation Pathways of the p35 Cdk5 (Cyclin-dependent Kinase) Activation Subunit, Dependent and Independent of Ubiquitination. In *The Journal of biological chemistry* 291 (9), pp. 4649–4657. DOI: 10.1074/jbc.M115.692871.

274. Tan, Jeanne M. M.; Wong, Esther S. P.; Kirkpatrick, Donald S.; Pletnikova, Olga; Ko, Han Seok; Tay, Shiam-Peng et al. (2008): Lysine 63-linked ubiquitination promotes the formation and autophagic clearance of protein inclusions associated with neurodegenerative diseases. In *Human molecular genetics* 17 (3), pp. 431–439. DOI: 10.1093/hmg/ddm320.

275. Tanaka, T.; Kato, N.; Cho, M. J.; Sugiyama, K.; Shimotohno, K. (1996): Structure of the 3' terminus of the hepatitis C virus genome. In *Journal of virology* 70 (5), pp. 3307–3312. DOI: 10.1128/JVI.70.5.3307-3312.1996.

276. Tanaka, Y.; Guhde, G.; Suter, A.; Eskelinen, E. L.; Hartmann, D.; Lüllmann-Rauch, R. et al. (2000): Accumulation of autophagic vacuoles and cardiomyopathy in LAMP-2-deficient mice. In *Nature* 406 (6798), pp. 902–906. DOI: 10.1038/35022595.

277. Tang, Hengli; Grisé, Henry (2009): Cellular and molecular biology of HCV infection and hepatitis. In *Clinical science (London, England : 1979)* 117 (2), pp. 49–65. DOI: 10.1042/CS20080631.

278. Tanida, Isei; Fukasawa, Masayoshi; Ueno, Takashi; Kominami, Eiki; Wakita, Takaji; Hanada, Kentaro (2009): Knockdown of autophagy-related gene decreases the production of infectious hepatitis C virus particles. In *Autophagy* 5 (7), pp. 937–945. DOI: 10.4161/auto.5.7.9243.

279. Tardif, Keith D.; Mori, Kazutoshi; Siddiqui, Aleem (2002): Hepatitis C virus subgenomic replicons induce endoplasmic reticulum stress activating an intracellular signaling pathway. In *Journal of virology* 76 (15), pp. 7453–7459. DOI: 10.1128/jvi.76.15.7453-7459.2002.

280. Tedbury, Philip; Welbourn, Sarah; Pause, Arnim; King, Barnabas; Griffin, Stephen; Harris, Mark (2011): The subcellular localization of the hepatitis C virus non-structural protein NS2 is regulated by an ion channel-independent function of the p7 protein. In *The Journal of general virology* 92 (Pt 4), pp. 819–830. DOI: 10.1099/vir.0.027441-0.

281. Tellinghuisen, Timothy L.; Foss, Katie L.; Treadaway, Jason C.; Rice, Charles M. (2008): Identification of residues required for RNA replication in domains II and III of the hepatitis C virus NS5A protein. In *Journal of virology* 82 (3), pp. 1073–1083. DOI: 10.1128/JVI.00328-07.

282. Tellinghuisen, Timothy L.; Marcotrigiano, Joseph; Gorbalenya, Alexander E.; Rice, Charles M. (2004): The NS5A protein of hepatitis C virus is a zinc metalloprotein. In *The Journal of biological chemistry* 279 (47), pp. 48576–48587. DOI: 10.1074/jbc.M407787200.

283. Terrault, Norah A. (2002): Sexual activity as a risk factor for hepatitis C. In *Hepatology (Baltimore, Md.)* 36 (5 Suppl 1), S99-105. DOI: 10.1053/jhep.2002.36797.

284. Tong, Yimin; Lavillette, Dimitri; Li, Qingchao; Zhong, Jin (2018): Role of Hepatitis C Virus Envelope Glycoprotein E1 in Virus Entry and Assembly. In *Frontiers in immunology* 9, p. 1411. DOI: 10.3389/fimmu.2018.01411.

285. Tsai, Chia-Ni; Pan, Ting-Chun; Chiang, Cho-Han; Yu, Chun-Chiao; Su, Shih-Han; Yu, Ming-Jiun (2019): Serine 229 Balances the Hepatitis C Virus Nonstructural Protein NS5A between Hypo- and Hyperphosphorylated States. In *Journal of virology* 93 (23). DOI: 10.1128/JVI.01028-19.

286. Tscherne, Donna M.; Jones, Christopher T.; Evans, Matthew J.; Lindenbach, Brett D.; McKeating, Jane A.; Rice, Charles M. (2006): Time- and temperature-dependent activation of hepatitis C virus for low-pH-triggered entry. In *Journal of virology* 80 (4), pp. 1734–1741. DOI: 10.1128/JVI.80.4.1734-1741.2006.

287. Ventura, Gustavo Tavares; Costa, Emmerson Corrêa Brasil da; Capaccia, Anne Miranda; Mohana-Borges, Ronaldo (2014): pH-dependent conformational changes in the HCV NS3 protein modulate its ATPase and helicase activities. In *PloS one* 9 (12), e115941. DOI: 10.1371/journal.pone.0115941.

288. Vieyres, Gabrielle; Thomas, Xavier; Descamps, Véronique; Duverlie, Gilles; Patel, Arvind H.; Dubuisson, Jean (2010): Characterization of the envelope glycoproteins associated with infectious hepatitis C virus. In *Journal of virology* 84 (19), pp. 10159–10168. DOI: 10.1128/JVI.01180-10.

289. Vogt, Dorothee A.; Ott, Melanie (2015): Membrane Flotation Assay. In *Bio-protocol* 5 (7). DOI: 10.21769/bioprotoc.1435.

290. Wakita, Takaji; Pietschmann, Thomas; Kato, Takanobu; Date, Tomoko; Miyamoto, Michiko; Zhao, Zijiang et al. (2005): Production of infectious hepatitis C virus in tissue culture from a cloned viral genome. In *Nature medicine* 11 (7), pp. 791–796. DOI: 10.1038/nm1268.

291. Wang, Ji; Kang, Rongyan; Huang, He; Xi, Xueyan; Wang, Bei; Wang, Jianwei; Zhao, Zhendong (2014): Hepatitis C virus core protein activates autophagy through EIF2AK3 and ATF6 UPR pathway-mediated MAP1LC3B and ATG12 expression. In *Autophagy* 10 (5), pp. 766–784. DOI: 10.4161/auto.27954.

292. Wang, Linya; Kim, Ja Yeon; Liu, Helene Minyi; Lai, Michael M. C.; Ou, Jing-Hsiung James (2017): HCV-induced autophagosomes are generated via homotypic fusion of phagophores that mediate HCV RNA replication. In *PLoS pathogens* 13 (9), e1006609. DOI: 10.1371/journal.ppat.1006609.

293. Wang, Linya; Ou, Jing-Hsiung James (2018): Regulation of Autophagy by Hepatitis C Virus for Its Replication. In *DNA and cell biology* 37 (4), pp. 287–290. DOI: 10.1089/dna.2017.4115.

294. Wang, Linya; Tian, Yongjun; Ou, Jing-Hsiung James (2015): HCV induces the expression of Rubicon and UVRAG to temporally regulate the maturation of autophagosomes and viral replication. In *PLoS pathogens* 11 (3), e1004764. DOI: 10.1371/journal.ppat.1004764.

295. Warkad, Shrikant Dashrath; Nimse, Satish Balasaheb; Song, Keum-Soo; Kim, Taisun (2018): HCV Detection, Discrimination, and Genotyping Technologies. In *Sensors (Basel, Switzerland)* 18 (10). DOI: 10.3390/s18103423.

296. WHO (2018): WHO HCV treatment. Available online at https://apps.who.int/iris/bitstream/handle/10665/260445/WHO-CDS-HIV-18.4-eng.pdf.

297. WHO HCV (2021): World Health Organization. HCV. Available online at https://www.who.int/news-room/fact-sheets/detail/hepatitis-c.

298. Wilfling, Florian; Haas, Joel T.; Walther, Tobias C.; Farese, Robert V. (2014): Lipid droplet biogenesis. In *Current opinion in cell biology* 29, pp. 39–45. DOI: 10.1016/j.ceb.2014.03.008.

299. Wooten, Marie W.; Geetha, Thangiah; Babu, J. Ramesh; Seibenhener, M. Lamar; Peng, Junmin; Cox, Nancy et al. (2008): Essential role of sequestosome 1/p62 in

regulating accumulation of Lys63-ubiquitinated proteins. In *The Journal of biological chemistry* 283 (11), pp. 6783–6789. DOI: 10.1074/jbc.M709496200.

300. Yanagi, M.; Purcell, R. H.; Emerson, S. U.; Bukh, J. (1997): Transcripts from a single full-length cDNA clone of hepatitis C virus are infectious when directly transfected into the liver of a chimpanzee. In *Proceedings of the National Academy of Sciences of the United States of America* 94 (16), pp. 8738–8743. DOI: 10.1073/pnas.94.16.8738.

301. Yen, Wei-Lien; Shintani, Takahiro; Nair, Usha; Cao, Yang; Richardson, Brian C.; Li, Zhijian et al. (2010): The conserved oligomeric Golgi complex is involved in double-membrane vesicle formation during autophagy. In *The Journal of cell biology* 188 (1), pp. 101–114. DOI: 10.1083/jcb.200904075.

302. Yu, Guann-Yi; Lee, Ki-Jeong; Gao, Lu; Lai, Michael M. C. (2006): Palmitoylation and polymerization of hepatitis C virus NS4B protein. In *Journal of virology* 80 (12), pp. 6013–6023. DOI: 10.1128/JVI.00053-06.

303. Zeisel, Mirjam B.; Felmlee, Daniel J.; Baumert, Thomas F. (2013): Hepatitis C virus entry. In *Current topics in microbiology and immunology* 369, pp. 87–112. DOI: 10.1007/978-3-642-27340-7_4.

304. Zeisel, Mirjam B.; Fofana, Isabel; Fafi-Kremer, Samira; Baumert, Thomas F. (2011): Hepatitis C virus entry into hepatocytes. Molecular mechanisms and targets for antiviral therapies. In *Journal of hepatology* 54 (3), pp. 566–576. DOI: 10.1016/j.jhep.2010.10.014.

305. Zhang, Wei; Aryan, Mahmoud; Qian, Steve; Cabrera, Roniel; Liu, Xiuli (2021): A Focused Review on Recent Advances in the Diagnosis and Treatment of Viral Hepatitis. In *Gastroenterology research* 14 (3), pp. 139–156. DOI: 10.14740/gr1405.

306. Zhong, Jin; Gastaminza, Pablo; Cheng, Guofeng; Kapadia, Sharookh; Kato, Takanobu; Burton, Dennis R. et al. (2005): Robust hepatitis C virus infection in vitro. In *Proceedings of the National Academy of Sciences of the United States of America* 102 (26), pp. 9294–9299. DOI: 10.1073/pnas.0503596102.

307. Zou, Dong-Mei; Sun, Wan-Ling (2017): Relationship between Hepatitis C Virus Infection and Iron Overload. In *Chinese medical journal* 130 (7), pp. 866–871. DOI: 10.4103/0366-6999.202737.

10 List of abbreviations

°C	Centigrade
µg	Microgram
µl	Microliter
µm	Micrometer
aa	Amino acids
AMPK	AMP-activated protein kinase
ApoE	Apolipoprotein E
APS	Ammonium persulfate
ARE	Antioxidative response element
ATF6	Activating transcription factor 6
Atg	Autophagy-related gene
ATP	Adenosine triphosphate
BFLA	Bafilomycin-A1
BODIPY	Boron-dipyrromethene
Bp	Base pairs
BSA	Bovines Serum Albumin
CAPN5	Calpain-5
CBLB	Casitas B-lineage lymphoma proto-oncogene B
cDNA	Complementary DNA
CHX	Cycloheximide
CLDN1	Claudin 1
CLF	Crude lysosomal fraction
CLIA	Chemiluminescence immunoassay
CLSM	Confocal laser scanning microscope
CMA	Chaperone-mediated autophagy
c-Raf	Rat fibrosarcoma 1
CRISPR-Cas9	Clustered Regularly Interspaced Short Palindromic Repeats-CRISPR associated protein 9
CTCF	Corrected total cell fluorescence
CTP	Cytidine triphosphate
DAAs	Direct-acting antivirals
DAPI	4,6-diamidino-2-phenylindole
DEPC-H_2O	Diethylpyrocarbonate H_2O
DFCP1	Double FYVE-containing protein 1
DGAT1	Diacylglycerol acyltransferase-1
DMEM	Dulbecco's Modified Eagles Medium
DMSO	Dimethyl sulfoxide
DMV	Double membrane vesicles
DNA	Deoxyribonucleic acid
DNase	Deoxyribonuclease
dNTP	Deoxyribonucleoside triphosphate
DTT	1,4-Dithiothreitol
DUB	Deubiquitinating enzyme
E6AP	E6-associated protein / Ubiquitin-protein ligase E3A (UBE3A)
E.coli	*Escherichia coli*
EDTA	Ethylenediaminetetraacetic acid
EE	Early endosome
EEA1	Early endosome antigen 1
EGFR	Epidermal growth factor receptor

ELISA	Enzyme-linked immunosorbent assay
EphA2	Ephrin type-A receptor 2
ER	Endoplasmatic reticulum
ERK	Extracellular-signal regulated kinase
ESCRT	Endosomal sorting complexes required for transport
et al.	et alii (and others)
FCS	Fetal calf serum
FIT	Fat storage-inducing transmembrane protein
Fwd	Forward
g	Gram
g/rcf	Gravity of g-force/relative centrifugal force
G418	Geneticin
GAPDH	Glyceraldehyde 3-phosphate dehydrogenase
GSK3	Glycogen synthase kinase 3
GTP	Guanosine triphosphate
h	Hour
HCC	Hepatocellular carcinoma
HCV	Hepatitis C virus
HCVcc	HCV cell culture
HCVpp	HCV pseudoparticles
hpe	Hours post electroporation
HRas	Harvey rat sarcoma viral oncogene homolog
HSPG	Heparan sulfate proteoglycan
Huh7.5	Human hepatoma cell line
HVR	Hypervariable region
IF	Immunofluorescence
IFN	Interferon
IκB	Inhibitor of nuclear factor kappa B
IM	Isolation membrane
IPS-1	Interferon-β promotor stimulator
IRE1	Inositol requiring enzyme 1
IRES	Internal ribosome entry site
IRGM	Immunity-associated GTPase family M
IRS1/2	Insulin receptor substrate 1/2
ISDR	Interferon-α-sensitivity-determining region
JFH1	Japanese fulminant hepatitis 1
JNK	c-Jun N-terminal kinase
Kb	Kilobases
kDa	Kilo Dalton
Keap1	Kelch-like ECH-associated protein 1
L	Liter
LAMP2	Lysosome-associated membrane protein 2
LB	Lysogeny Broth
LC3	Microtubule-associated protein 1 light chain 3
LD	Lipid droplet
LDL	Low density lipoprotein
LDLR	Low-density-lipoprotein receptor
LE	Late endosome
LIMP	Lysosome integral membrane protein
LMP7	Low-molecular-mass protein 7
LVP	Lipoviral particle

M	Molar (mol/l)
mA	Milliampere
MAPK	Mitogen-activated protein kinase
MEK	Mitogen-activated protein kinase kinase
mg	Milligram
MHC II	Major histocompatibility complex class II
min	Minute
miRNA	MicroRNA
ml	Milliliter
mM	Millimolar
MMV	Multi membrane vesicle
mRNA	Messenger RNA
mTOC1	Mammalian target of rapamycin complex 1
mTOR	Mammalian target of rapamycin
MVB	Multivesicular body
MW	Membranous web
NAT	Nucleic acid test
Nm	Nanometer
nM	Nanomolar
NOX	NADPH oxidases
NPC1L1	Niemann-Pick C1-like
Nrf2	Nuclear factor-E2 related factor 2
NS	Nonstructural
NTP	Nucleoside triphosphate
OCLN	Occludin
ORF	Open reading frame
PA28γ	Proteasome activator 28 gamma
PBS	Phosphate buffered saline
PBS-T	Phosphate buffered saline + Tween
PE	Phosphatidylethanolamine
PEI	Polyethylenimine
PERK	Protein kinase R-like ER kinase
PGC-1α	Peroxisome proliferator-activated receptor-gamma coactivator 1α
PHH	Primary human hepatocytes
PI3K	Phosphatidylinositol 3-kinase
PI3P	Phosphatidylinositol 3-phosphate
PI4KIIIα	Phosphatidylinositol-4 kinase III α
PI4P	Phosphatidylinositol-4 phosphate
PKA	Protein kinase A
PKR	Protein kinase R
PLA2G4	Phospholipase A2
PMSF	Phenylmethylsulfonyl fluoride
PNS	Post-nuclear supernatant
PSMB4	Proteasomal subunit beta 4
PSMB5	Proteasomal subunit beta 5
PVDF	Polyvinylidene fluoride
q-PCR	Quantitative polymerase chain reaction
Rab	Ras-related in brain
RC	Replication complex
RdRp	RNA-dependent RNA-polymerase
Rev	Reverse

RIG-I	Retinoic acid inducible gene I
RIPA	Radioimmunoprecipitation assay buffer
RNA	Ribonucleic acid
ROI	Reactive oxygen intermediate
ROS	Reactive oxygen species
RPM	Rounds per Minute
RT	Room temperature
RT-qPCR	Real Time-qPCR
s	Seconds
scrRNA	Scrambled RNA
SDS	Sodium Dodecyl Phosphate
SDS-PAGE	Sodium dodecyl sulfate-polyacrylamide gel electrophoresis
SEM	Standard error of the mean
siRNA	Small interfering RNA
sMAF	Small musculoaponeurotic fibrosarcoma
SN	Supernatant
SNAP29	Synaptosomal-associated protein 29 kDa
SNARE	Soluble N-ethylmaleimide-sensitive fusion protein-attachment protein receptor
SOCS-3	Suppressor of cytokine signaling
SPCS1	Signalpeptidase complex unit 2
SRB1	Scavenger receptor B1
STX17	Syntaxin 17
STX4	Syntaxin 4
SVR	Sustained virologic response
TAE	Tris-Acetat-EDTA
TAG	Triacylglycerides
TBS	Tris Buffered Saline
TBS-T	Tris Buffered Saline + Tween 20
TEMED	N,N,N',N'- Tetramethylethylenediamine
TfR	Transferrin receptor
TIP47	Tail-interacting protein 47
TMD	Transmembrane domain
tMOC	Threshold Manders overlap coefficient
TRIM26	Tripartite Motif Containing 26
t-SNARE	Target-soluble N-ethylmaleimide-sensitive fusion protein-attachment protein receptor
U	Unit
ULK1/2	Unc-like kinase 1 and 2
UPR	Unfolded protein response
UTP	Uridine triphosphate
UTR	Untranslated region
UVRAG	UV radiation resistance-associated gene protein
V	Volt
v/v	Volume/volume
VAMP8	Vesicle associated membrane protein 8
VAR	Variable sequence
v-ATPase	Vacuolar type H^+-ATPase
VLDL	Very-low density protein
Vps34	Vacuolar protein sorting
w/o	Without

w/v	Weight/volume
WB	Western blot
WCC	Weighted Correlation Coefficient
WHO	World health organization
WIPI	WD-repeat domain phosphoinositide interacting protein
wt	Wildtype
Δ	Deletion
λ	Wavelength

11 List of figures

12 List of tables

13 Publications

Personal publications

Vanessa Haberger; Fabian Elgner; Jessica Roos; Daniela Bender; Eberhard Hildt (2020): Regulation of the Transferrin Receptor Recycling in Hepatitis C Virus-Replicating Cells. In: Front Cell Dev Biol 8 (44) DOI: 10.3389/fcell.2020.00044.

Posters

13th Annual Meeting, Retreat on Biomedical Research, 2019, Ronneburg, Germany.
Vanessa Haberger, Fabian Elgner and Eberhard Hildt.
Regulation of the Transferrin Receptor Recycling in Hepatitis C Virus-Replicating Cells.

29th Annual Meeting of the Society of Virology, 2019, Düsseldorf, Germany.
Vanessa Haberger, Fabian Elgner and Eberhard Hildt.
Regulation of the Transferrin Receptor Recycling in Hepatitis C Virus-Replicating Cells.

14th Annual Meeting, Retreat on Biomedical Research, 2020, Ronneburg, Germany.
Vanessa Haberger, Daniela Bender and Eberhard Hildt.
Characterizing the turnover of viral nonstructural proteins of the hepatitis C virus.

14th Annual Meeting, Retreat on Biomedical Research, 2020, Ronneburg, Germany.
Xingjian Wen, Fabian Elgner, Mirco Glitscher, Daniela Bender, Bingfu Jiang, Marie-Luise Herrlein, Vanessa Haberger, Gerrit Praefcke and Eberhard Hildt.
The impact of guanylate-binding protein 1 on the HCV life cycle.

30th Annual Meeting of the Society of Virology, 2021, digital.
Vanessa Haberger, Marie-Luise Herrlein, Nagihan Aydin, Fabian Kortum, Daniela Bender and Eberhard Hildt.
Characterizing the turnover of viral nonstructural proteins of the hepatitis C virus.

14 Danksagung

15 Curriculum vitae

16 Eidesstattliche Erklärung

Hiermit erkläre ich an Eides statt, dass ich die vorliegende Dissertation selbstständig und ohne unerlaubte Hilfe angefertigt und andere als die in der Arbeit angegebenen Hilfsmittel nicht benutzt habe. Alle Stellen, die wörtlich oder sinngemäß aus anderen Schriften entnommen sind, habe ich als solche kenntlich gemacht. Diese Arbeit hat in gleicher oder ähnlicher Form noch keiner Prüfungsbehörde vorgelegen. Des Weiteren bin ich mit der späteren Ausleihe meiner Doktorarbeit an die Fachbereichsbibliothek einverstanden.

Mainz, den

_____

Vanessa Haberger